Universidade de Aveiro
Ano 2018
Departamento de Química

Celso Eduardo Dias Cardoso

Recuperação de terras raras de águas naturais usando nanomateriais à base de carbono

Recovery of rare earths from natural waters using carbon--based nanomaterials

Universidade de Aveiro
Ano 2018
Departamento de Química

Celso Eduardo Dias Cardoso

Recuperação de terras raras de águas naturais usando nanomateriais à base de carbono

Recovery of rare earths from natural waters using carbon--based nanomaterials

Dissertação apresentada à Universidade de Aveiro para cumprimento dos requisitos necessários à obtenção do grau de Mestre em Química, realizada sob a orientação científica da Doutora Cláudia Maria Batista Lopes, Bolseira de pós-doutoramento do Departamento de Química da Universidade de Aveiro, da Doutora Maria Eduarda da Cunha Pereira, Professora Associada do Departamento de Química da Universidade de Aveiro, e co-orientação do Doutor Tito da Silva Trindade, Professor Catedrático do Departamento de Química da Universidade de Aveiro.

o júri

presidente

Doutora Helena Isabel Seguro Nogueira
professora auxiliar do Departamento de Química da Universidade de Aveiro

Doutora Maria Eduarda Pereira
professora associada do Departamento de Química da Universidade de Aveiro

Doutor Carlos Alberto Garcia do Vale
Investigador principal do Centro Interdisciplinar de Investigação marinha e Ambiental (CIMAR) da Universidade do Porto

agradecimentos

No decorrer desta dissertação de mestrado diversas pessoas contribuíram de forma direta ou indireta para o sucesso deste trabalho.

Gostaria de começar por agradecer à professora Eduarda Pereira pela oportunidade e por me ter integrado tão bem neste trabalho. Agradeço-lhe todos os ensinamentos e a motivação que me transmitiu ao longo deste ano. Um grande obrigado pela paciência e pelas longas conversas que contribuíram para o sucesso deste trabalho.

À Drª Cláudia Lopes pelos ensinamentos transmitidos, pelo acompanhamento e por todo o apoio e dedicação ao longo deste trabalho, sobretudo na ajuda em solucionar alguns obstáculos que foram aparecendo ao longo do trabalho.

Ao professor Tito Trindade por todo o apoio e ajuda indispensável que me deu a nível científico e pela disponibilização do seu laboratório, o nanolab.

À professora Paula Marques do TEMA pela disponibilização de alguns dos materiais utilizados neste trabalho.

Ao Dr. Bruno Henriques e à Daniela Tavares agradeço pelo seu interesse, sugestões, simpatia e amizade, bem como toda a sua vontade e disponibilidade de ajuda manifestada ao longo de todo o trabalho.

A todas as pessoas que me ajudaram com diversas técnicas, no departamento de Química, no departamento de Cerâmica e do Vidro e no Laboratório Central de Análises.

Aos meus colegas de laboratório (Inorgânica e Analítica) pelo companheirismo.

Aos meus amigos que sempre me apoiaram e acompanharam neste grande percurso, pela amizade e carinho que sempre me transmitiram, um grande obrigado do fundo do coração.

À Joana Almeida por todo o apoio e ajuda em todos os momentos.

À minha família pelo esforço, apoio e motivação dada ao longo do ano.

A todos os meus sinceros agradecimentos!

palavras-chave Lixo eletrónico, Magnetite, Óxido de grafeno, Recuperação, Sorção, Terras raras, ácidos húmicos, polietilenimina, quitosana.

Resumo

A sociedade nunca foi tão dependente de dispositivos eletrónicos e elétricos como é hoje. Como resultado desta crescente utilização, o lixo eletrónico tornou-se um problema mundial, não apenas devido às alterações ambientais que surgiram com o seu tratamento e armazenamento incorreto, mas também porque a quantidade de lixo eletrónico aumenta a cada ano. Outro problema inerente aos dispositivos elétricos e eletrónicos é o facto de dependerem de elementos de terras-raras para serem produzidos. Atualmente, eles são considerados as "vitaminas" da indústria moderna, devido ao seu papel crucial no desenvolvimento de novas tecnologias e às suas propriedades químicas e físicas distintas. No entanto, a elevada procura e os recursos limitados de elementos de terras-raras (REEs), combinados com os problemas ambientais associados à sua exploração pelas atividades de mineração, reforçam a necessidade de desenvolver novas formas de recuperar estes elementos a partir de lixo eletrónico e de águas residuais que os contenham. Portanto, o desenvolvimento de técnicas e materiais de baixo custo para a recuperação destes elementos é extremamente importante.

Desta forma, o principal objetivo deste trabalho foi desenvolver materiais compósitos à base de carbono que fossem eficientes para a recuperação de terras-raras. A maioria dos estudos de sorção reportados na literatura foram realizados em água ultrapura e com soluções monoelementares de concentrações elevadas de terras-raras; assim, o objetivo é estudar a recuperação destes elementos em matrizes mais complexas, tais como na presença de outros iões, e usando concentrações mais realistas de terras-raras. Os materiais sintetizados e usados neste trabalho foram a grafite esfoliada magnética funcionalizada com ácidos húmicos (MEG-HÁ), óxido de grafeno funcionalizado com 25% de polietilenimina (GO-PEI) e óxido de grafeno funcionalizado com quitosana (GO-CH) e estes foram avaliados quanto à sua capacidade de recuperação de REEs, utilizando diferentes quantidades de material/sorvente e na presença de diferentes tipos de águas. Em água ultrapura, foram obtidas percentagens médias de recuperação de 47%, 97% e 71%, utilizando 100 mg/L de MEG-HÁ, GO-PEI e GO-CH. O comportamento de sorção dos compósitos permitiu verificar que a recuperação é mais eficiente em água mineral, quer usando MEG-HÁ ou GO-PEI, atingindo percentagens de recuperação de cerca 100%. No entanto, em água do mar, as percentagens de recuperação diminuem para cerca 60 e 50% usando 100 mg/L de GO-PEI e MEG-HÁ, respetivamente. Os resultados foram ajustados utilizando modelos cinéticos de pseudo primeira ordem, pseudo segunda ordem e Elovich e o mecanismo de sorção que melhor descreveu a interação entre os nanocompósitos e as REEs foi a quimiossorção. A aplicação dos nanocompósitos testados para a recuperação de REEs a partir de soluções aquosas confirma que os compósitos MEG-HÁ e GO-PEI têm um elevado potencial para serem utilizados na recuperação de REEs de águas.

keywords E-waste, Graphene oxide, Magnetite, Rare earths elements, Recovery, Sorption, humic acids, polyethylenimine, chitosan.

abstract

The society has never been so much dependent on electronic and electric devices as it is today. As a result, e-waste has become a worldwide problem not only due to environmental changes that have emerge from the incorrect treatment and storage of e-waste but also because the amount of e-waste is increasing each year. Another problem inherent to electrical and electronic devices is their dependence on rare earth elements. Currently, they are considered as the “vitamins” of modern industry due to their vital role on the development of new cutting-edge technologies due to their distinctive chemical and physical properties. However, the high demand and the limited resources of rare earth elements, combined with the environmental problems associated with their exploration by mining activities, enforce the development of new ways to recover these elements from e-waste and wastewaters. Therefore, the development of low cost techniques and materials for recovery these valuable elements from e-waste is important to face and resolve both issues.

In this way, the main objective of this work was to develop an efficient carbon-based composite towards the recovery of rare earths. Most of the sorption studies reported in the literature were performed with ultrapure waters spiked with tens to hundreds mg/L of single rare earth elements; so the objective is to study the recovery from waters of different matrices and using lower element concentrations.

The materials synthesized in this work were magnetic exfoliated graphite functionalized with humic acids (MEG-HA), graphene oxide functionalized with *ca.* 25% of polyethylenimine (GO-PEI) and graphene oxide functionalized with chitosan (GO-CH), and they were evaluated for the REEs recovery capacity, using different amount of sorbent and in the presence of different type of waters. In ultrapure water, average recovery percentages of 47%, 97% and 71% were obtained using 100 mg/L of MEG-HA, GO-PEI and GO-CH, respectively. The sorption behaviour of the composites showed that the recovery is more efficient in mineral water, either using MEG-HA or GO-PEI, achieving recovery percentages around 100%. However, in saline water, the recovery percentages decrease to *ca*. 60 and 50% using 100 mg/L of GO-PEI and MEG-HA, respectively. The results were adjusts using kinetic models of pseudo first order, pseudo second order and Elovich and the sorption mechanism that better described the interaction between the nanocomposites and REEs was chemisorption. The application of the nanocomposites tested for the recovery of rare earth elements from aqueous solutions confirms that the carbon-based composites have a great potential to be used in the recovery of REEs.

List of Contents

List of Figures

List of Tables

Chapter 1

Introduction and objectives

1.1. Contextualization

The development of emerging key technologies – including renewable energy, energy efficiency, electronics and aerospace industries – are taking an important role in the current socio-economic, environmental and public health challenges that countries are facing and therefore the pursuit for solutions to support our transition towards an economy and lifestyle sustainable is crucial. In this context, the increasing use of technology-critical elements (TCEs) – that are essentials to this emerging key technologies – and their associated environmental impacts (from mining to end-of-life waste products) are a big concern for all the countries nowadays. These elements – which includes Ga, Ge, In, Te, Nb, Ta, Tl, the platinum group elements (PGEs: Pt, Pd, Rh, Os, Ir, Ru), and most of the rare earth elements (REEs: Y, La, Ce, Pr, Nd, Sm, Eu, Gd, Tb, Dy, Ho, Er, Yb, Lu) – have gained an enormous importance due to their high economic relevance and to European Union (EU) dependency on their imports, mainly from China. For this reason, EU labelled these elements as TCEs since there are, at the moment, no mining zones with an acceptable short/mid-term profit within the EU borders (Cobelo-García et al., 2015).

Currently, the extraction of TCEs from ores involves large energy costs and serious environmental risks due to the chemicals involved in the mining (Environmental Law Alliance Worldwide, 2014). An alternative source to obtain and to produce TCEs is Waste Electrical and Electronic Equipment (WEEE or e-waste). However, the current processes of recycling and treatment of this waste have very low efficacy and are expensive. This means that the recovery of TCEs from this growing "source" is very small, and therefore large amounts of TCEs are wasted. In addition, several inadequate and careless recycling approaches by developing countries and/or countries with less environmental awareness are causing serious health and environmental damage (Atibu et al., 2016; Gonzalez et al., 2014; Hao et al., 2015; Medas et al., 2013; Meryem et al., 2016; Pagano et al., 2015; Ramos et al., 2016; Rim, 2016; Rim et al., 2013; Wei et al., 2013; Yang et al., 2016; Zhuang et al., 2016). It is not yet entirely understood neither there are not enough data about the full impact of this exponential use of TCEs since these studies are only now being done. However, recent studies report, for example, the disturbance of the natural environmental distributions of various rare earth elements (REEs) in the waters of the Rhine River in Germany (Kulaksiz and Bau, 2013) and San Francisco Bay in USA (Hatje et al., 2014), indicating that human activities are already impacting the geochemical cycles of these elements. It should be noted

that these TCEs can be released into the environment and become in contact with the biosphere at any stage of their life cycle (Zaimes et al., 2015). Hence, it is essential to develop more effective and ecologically systems to respond to these manifold challenges of the recovery of TCEs from WEEE like concerted collection, pre-treatment and refining processes for an utmost efficient recovery.

1.2. Waste electrical and electronic equipment

There are several definitions and different classifications about what waste electrical and electronic equipment (WEEE or e-waste) is or is not. In general, e-waste is a chemical and physical specific form of municipal and industrial waste that covers, mainly, old, end-of-life and/or discarded appliances that use electricity, such as consumer electronics (like computers, LCD screens, smartphones), large appliances (like refrigerators, washers or dryers) and similar consumer products that have been discarded by their original users or by having a manufacturing defect (Hobohm and Kuchta, 2015; Tansel, 2017).

The global quantity of e-waste generated in 2014 was around 41.8 million tonnes (Mt). However, in 2016, the amount of e-waste generated worldwide increase to 44.7 Mt (figure 1), approximately more 3 million tonnes of e-waste produce in just 2 years, which is equivalent to 6.1 kilogram of e-waste per inhabitant (kg/inh) in 2016 - in contrast to the 5.8 kg/inh generated in 2014. The amount of e-waste is expected to increase to 52.2 million tonnes, or 6.8 kg/inh by 2021 (figure 1). Most of the e-waste was generated in Asia: 16 Mt in 2014 and 18.2 Mt in 2016, which corresponds, respectively, to 3.7 and 4.2 kg for each inhabitant (kg/inh). Although the Asia is the continent that produces more quantity of e-waste, Asia is also the continent that generates less e-waste per inhabitant. In this case, the highest per inhabitant e-waste quantity (15.6 kg/inh) was generated in Europe (including Russia), which correspond to a total of 11.6 Mt e-waste generated. Of the 44.7 Mt of e-waste generated in 2016, approximately 1.7 Mt are thrown into the residual waste in higher-income countries, and are likely to be incinerated or land-filled; furthermore, only 8.9 Mt (about 20%) of e-waste are documented to be collected and recycled (Baldé et al., 2017, 2015).

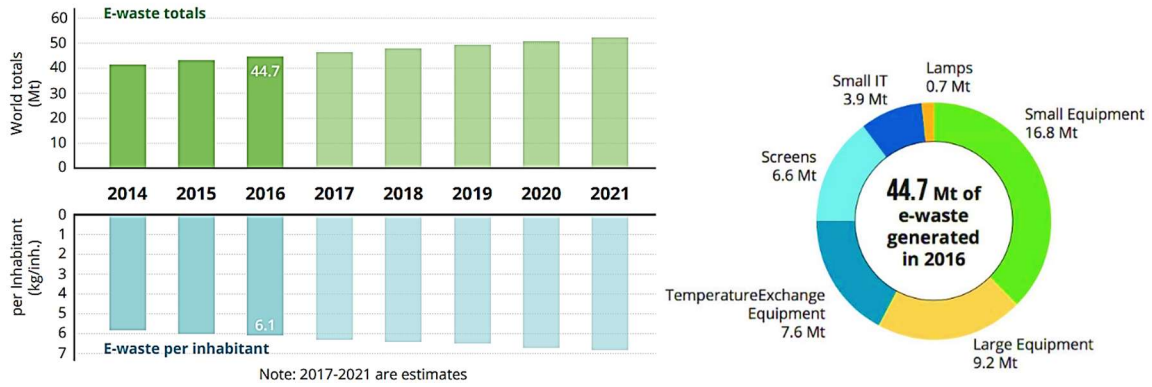

Figure 1 - Amount of global e-waste generated from 2014 to 2016 and the estimate values for the following years (2017 to 2021) (left, retired from Baldé et al. (2017)), and the typology of e-waste produced in 2016 (right, adapted from Baldé et al. (2017)).

The total value of all raw materials present in e-waste is estimated at approximately 55 Billion Euros in 2016 (Baldé et al., 2017). According to an European report (Tsamis and Coyne, 2015), the European recycling market for REEs is estimated to be worth 1 billion euros. Although, recycling of e-waste is strongly encouraged, only 9% is collected and recovered for recycling (the remaining e-waste is exported to developing countries or ends up in electronic waste crusher without pre-separation and appropriate treatment (Hobohm and Kuchta, 2015)) and the recycling ("urban mining") rate of REEs is less than 1% worldwide. This can be explained by the unbridled proliferation of the electronic and electric equipment (EEE) in the society, the short lifetime of these products as well as the complexity of the process of recycling and recovery of these critical elements. According to the existing literature on recovery technologies of REEs from e-waste, although there has been a significant level of R&D, very little activity has moved to an industrial scale. Perhaps it is for this reason that there are only a few companies, in Europe, which are actively involved in REEs recovery (Hobohm and Kuchta, 2015). In terms of industrial scale applications, the recovery of REEs from lamp phosphors is the most developed process (Tsamis and Coyne, 2015).

Fortunately, there is an increasing awareness of this global problem of environmental and public health, and a higher perception of the socio-economic impact that the recycling of these elements has nowadays. A clear example of this change is this new quest of the technologies companies that aiming closing the loop in their supply chain. Namely, Apple published in its annual environmental responsibility report along with a public statement announcing their goal of using 100% recycled materials or renewable resources to produce

iPhones, Macbooks and other electronic products in the future in order to reduce its reliance on mined raw materials (figure 2). In the case of REEs, Apple manages to recover about 24 kg of rare earths in 100 000 iPhone 6 devices (Schischke and Clemm, 2016). Recovery of the REEs content is the most drastic method of recycling, but it delivers the purest end products, in the form of high-purity rare-earth oxides.

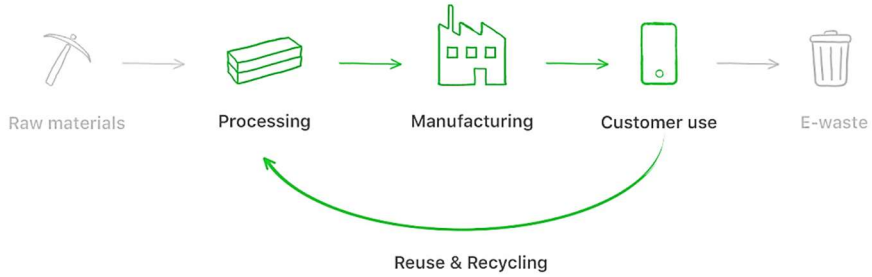

Figure 2 - Representation of the supply chain of the Apple production products (Schischke and Clemm, 2016).

1.3. Technology-critical elements

Technology-critical elements (TCEs) - represented in figure 3 - are all the elements which have an important role in high-technology, energy supply and green applications, but their supply and demand is unbalanced. Generally, they include Ga, Ge, In, Te, Nb, Ta, Tl, the platinum group elements (PGEs: Pt, Pd, Rh, Os, Ir, Ru), and most of the rare earth elements (REEs: Y, La, Ce, Pr, Nd, Sm, Eu, Gd, Tb, Dy, Ho, Er, Yb, Lu) (Directorate General Enterprise and Industry, 2014).

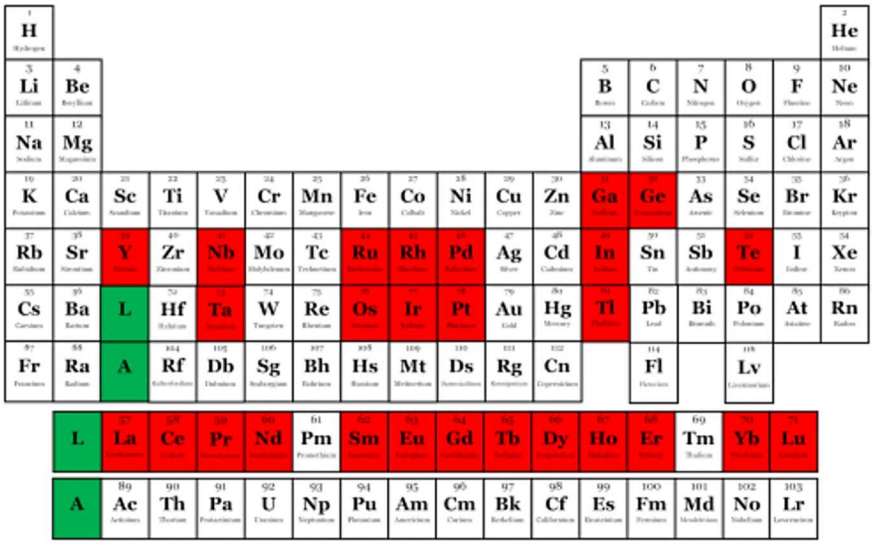

Figure 3 – Periodic table with the technology-critical elements in red (European Comission, 2014)

1.3.1. Rare earth elements

The International Union of Pure and Applied Chemistry (IUPAC) defines the rare earth elements (REEs) as a group of 17 elements consisting of the 15 lanthanoids (La to Lu), Sc and Y. Scandium and Yttrium are also considered REEs since they tend to occur in the same ore deposits as the lanthanoids and share many chemical and physical properties (Tsamis and Coyne, 2015). The REEs are usually subdivided into groups: light REEs (LREEs), the heavy REEs (HREEs) and sometimes medium or middle REEs (MREEs). The grouping to these three classes is not consistent among different authors, as can be seen in Zepf (2013). The LREEs includes, generally, the elements La to Pm, the elements Sm, Eu and Gd are MREEs, and the elements Tb to Lu, including Y are designated as HREEs. Yttrium is included in the HREEs group based on its similar ionic radius and chemical properties. On the contrary, Scandium, although its trivalent state, the other properties are not similar enough to classify it in any group. REEs naturally occur together in mineral deposits, however they are often widely dispersed and found in very low concentrations (typical the concentration range is 10 to a few hundred ppm by weight), resulting in energy intensive, large amounts of waste and environmental taxation of mining, extraction, and refining processes which represents an additional difficulty in obtaining these metals (European Rare Earths Competency Network (ERECON), 2014). For example, the values reported to produce 1 tonne of rare earth oxide (REO) in China are 60 000 m^3 of waste gases, 200 m^3 of acidified water and 1.4 tonnes of radioactive waste since most REEs deposits contain uranium or thorium; besides the electricity required for its production that generally comes from unclean sources (Royen and Fortkamp, 2016).

Towards the expected growth of demand for REEs and possible supply restrictions, it is important to characterise the “criticality” of raw materials and metals, including rare earths (Tsamis and Coyne, 2015). In this way, REEs – mostly dysprosium, terbium, yttrium, europium, and neodymium (Dutta et al., 2016) – were described as critically at-risk marketable elements (figure 4).

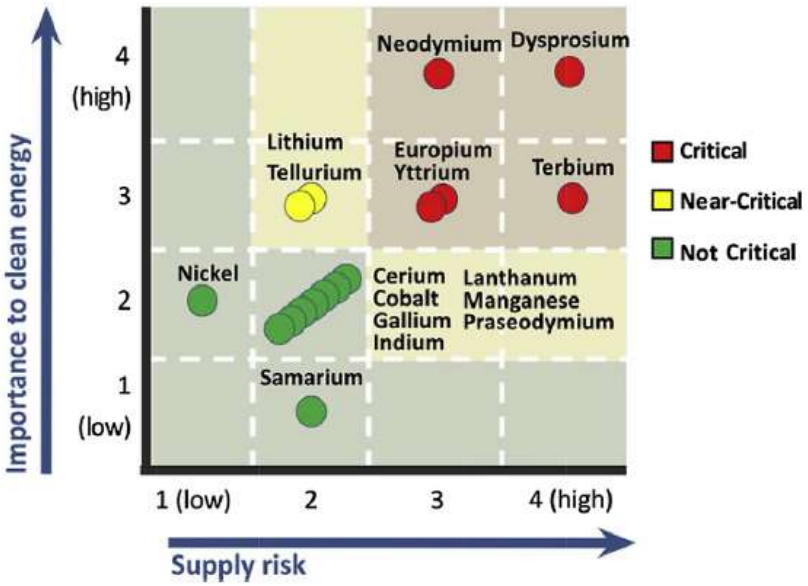

Figure 4 - Criticality assessment of REEs and other elements.

Moreover, the rare earths supply crunch in 2010/2011 served as a "wake-up call" to businesses and governments, bringing up the discussion about the future rare earths supply. Consequently, China – which is the main country supplying rare earth elements – imposed tight export restrictions and a ban on exports to Japan leading to speculative price increase where prices of different REEs ranged between four and nine times. The price spike led to a global exploration boost of REEs, with miners scrambling to access old mines and hundreds of new exploration projects being announced around the world, including some in Europe (European Rare Earths Competency Network (ERECON), 2014). In figure 5, it is possible to observe a prediction of the evolution of global rare earth demand and supply from 2016 to 2020 (Dutta et al., 2016).

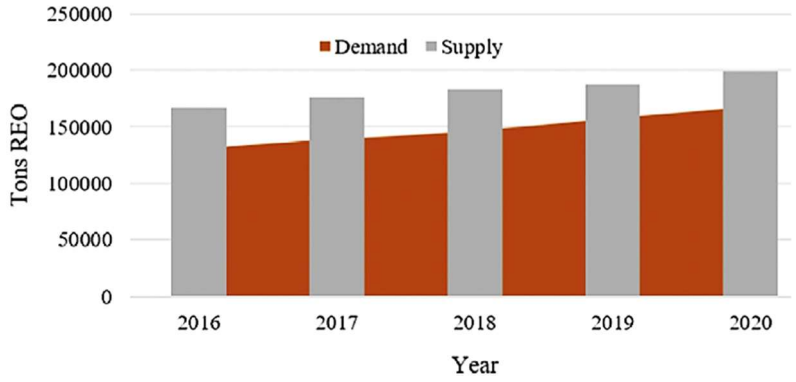

Figure 5 - Anticipated evolution of global rare earth demand and supply from 2016 to 2020 (Dutta et al., 2016).

REEs usually occur together with oxygen in oxide, silicate or phosphate combinations and always together with other REEs as accessories in minerals. Typical occurrences of REE are in granites, pegmatites, carbonatites – usually enriched with phosphate-minerals (like apatite, monazite or xenotime), bastnaesite and others – and perovskites. In general, there is an aggregation as LREE or HREE and some complex mineral ores. Thus, monazite and bastnaesite are the main minerals of LREEs and xenotime is the main font of HREEs (specifically Y, Dy, Ho, Er, Tm, Yb and Lu) (Vogel, 2011).

1.3.1.1. Chemistry of the rare earth elements – the singularity of lanthanoids

In the periodic table, lanthanoids (Lns) as well as scandium, yttrium and actinides belong to the third subgroup of the transition metals – designated as the Sc-group. The lanthanoids are soft and white metals which have special electronic configurations on the atomic level providing them unique properties. Instead of the valence electrons attach to the outer orbitals, they are accommodated in a deeper lying orbital, the 4f-orbital. This leads to the outer orbital of Lns being the same for all of them and, consequently, to its chemical resemblance. A clear example is their oxidation state, since Lns favour the oxidation state Ln(III) with unprecedented uniformity in the periodic table. The prevalence of their trivalent oxidation state regardless of atomic number is due to the nature of their 4f-orbitals (Shriver et al., 2014; Vogel, 2011). However, some lanthanoids (Lns) may show other states (like Ln^{2+} or Ln^{4+}); thus, the preferred stable states are those attained by empty, half or full occupied orbitals: La^{3+} (f^0), Ce^{4+} (f^0), Eu^{2+} (f^7), Gd^{3+} (f^7), Tb^{4+} (f^7), Yb^{2+} (f^{14}) and Lu^{3+} (f^{14}) (Vogel, 2011). Other consequence of the 4f subshell is the Lns size, since as the atomic number increases, the ionic radii gets smaller along the period (from La to Lu) which is known as lanthanoid-contraction. Complexes of Ln(III) are usually form by electrostatic interactions – due to the anionic polydentate ligands containing oxygen-atom donors – rather than covalent interactions which are very stable. Coordination numbers usually exceed 6 and the ligands adopt geometries that minimize interligand repulsions; all Lns form complexes with complexing agents like EDTA, however, lutetium forms a stronger complex than cerium because it is the smallest in the series (Huang, 2010). Nevertheless, their chemical resemblance does not have influence on the physical properties since lanthanoids (Lns) display different physical behaviours. Among its physical properties, the Lns – which are metals - have relatively poor thermal and electrical conductivities (about 25 and 50 times

lower than copper, respectively). Most metals adopt the hexagonal close-packed structure type, although cubic close-packed forms are also known for most of the elements, particularly under high pressure (Zepf, 2013).

1.3.1.2. Rare earth elements in devices

Among the wide variety of REEs applications, there are four markets – magnets, metallurgy, catalysts and polishing powder – which account for nearly three quarters of total rare earth used in 2012. However there are other applications important for several rare earths, such as glass, phosphors and ceramics (European Rare Earths Competency Network (ERECON), 2014). Figure 6 shows the current consumption of REEs in several applications, as well as the respective susceptibility to be replaced.

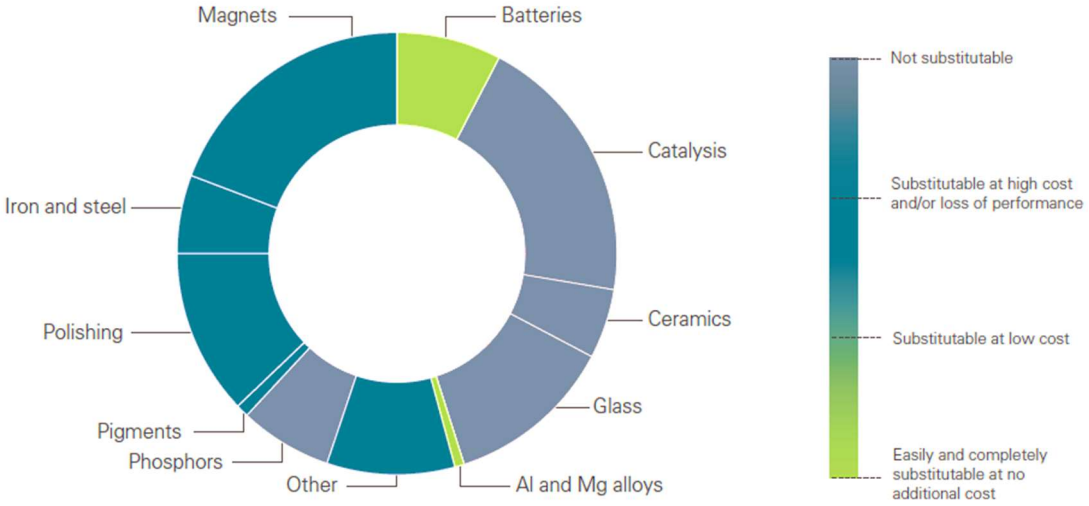

Figure 6 - Current consumption of REEs in several applications, as well as the respective susceptibility to be replaced (European Rare Earths Competency Network (ERECON), 2014).

In this figure, it is possible to observe the areas where REEs have the most impact and where they are irreplaceable – like the catalysis, phosphors, ceramics and glass industry – but also other areas where they have a huge impact and where they are very difficult to replace – as is the case of magnets, and iron and steel applications, for example.

1.3.1.3. Rare earth elements in effluents

REEs contained in non-recycled waste materials may end up in surface waters and oceans. For example, the highest REEs concentration in well water in Chinese mining areas is 130 µg/L. However, Sidaosha River – which has highest level of REEs – has a total of

REEs concentration in suspended particles and surface sediments of 31 524 and 30 461 μg/L, respectively (Liang et al., 2014). Recently, significantly high concentrations of rare earths were detected in the surface water of San Francisco Bay area (Hatje et al., 2014) presumably due to the wastewater treatment plant discharges of refractory magnetic resonance imaging (MRI) contrast agents used in hospitals and medical research centres (Dutta et al., 2016). In addition, it has been found that anthropogenic gadolinium contaminates surface and ground water. Therefore, it is necessary the treatment of these wastewaters. Furthermore, wastewater could also be a source of REEs, but its potential remains largely unexplored. In the first instance, rare earths could be recovered from wastewater produced during the extraction and separation of rare earths. However, the recovery of REEs from acidic industrial waste water streams and mining effluents is still in its infancy since their concentrations in industrial waste residues are very low compared to primary rare earth ores and e-waste, whereby it is necessary develop special processes dedicated to the recovery of rare earths from these dilute waste streams.

1.3.1.4. Recycling of rare earth elements and barriers to end-of-life recycling

A major challenge in recycling REE has been its low yield rate which can be explained by the lack of proper recycling design and by the tedious steps involved in their separation. These problems have led to a false premise that is the virtual impossibility to recycle REE in any profitable quantity, since they are used in very small quantities (Dutta et al., 2016). In the last years, several examples of REE recovery from end-of-life products have been presented such as wastes from fluorescent lamps (Binnemans and Jones, 2014; Ruiz-Mercado et al., 2017; Tan et al., 2015; Wu et al., 2014), magnets (Abrahami et al., 2015; Firdaus et al., 2016; München and Veit, 2017; Yang et al., 2017; Yoon et al., 2016), batteries (Innocenzi et al., 2017) and mobile phones (Lister et al., 2014). Many of these studies report a reasonably good yield, which in some cases may goes up to 99% of re-usable REEs. An example of this scenario is the study of Kim et al. (2015) where the recovery of REEs oxides (namely Nd, Pr and Dy) was made from commercial magnets and industrial scrap magnets by employing membrane-assisted solvent extraction. Good yields without any co-extraction of non-REEs over the 120 hours run were obtained. Although many lab-scale experiments have reported a good REEs recovery (Sun et al., 2016), cooperation among

companies to develop techniques and processes in order to recover high purity REE from e-waste are scarse (Dutta et al., 2016). A mature recycling route for REE could offer a number of important advantages over primary production, such as a smaller environmental footprint (even because recycling does not leave radioactive elements to dispose of), shorter lead times and a cheaper source of material compared to primary production.

Regardless of the recycling techniques used, there are several barriers to overcome and to the recycling of REEs content products become a reality on a large scale, such as (European Rare Earths Competency Network (ERECON), 2014):

- Insufficient and often non-selective collection rates;
- Lack of information about the quantity of REE materials available for recycling;
- Dissipative use, since the quantity of rare earths per component or device is often very small, which can make it difficult to detect the REEs products in mixed waste streams and uneconomical to separate them;
- Presence of contaminants;
- Price volatility for scrap and products like magnets or phosphors;
- Shipping of e-waste.

1.4. Pre-treatment of e-waste

Most of the REE are intricately embedded into e-wastes, and hence pre-treatment procedures towards their recovery from goods at end-of-life vary with their typology. The first step that e-waste undergo is dismantled, separated and crushed by mechanical processes such as shredding, cutting, grinding or milling, followed by physical processes which may be separation by vibration, gravity, buoyancy, magnetic or Eddy current. It follows a chemical decomposition step through leaching or other chemical treatment to solubilise the REE (Kaya, 2016), for later recovery of REEs from aqueous systems (figure 7).

Figure 7 - Steps of a general process of REEs recycling from e-waste.

Liquid-liquid extraction (LLE) and solid phase extraction (SPE) procedures have been applied to separate and extract REE from aqueous solutions.

LLE implies two different immiscible liquids, such as aqueous and organic solvents, to separate compounds through the attraction of the desired element from one side of the liquid phase towards another liquid phase (Hidayah and Abidin, 2017). Among the LLE procedures commonly used in metallurgy, there are the pyrometallurgical and hydrometallurgical techniques, in which metals are melted by heat or dissolved by a liquid, respectively (Kaya, 2016). Low extraction, loss of extractant into aqueous, and low purity in the final product are the major limitations of those processes (Hidayah and Abidin, 2017).

SPE consists of the extraction of the desired element from liquid phase towards the solid phase of large surface (Hidayah and Abidin, 2017). Among of the SPE, batch (offline) and column (online) procedures have been widely used (Pyrzynska et al., 2016). In batch pre-concentration procedure, the solids are manually mixed with the liquid, filtered, and finally the enriched solid phase is transferred to the detector. On the contrary, all operations are automatic in the column procedure. High extraction, selectivity, quality of the products in the separation and extraction of REE are generally obtained (Xiaoqi et al., 2009; Zhu et al., 2012). When compared to LLE, the solid phase extraction offers a number of important advantages, such as reduced organic solvents use and exposure, high enrichment factor, rapid phase separation and the possibility of combination with different detection techniques (Płotka-Wasylka et al., 2015; Pyrzynska et al., 2016).

1.5. Materials commonly used as solid phase sorbent

Several nanomaterials have been investigated as solid phase sorbents in batch technique, such as polymers supports, carbon-based composites (carbon nanotubes and graphene oxide) and nanoparticles (NPs); particularly, magnetic NPs which have very interesting magnetic properties (Cao et al., 2015; Ghazaghi et al., 2016; Giakisikli and Anthemidis, 2013). Examples are:

(i) Ion imprinted polymers (IIPs) of specific binding sites for a particular metal ion; interactions between the polymer framework and the complexed ion are based on coordinative bonds from some electron donating heteroatoms (such as oxygen, nitrogen or sulphur) to the unfilled orbitals of the outer sphere of the metal ions (Branger et al., 2013; Hu et al., 2013; Pyrzynska et al., 2016).

(ii) Silica-based materials due to their good porous structure, good quality of mechanical properties, good physical and chemical stability, and the possibility to immobilised

various functional groups on its surface to enhance the sorption to metal ions; drawbacks are related to easy degradation at high pH and difficult separation from water under continuous industrial operation (Fisher and Kara, 2016; Hidayah and Abidin, 2017; Pyrzynska et al., 2016).

(iii) ***Membrane supports*** as poly(tetrafluoroethylene), poly(vinylidene) fluoride, polyamide, and ceramic membranes are common supporting material used in SLE with the advantage of low consumption of energy, high selectivity, and the easy to manage (Fisher and Kara, 2016; Hidayah and Abidin, 2017; Pyrzynska et al., 2016).

(iv) ***Microorganisms***, such as *Bacillus subtilis, Escherichia coli, Pseudomonas fluorescens, Paracoccus denitrificans, Schwanella putrefaciens, and Alcaligenes faecalis* have efficient and environmentally friendly interactions with metal ions through surface adsorption, adsorption on extracellular biopolymer, biologic absorption, and adsorption on extracellular bio-mineral (Fisher and Kara, 2016; Hidayah and Abidin, 2017; Pyrzynska et al., 2016);

(v) ***Nanomaterials*** have an enormous potential for water remediation and elements recovery due to their size dependent properties and surface characteristics (Martins and Trindade, 2012; Quina, 2004). Among these properties, specific surface area is obviously of paramount relevance because leads to higher chemical activity at the solids surfaces. Additionally, nanomaterials can be surface functionalized with specific ligands to increase the affinity to specific targets (elements or compounds) (Francisquini et al., 2014; Martins and Trindade, 2012). More recently, there has been an increasing interest for magnetic nanosorbents because their easy separation from aqueous solutions by using an external magnetic field (Carvalho et al., 2016). This property is a great practical improvement for water treatment units due to practicability and time saving because there is no need of conventional separation methods.

(vi) **Carbon-based nanomaterials** are essential building blocks due to their capability of having variable oxidation states and/or coordination numbers which makes carbon one of the few elements to have multiple numbers of allotropic forms like graphite, graphene, graphene oxide, carbon nanotubes, carbon nanofibers, carbon dots, among others (figure 8); sorption of REEs to those forms is mainly controlled by electrostatic forces, which are related to the various surface oxygen-containing functional groups, such as hydroxyl, carbonyl and carboxyl groups O donors (Pyrzynska et al., 2016). Nowadays, it has been

very frequent combine these materials with ferrites or iron oxide nanoparticles to provide magnetic properties to the materials.

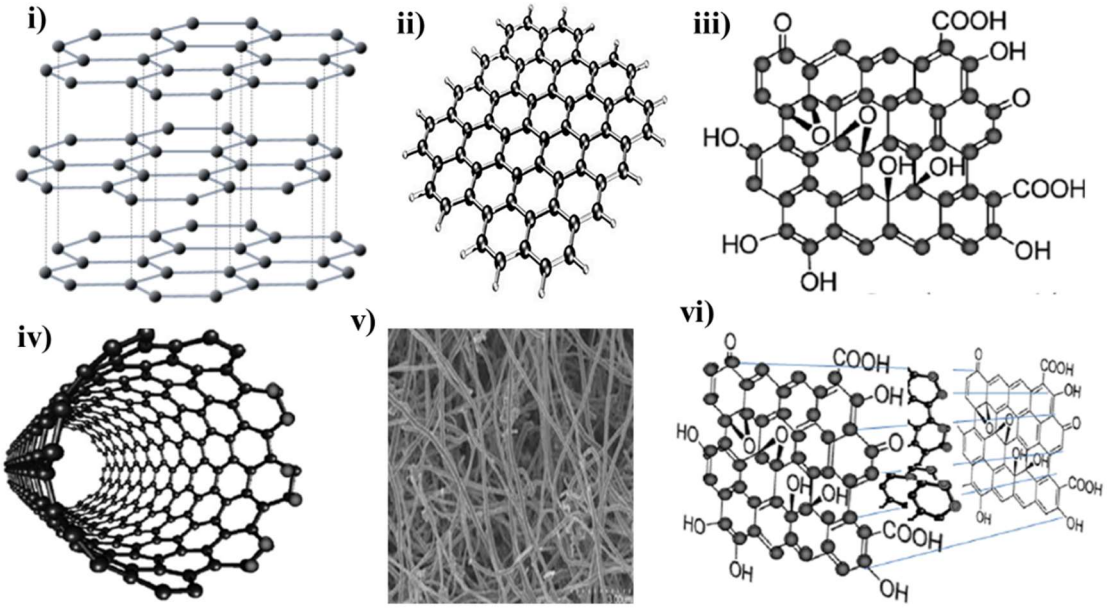

Figure 8 - Carbon allotropic forms: i) graphite, ii) graphene, iii) graphene oxide, iv) carbon nanotube, v) carbon nanofibers, vi) carbon dot. Figure adapted from Kiew et al. (2016) and Tripathi et al. (2015).

1.5.1. Functionalizations

As already mentioned, REEs show a great affinity to O donors and although the graphene oxide has great adsorption properties (essentially due to its O-based surface functional group), in more complex aqueous environments it loses some efficiency. In this context, a variety of methods for the graphene surface modification have been developed in order to improve its sorption efficiency and to give new properties to the material. Therefore, in table I, it was collected a number of ligands that have already been used to functionalised graphene oxide and others ligands that have a great potential to be used in carbon functionalizations for REEs recovery at low pH, due to their low pka values – which makes the surface of the material negative and, therefore, available for sorption of REEs – and their level of proticity – since, theoretically, a higher level of proticity correspond to a higher number of sites, which may mean a higher sorption capacity of the material. Note that the majority of these ligands have already been used to functionalized different nanomaterials (ferrites NPs, silica NPs, among others) to recovery critical elements such as rare earth elements. In the preparation of this table, a number of factors were taken into account in

order to propose the best functionalization hypotheses. They are: water solubility, number of O donors, low pka values and number of sites to interact with REEs. Many of these ligands have already been applied to REEs recovery in various ways as it is the case of ethylenediaminetetraacetic acid (EDTA) (Dupont et al., 2014; Zhao et al., 2016), diethylenetriaminepentaacetic acid (DTPA) (Noack et al., 2016), diglycolamic acid (DGA) (Juère et al., 2016; Ogata et al., 2016; Sengupta et al., 2017), humic acids (Yang et al., 2012) and others chelating ligands (Huang and Hu, 2008), for example. These functionalizations can be obtain, for example, through the preparation of nanostructured silica-coated magnetite (in a first step) and then coating them with the proposed functionalizations. Applying this method, the resulting material would get not only higher sorption capacity of REEs, but also magnetic properties that would be very important in the separation process of the material in aqueous media.

Table I - Carbon functionalization hypotheses for REEs recovery at low pH.

Functionalizations	**Formula**	**Level of proticity**	**pka**
Pentetic acid (DTPA)	$C_{14}H_{23}N_3O_{10}$	Penta	1.80
Ethylenediamine tetraacetic acid (EDTA)	$C_{10}H_{16}N_2O_8$	Tetra	0.0, 1.5, 2.00, 2.69, 6.13, 10.37
Ethylene glycol tetraacetic acid (EGTA)	$C_{14}H_{24}N_2O_{10}$	Tetra	<2, 2.7, 8.8, 9.5
Nitrilotriacetic acid (NTA)	$C_6H_9NO_6$	Tri	1.89, 2.49, 9,73
Perchloric acid	$HClO_4$	Mono	-10
Hydrochloric acid	HCl	Mono	-7
Sulfuric acid	H_2SO_4	Tri	-3, 1.92, 6.91
Nitric acid	HNO_3	Mono	-1.3
(Chloro)acetic acids	CCl_3COOH $CH_2ClCOOH$ CH_3COOH	Mono	0.52 2.85 4.75
Argininosuccinate	$C_{10}H_{18}N_4O_6$	Tetra	1.62, 2.70, 4.26, 9.58
Histidine	$C_6H_9N_3O_2$	Tri	1.80, 6.04, 9.33
Aspartic acid	$C_4H_7NO_4$	Tri	1.99, 3.90, 9.90
Phosphoric acid	H_3PO_4	Tri	2.12, 7.21, 12.3
Citric acid	$C_6H_8O_7$	Tri	3.08, 4.74, 5.40
Pyruvic acid	$C_3H_4O_3$	Mono	2.39
Glutamic acid	$C_5H_9NO_4$	Di	2.13, 4.31
Malonic acid	$C_3H_4O_4$	Di	2.83, 5.69
Tartaric acid	$C_4H_6O_6$	Di	2.98, 4.34

Mesaconic acid	$C_5H_6O_4$	Di	3.09, 4.75
Malic acid	$C_4H_6O_5$	Di	3.40, 5.11
Glyceric acid	$C_3H_6O_4$	Mono	3.52
Formic acid	HCOOH	Mono	3.77
Glycolic acid	$C_2H_4O_3$	Mono	3.83
Thioglycolic acid	$C_2H_4O_2S$	Di	3.83, 9.3
Lactic acid	$C_3H_6O_3$	Di	3.86, 15.1
Ascorbic acid (Vitamin C)	$C_6H_8O_6$	Di	4.10, 11.8
Benzoic acid	$C_7H_6O_2$	Mono	4.19
Succinic acid	$C_4H_6O_4$	Di	4.22, 5.64
Carboxylic acids	RCOOH		4.8 (4 to 5)
Humic acid (HA)			
Fulvic Acid			
Chitiosan			~5.5
PEG			~3
PEI			
Crown ethers			
Chalcogenides	(S^{2-}, Se^{2-}, Te^{2-}, O^{2-})		
Carbonic acid	H_2CO_3	Di	6.35, 10.2

1.6. Sorption as a recovery of rare earth elements process

As already mentioned, there are a lot of materials which can be used as sorbents for the REEs recovery. Also, sorption has many other advantages when compared to the common techniques, namely high removal efficiency, easy to operate and installation, and low maintenance costs.

Nevertheless, the efficiency of this process is dependent from some factors, which will, consequently, influence the REEs recovery (either the kinetics or the sorption capacity). These factors are the typology of the sorbent and the metal ion (to be recovered), as well as the experimental conditions. Among the experimental parameters, there are:

- pH of the batch, because it will affect either the metal ions and the sorbent. The surface charge of the sorbents depends on the acidity of the surrounding electrolyte. Since the sorption of REEs occur mainly by electrostatic forces, the surface charge of the sorbents need to be negative;
- temperature, since inadequate temperatures can decrease the efficiency of the sorption process;
- dose of sorbent, since theoretically, as higher it become, better will be the recovery rate;

- REEs initial concentration because, for the same dose of sorbent, higher values of concentration, lead to lower sorption rates;
- stirring speed, which control the dispersion of particles and the mass transfer rate.

Besides these, the presence of other metal ion species – that is a reality in real effluents – can influence the recovery of REEs due to the competition for the binding site. Therefore, these factors should be considered for an efficient recovery of REEs. These factors will be discussed in more detail in the following sections

1.7. Recovery of rare earth elements using different carbon materials: a literature review

In the literature, several papers describe the use of carbon (nano)composites for the recovery of REEs either in batch or column experiments. Table II shows the carbon materials and batch experimental conditions used in different studies. It should be noted that this table was divided into three sections: -A) GO composites, -B) CNTs and -C) other types of carbon materials for the recovery of REEs. This division is mainly based on the number of papers found in the literature for each nanomaterial. More specifically, the following materials – activated carbon, fullerenes, carbon dots, mesoporous carbon, carbon nanofibers and carbon black – were placed in the third section due to the reduced number of reports found in the literature. However, the volume of studies of GO and CNTs composites reported in the literature made it possible to placed them into individual sections, leading to a more easier and full understanding of the experimental conditions employed. It should also be noted that the optimal experimental conditions are represented by shading and the other conditions tested and described in the papers are represented on a white background (without shading).

Recovery of rare earth elements using graphite oxide composites

The first section of the table (table II-A) presented several studies of the recovery of REEs using GO composites. In this section, it is possible to conclude that almost all the studies were performed in Milli-Q water with the exception of one study that used $HClO_4$ (aq, 0.01 mol/L) performed by Sun et al. (2013). This is expected since Milli-Q water has no competitive ions, so the most studies are performed in this type of water because it is the simplest system to study. Regarding the contact time between the nanomaterial and the rare

earth solution there was a widely range of times used, nevertheless, there are no published studies over 48 hours. In the case of the temperature, most of reported studies were performed at room temperature. However, it is possible to verify that the increase of the temperature provides better rates of rare earth sorption. Thus, the reason to work at room temperature, even with a slight decrease of the sorption rate, is due to the lack of practicality and associated cost of working at higher and controlled temperature environments particularly on an industrial scale; even because the purpose of most of these studies is to have industrial applicability. This is also the reason to not study the sorption during a period over 48 hours.

A set of materials based on graphene oxide with different C:O ratios were found. In addition, to the GO several functionalizations were performed to make the material more efficient, such as: magnetite (Fe_3O_4) (D. Li et al., 2015) with the purpose of afford magnetic proper ties to the material, making the material more efficient for the REEs separation from solution, or polyaniline (PANI) (Sun et al., 2013) to increase the maximum adsorption capacity of the material. It is possible to find in the literature ratios mass of sorbent per volume of solution between the minimum of 40 mg/L and the maximum of 5 000 mg/L for the REEs recovery, being that the m/v ratio most reported in the literature equal to 1 000 mg/L. The studies of Chen et al. (Chen et al., 2014a) and Chen et al. (Chen et al., 2014b) were the ones that reported the lowest value of sorbent mass/volume (40 mg/L), which was used in the recovery of Gd(III) and Y(III) ions, respectively, at pH 5.9 ± 0.1.

Regarding the study of rare earth elements, it is possible to verify that most studies use mono-elemental systems in order to obtain the simplest system to study; there are only two studies – of Ashour et al. (Ashour et al., 2017) and Su et al. (Su et al., 2014) – reported in the literature that used multielementar system. In the mono-elemental system, Europium is the rare earth element most studied by far, but there are also studies with other REEs like two studies with Cerium by Fakhri et al. (2017) and Farzin et al. (Farzin et al., 2017) and one study of Gadolinium, Scandium and Yttrium by W. Chen et al. (Chen et al., 2014a), Kilian et al. (2017) and Chen et al. (Chen et al., 2014b), respectively. In the multi-elemental systems, Ashour et al. (Ashour et al., 2017) used a quaternary system with Lanthanum, Neodymium, Gadolinium and Yttrium, and Su et al. (Su et al., 2014) studied a mixture of fifteen REEs (leaving only the Pm(III) and Sc(III) ions). As for the rare earth concentration, a wide variety of intervals are published, as shown in table II-A. Most of the studies to the

date have used concentrations between the minimum of 10 µg/L (Xie et al., 2016) and the maximum of 300 000 µg/L (Kilian et al., 2017), being that the majority of the used concentrations varies between 1 and 100 µg/L (Ashour et al., 2017; Chen et al., 2014a, 2014b; Fakhri et al., 2017; D. Li et al., 2015; Sun et al., 2013, 2012; Yao et al., 2016). The studies that used lower concentration values, namely 10 and 50 µg/L of Eu(III) and Ce(III) ions, in mono-elemental solutions, were the studies of Xie et al. (Xie et al., 2016) and Farzin et al. (Farzin et al., 2017), respectively; moreover, Su et al. (Su et al., 2014) used 10 µg/L for 15 elements in multi-elemental solution. Concerning the pH, the rates of rare earth adsorption are strongly pH dependent, so the maximum adsorption values of REEs using different types of GO composites are highly dependent on the chosen working pH. In this way, several authors have done the study of pH, varying mostly between 2-11, in order to find out the optimal pH and/or the working pH. The most used working pH is 6 (Ashour et al., 2017; Chen et al., 2014a, 2014b; Fakhri et al., 2017; Sun et al., 2012); also, the lowest pH used was 2 (Kilian et al., 2017; Sun et al., 2012) whereas the highest working pH chosen was 7 (Li et al., 2014; D. Li et al., 2015; Sun et al., 2012). A clear example that evidences this pH dependence on REEs adsorption is the study of Li et al.(2014) in which approximately 7% and 10% of Eu(III) adsorption was obtained for pH 1 using GO and titanium phosphate modified GO composite (GTiP-2), respectively; at pH 3.7 and 5, it was possible to obtained 20% with GO and 45-50% using GTiP-2 ; and finally, at pH 7.3, they achieved an Eu(III) adsorption rate of 28% using GO and 80% using GTiP-2. Nevertheless, at least two studies have been reported in the literature that have achieved adsorption of approximately 100% using a pH of 5.5 (Yao et al., 2016) and 7 (Sun et al., 2012), and it is possible to find more studies with values around 80% and 90% of adsorption. Finally, the material with the highest maximum adsorption capacity (qm) of REEs reported in the literature to date was PANI@GO with 250.74 mg/g achieved (Sun et al., 2013).

Table II-A - Recovery of REEs using graphene oxide (GO) composites and the respectively experimental conditions used as reported in the literature. Note that in this table it is only presented the best results and consequently the optimal experimental conditions (see complete table in the attachments present in chapter 6, table A1).

Ref.	Sorbent	Type of water	Type of system	REEs (III)	$[REEs]_0$ (µg/L)	pH	T (ºC)	Time of contact (h)	m (sorbent)/ V(solution) (mg/L)	q_m (mg/g) or REEs adsorption (%)
(Ashour et al., 2017)	GO colloid	Ultrapure	Multi elemental	La, Nd, Gd, Y	5×10^3	6	r.t.	0.5	10×10^2	La = 85.67 mg/g Nd = 188.6 mg/g Gd = 225.5 mg/g Y = 135.7 mg/g
(Li D. et al., 2015)	GO (Graphene Oxide)	Ultrapure	Mono elemental	Eu	10×10^3 $NaClO_4$= 0.01 mol/L	4.5, 7	20	0-24	10×10^2	90 %, 89.654 mg/g
(Li D. et al., 2015)	MGO (Magnetic Graphene Oxide)	Ultrapure	Mono elemental	Eu	10×10^3 $NaClO_4$= 0.01 mol/L	4.5, 7	20	0-24	10×10^2	80 %, 70.15 mg/g
(Sun et al., 2012)	GONS (Graphene Oxide Nanosheets)	Ultrapure	Mono elemental	Eu [(1)]	51×10^3 $NaClO_4$= 0.01 mol/L	7	25	48	2×10^2	100 %
(Farzin et al., 2017)	TGA/CdTeQDs/Fe_3O_4/rGONS	Distilled	Mono elemental	Ce	0.05×10^3 $(1\text{-}100)\times10^3$	5.0	35	0.17	7×10^2	95 % 56.82 mg/g
(Yao et al., 2016)	GO GO-OSO_3H	Ultrapure	Mono elemental	Eu	10×10^3 NaCl= 0.1, 0.01, 0.001 mol/L	5.5	20	0-24	5×10^2	100%, 142.8 mg/g 90%, 125.0 mg/g

Ref.	Sorbent	Type of water	Type of system	REEs (III)	$[REEs]_0$ (µg/L)	pH	T (ºC)	Time of contact (h)	m (sorbent)/ V(solution) (mg/L)	q_m (mg/g) or REEs adsorption (%)
(Chen et al., 2014a)	GO colloid	Ultrapure	Mono elemental	Gd	12×10^3	5.9 (2-11)	30	0.5	0.4×10^2	286.86 mg/g
(Chen et al., 2014b)	GO colloid	Ultrapure	Mono elemental	Y	12×10^3	5.9	30, 40	0.42	0.4×10^2	190.48 mg/g
(Xie et al., 2016)	GO	Ultrapure	Mono elemental	Eu	0.01×10^3 NaCl= 0.01M	5.0,	r.t.	48	1×10^2	78 mg/g
(Kilian et al., 2017)	GO	Ultrapure	Mono elemental	Sc	300×10^3	2	r.t.	4	50×10^2	~ 95%, 36.5 mg/g
(Fakhri et al., 2017)	30%Mo_4W_8@EDMG, 30%Mo_2W_{10}@EDMG	Ultrapure	Mono elemental	Ce	10×10^3	6 (2-6)	20	0.08-3	17×10^2	90.90 mg/g, 96.15 mg/g
(Su et al., 2014)	MPANI-GO	Ultrapure	Multi elemental	All REEs	0.01×10^3	4	r.t.	0.33	4×10^2	~ 95%
(Sun et al., 2013)	PANI@GO	$HClO_4$ (aq) 0.01 mol/L	Mono elemental	Eu	15×10^3	3	25	48	2.5×10^2	250.74 mg/g
(Li C. et al., 2014)	GTiP-1 (titanium phosphate modified GO composite) GTiP-2 GO	Ultrapure	Mono elemental	Eu	100×10^3	7.3	25	2	10×10^2	~ 72 % ~ 80 % ~ 28 %

(1) Adsorptions experiments were conducted under N_2 conditions.

Recovery of rare earth elements using carbon nanotubes

In the table II-B, studies of the recovery of REEs using carbon nanotubes composites are presented. It is possible to observe that all the studies were performed in Milli-Q or distilled water, with the exception of only one study performed by Yadav et al. (2015) that used HCl (aq, 0.5 mol/L). Regarding the contact time between the nanocomposite and the rare earth solution there was a widely range of times used, nevertheless, there are no studies published over 96 hours and the majority of the studies performed had a duration time of 2 and 4 hours (Behdani et al., 2013; Kilian et al., 2017; Koochaki-Mohammadpour et al., 2014; K. Li et al., 2015; Yadav et al., 2015). In the case of the temperature, there was also a widely range used such as 20, 25, 30, 43 and 65 ºC, but most of reported studies were performed at 30 ºC (Behdani et al., 2013; Koochaki-Mohammadpour et al., 2014; Yadav et al., 2015).

For a set of materials based on carbon nanotubes, in most studies the oxidized multi-walled carbon nanotubes (MWCNTs-oxidized) were chosen since they are a more efficient and cheaper material when compared to the single-walled carbon nanotubes (SWCNTs-oxidized). In addition to the CNTs, some studies show some sorption experiments using CNTs with several functionalizations to improve even more the efficiency of the material or to introduce others properties in the material, such as: magnetite (Fe_3O_4) (Chen et al., 2009) with the purpose of afford magnetic properties to the material, or chitosan (K. Li et al., 2015) to increase the maximum adsorption capacity of the material. It is possible to find, in the literature, ratios mass of sorbent per volume of solution between the minimum of 600 mg/L and the maximum of 100 000 mg/L for the REEs recovery, however, the m/v ratio most reported in the literature was 600, 1 000 and 5 000 mg/L. The studies of Fan et al. (2009), Chen et al. (2009) and Chen et al. (2008) were the ones that reported the lowest value of sorbent mass/volume (600 mg/L), which was used in the recovery of Eu(III) in mono-elemental solutions and at a pH between 5 and 6. Finally, the material with the highest maximum adsorption capacity (qm) of REEs reported in the literature to the date was mIIP-CS/CNT composite with 121.51 mg/g achieved (K. Li et al., 2015).

In REEs sorption studies using CNTs composites, it is easily perceptible that there are a higher number of studies using multi-elemental systems when compared with the number of the REEs sorption studies using GO composites, since half of the studies in this section were performed in multi-elemental systems. The REEs studied in mono-elemental systems were scandium and europium; in multi-elemental systems cerium, samarium,

lanthanum, dysprosium, terbium, lutetium and gadolinium ions were the only ones studied; and yttrium was studied in both types of system. The two elements most studied were La(III) and Eu(III). It should also be noted that the adsorption studies in multi-elemental systems were performed with a maximum of 3 elements by Tong et al. (2011) and Yadav et al. (2015). As for the rare earth concentration, a wide variety of intervals are published, as shown in table II-B. Most of the studies to the date have used concentrations between the minimum of 30 µg/L (Chen et al., 2008) and the maximum of 1 000 000 µg/L (Yadav et al., 2015), being that most of them used concentrations varies between 10 000 and 40 000 µg/L. The studies that used lower concentration values, namely 30 and 61 µg/L of Eu(III), in mono-elemental solutions, were the studies of Chen et al. (2008) and Chen et al. (2009), respectively; moreover, K. Li et al. (2015), Koochaki-Mohammadpour (2014) and Behdani et al. (2013) used 10 000 µg/L for different REEs like La(III) and Dy(III) or Ce(III) and Sm(III), in multi-elemental solutions.

Concerning the pH, the maximum adsorption values of REEs using CNTs composites are highly dependent on the chosen working pH, as previously mentioned. In other words, for different pH values, the acidity of the surrounding electrolyte will be different, which affects the surface charge and, consequently, the sorption of metal ions on CNTs. Generally, by increasing the pH, the sorption of metal ions increases; this occurs because, at pH superior to pH_{PZC} (point of zero charge), the positively-charged metal ions can be adsorbed on the negatively-charged oxidized CNTs (Pyrzynska et al., 2016). In this way, several authors have done the study of pH, varying mostly between 5-7, in order to find out the optimal pH and/or the working pH. The most used working pH is 5 (Behdani et al., 2013; Chen et al., 2009; Fan et al., 2009; Koochaki-Mohammadpour et al., 2014; Tong et al., 2011); also, the lowest pH used was 1.5 (Kilian et al., 2017; Tong et al., 2011) whereas the highest working pH chosen was 8 (Behdani et al., 2013; Fan et al., 2009). Nevertheless, at least two studies have been reported in the literature that have achieved adsorption rates of approximately 100% using a pH of 5 (Behdani et al., 2013) and 5.5 (Chen et al., 2009), and it is possible to find studies with values around 90% of adsorption.

Table II B - Recovery of REEs using Carbon nanotubes (CNTs) and the respectively experimental conditions used as reported in the literature. Note that in this table it is only presented the best results and consequently the optimal experimental conditions (see complete table in the attachments present in chapter 6, table A2).

Ref.	Sorbent	Type of water	Type of system	REEs (III)	$[REEs]_0$ (µg/L)	pH	T (ºC)	Time of contact (h)	m (sorbent)/ V (solution) (mg/L)	qm (mg/g) or REEs adsorption (%)
(Kilian et al., 2017)	CNTs-COOH	Ultrapure	Mono elemental	Sc	300 x 10^3	2 4	r.t.	4	50 x 10^2	37.9 mg/g 42.5 mg/g
(Behdani et al., 2013)	MWCNTs-oxidized	Distilled	Multi elemental	Ce Sm	10 x 10^3	5	30	2	10 x 10^2	~ 97 % ~ 100 %
(Koochaki-Mohammadpour et al., 2014)	MWCNTs-oxidized	Distilled	Multi elemental	La Dy	10 x 10^3	5	30	2	10 x 10^2	93 % 98%
(Tong et al., 2011)	TA-MWCNTs	Distilled	Multi elemental	La Tb Lu	40 x 10^3	5	20	1	50 x 10^2	5.35 mg/g, 8.55 mg/g, 3.97 mg/g
(Chen et al., 2008)	MWCNTs-oxidized	Distilled	Mono elemental	Eu	0.03 x 10^3 $NaClO_4$= 0.001, 0.01, 0.1 mol/L	6	25	48	6 x 10^2	98 % for all the ionic strengths
(Li K. et al., 2015)	mIIP-CS/CNT composite	Distilled	Multi elemental	Gd [b]	10 x 10^3	7	43	4	20 x 10^2 [c]	121.51 mg/g

Ref.	Sorbent	Type of water	Type of system	REEs (III)	$[REEs]_0$ (µg/L)	pH	T (ºC)	Time of contact (h)	m (sorbent)/ V (solution) (mg/L)	qm (mg/g) or REEs adsorption (%)
(Tong et al., 2011)	TA-MWCNTs	Distilled	Mono elemental	La	40×10^3	5	20	1	50×10^2 (with 0.12×10^2 being TA)	75 %
(Tong et al., 2011)	TA-MWCNTs	Distilled	Multi elemental	(La, Tb, Lu)	40×10^3	1.5-4	20	1	50×10^2	0.4-6.0 mg/g
(Fan et al., 2009)	MWCNTs-oxidized	Ultrapure	Mono elemental	Eu	0.99×10^3	5 (2-8)	25	96	6×10^2	90 %
(Chen et al., 2009)	MWCNTs/Fe_3O_4 composite	Ultrapure	Mono elemental	Eu [a]	0.061×10^3 $NaClO_4$= 0.1 mol/L	5.5	25	48	6×10^2	~ 100 %
(Yadav et al., 2015)	PES/PVA/MWCNT/ D2EHPA beads	HCl (aq, 0.5 mol/L)	Mono elemental	Y	1000×10^3	–	30	8	1000×10^2	95 %
(Yadav et al., 2015)	PES/PVA/MWCNT/ D2EHPA beads	HCl (aq, 0.5 mol/L)	Mono elemental	Y	(80-3300) $\times 10^3$	–	30-65	0-8	1000×10^2	44.09 mg/g
(Yadav et al., 2015)	PES/PVA/MWCNT/ D2EHPA beads	HCl (aq, 0.5 mol/L)	Multi elemental	Y Sm La	100×10^3	–	30	4	1000×10^2	94 % 82% 30%

[a] Adsorptions experiments under N_2 conditions.
[b] Gd^{3+} adsorption experiments with two competitive ions (La^{3+} and/or Ce^{3+}).
[c] 10 mg of IIP-CS/CNT (or NIP-CS/CNT) and 30 mg of SiO_2@Fe_3O_4 were added into a vial, which contained 20 mL of REEs.

Recovery of rare earth elements using other carbon materials

Table II-C has the studies of the REEs recovery using the other types of carbon materials which do not belong to the graphene or carbon nanotubes families (activated carbon, fullerenes, carbon dots, mesoporous carbon, carbon nanofibers and carbon black). This review is focused in batch experimental studies whereby there are a few studies in the literature that are not been explored in this review because they are column experiments (Agrawal, 2007; Chen et al., 2007a, 2007b; Pyrzynska et al., 2016). However, it was possible to verify that carbon nanotubes and carbon nanofibers are the most used materials for column experimental studies.

It is possible to observe that all the studies were performed in Milli-Q, with the exception of two studies performed by Gad and Awwad (2007) that used laboratory wastewaters beyond Milli-Q water and Marwani et al. (2017) that used distilled water, tap water, lake water and seawater. Regarding the contact time between the nanocomposite and the rare earth solution there was a widely range of times used, nevertheless, there are no studies published over 48 hours (Sun et al., 2012) and the majority of the studies performed had a duration time of 1 and 24 hours (Gad and Awwad, 2007; Marwani et al., 2017; Smith et al., 2016). In the case of the temperature, there was also a widely range used such as 20, 25, 40, 60 and 80 ºC, but most of reported studies were performed at room temperature, 25 ºC.

The most used material was activated carbon. In addition to these carbon materials, several studies used different types of functionalizations to improve the efficiency and to increase the maximum adsorption capacity of the material. It is possible to find, in the literature, ratios mass of sorbent per volume of solution between the minimum of 3 and 25 mg/L and the maximum of 5 000 mg/L for the REEs recovery, however, the m/v ratio most reported in the literature was 1 000 mg/L. The study of Smith et al. (2016) reported the lowest values of sorbent mass/volume (3 and 25 mg/L), which was used in the recovery of La(III), Ce(III), Nd(III), Sm(III) and Y(III) in multielementar solutions and at natural pH. Finally, the material with the highest maximum adsorption capacity (qm) of REEs reported in the literature to the date was oxygen and phosphorus functionalized nanoporous carbon with 335.5 mg/g and 344.6 mg/g achieved of Nd and Dy, respectively, at pH 6.1 and 6.6 in multielementar solution (Saha et al., 2017). However, the best removal achieved was 99.60% of La by BETADHBA functionalized activated carbon at pH 6 (Saha et al., 2017).

In REEs sorption studies using the carbon composites of these section, it is easily perceptible that there are a higher number of studies using multielementar systems when compared with the number of the REEs sorption studies using GO composites, since there are at least two times more studies in this section that were performed in multi-elemental solutions when compared with the studies performed in monoelementar solutions. The elements most studied were La(III), Nd(III) and Eu(III). As for the rare earth concentration, a wide variety of intervals are published, as shown in table II-C. Most of the studies to the date have used concentrations between the minimum of 0.3 µg/L (Perreault et al., 2017) and the maximum of 300 000 µg/L (Kilian et al., 2017), however, most of the concentrations used were 50 000 and 100 000 µg/L. The studies that used lower concentration values, namely 70 µg/L of Sm(III), in monoelementar solutions, was the study of Perreault et al. (2017), which also used 0.3 µg/L for different REEs like La(III). Concerning the pH, the rates of rare earth adsorption are once again strongly pH dependent, so the maximum adsorption values of REEs using these types of composites are highly dependent on the chosen working pH. The most used working pH were 5 and 6; also, the lowest pH used was 2 (Gad and Awwad, 2007; Kilian et al., 2017; Perreault et al., 2017) whereas the highest working pH chosen was 7 (Saha et al., 2017; Smith et al., 2016). A clear example that evidences this pH dependence on REEs adsorption is the study of Gad and Awwad (2007) which got an increase of adsorption capacity from 20 mg/g at pH 2 for 32 mg/g at pH 5, 47 mg/g at pH 6 and 50 mg/g of Eu at pH 7. Furthermore, the study of Marwani et al. (2017) demonstrate an increase of sorption rate from 40% of La(III) at pH 4 to 85% at pH 5 and 99.60% at pH 6. This study reported the best sorption rate in the literature. Finally, the material with the highest maximum adsorption capacity (qm) of REEs reported in the literature to date was oxide and phosphorous functionalized nanoporous carbon with 344.6 mg/g of Dy achieved (Saha et al., 2017); and, the best maximum adsorption capacity by an activated carbon was BETADHBA functionalized activated carbon (AC-BETADHBA) with 144.80 mg/g for La(III) (Marwani et al., 2017).

Table II C - Recovery of REEs using other carbon materials (Activated Carbon, Fullerene, C-Dots, Carbon Black, Mesoporous Carbon, Carbon nanofibers) and the respectively experimental conditions used as reported in the literature. Note that in this table it is only presented the best results and consequently the optimal experimental conditions (see complete table in attachments present in chapter 6, table A3).

Ref.	Sorbent	Type of water	Type of system	REEs (III)	$[REEs]_0$ (µg/L)	pH	T (ºC)	Time of contact (h)	m (sorbent)/ V(solution) (mg/L)	qm (mg/g) or REEs adsorption (%)
(Sun et al., 2012)	AC (Activated Carbon)	Ultrapure	Mono elemental	Eu	10×10^3 $NaClO_4$= 0.01 mol/L	4.5	25	48	2×10^2	20 mg/g
(Saha et al., 2017)	Phosphorous functionalized nanoporous carbon	Ultrapure	Multi elemental	Nd Dy	0.5×10^3	6.1 6.6	25	4	10×10^2	Nd= 335.5 mg/g Dy= 344.6 mg/g
(Smith et al., 2016)	F-CCB (Functionalized commercial carbon black)	Ultrapure	Multi elemental	La, Ce, Nd, Sm, Y	100×10^3	Natural pH	25	24	0.25×10^2	La = 15 %, Ce = 41 % Nd = 22.5 %, Sm = 14 % Y = 17 %
	RTCB (Recycled tire carbon black)				100×10^3		80	24	0.5×10^2	La= 69%, Ce = 90% Nd = 75%, Sm = 75% Y = 75%
	RTCB (Recycled tire carbon black)				20×10^3		25	12	0.5×10^2	La = 60%, Ce = %, 95% Nd = 83%, Sm = 88% Y = 77%
	RTCB (Recycled tire carbon black)				20×10^3		80	12	0.5×10^2	La = 75%, Ce = 95% Nd = 91%, Sm = 95% Y = 90%
	RTCB (Recycled tire carbon black)				100×10^3		60	24	0.5×10^2	La= 51.5%, Ce = 90% Nd = 70%, Sm = 72% Y = 70%

Ref.	Sorbent	Type of water	Type of system	REEs (III)	$[REEs]_0$ (µg/L)	pH	T (ºC)	Time of contact(h)	m (sorbent)/ Vsolution (mg/L)	qm (mg/g) or REEs adsorption (%)
(Gad and Awwad, 2007)	H-APC AC (HPO_4-APC activated carbon)	Ultrapure	Mono elemental	Eu	50×10^3	5	20	2	5×10^2 17.5×10^2	60 % 93 %
	H-APC AC	Ultrapure	Mono elemental	Eu	50×10^3	7	20	2	10×10^2	50 mg/g
	H-APC AC	Ultrapure	Mono elemental	Eu	50×10^3	5	20	2	10×10^2	29 mg/g
	H-APC AC	Laboratory wastewaters	Mono elemental	Eu	-	5	20	0.7	25×10^2	99.10 %
(Marwani et al., 2017)	AC-DETADHBA	Distilled	Multi elemental	La	5×10^3	6	25	1	25 mg*	99. 60%, 144.80 mg/g
	AC-COOH	Distilled	Multi elemental	La	5×10^3	6	25	1	25 mg*	89.50 mg/g
	AC-DETADHBA	Tap water	Mono elemental	La	10×10^3	6	25	1	25 mg*	100 %
	AC-DETADHBA	Lake water	Mono elemental	La	5×10^3 10×10^3	6	25	1	25 mg*	100 % 100 %
	AC-DETADHBA	Seawater	Mono elemental	La	10×10^3	6	25	1	25 mg*	99.65 %
(Perreault et al., 2017)	CMK-8-O (CMK-8-Oxidezed)	Ultrapure	Multi elemental	Sm	0.07×10^3	2.6	r.t.	0.5	10×10^2	14 mg/g
	CMK-8-DGO (DGO: diglycolyl-type organic)	Ultrapure	Multi elemental	La	0.0003×10^3	2.6 3.8 5.7	r.t.	4	10×10^2	23 mg/g 27 mg/g 22 mg/g

*There are not any mention of the volume of REEs solution used.

1.8. Hypothesis of work and objectives

The main goals of this master thesis are to draw attention to the growing problem of e-waste and to change the misconception currently associated with e-waste: a nightmare for business and governments, which need to manage and treat it. In the near future, e-waste will no longer be an expense for companies and governments and will become a source of profit; but, for this, we must invest in the research of technologies and methods for recovery of TCEs.

The objectives are:

- Synthesize, functionalize and characterize carbon-based nanocomposites;
- Evaluate the efficiency of the different carbon-based materials in the recovery of REE;
- Evaluate the influence of the experimental conditions (mass of sorbent, ionic strength, time of contact) in order to visualize which are the key parameters for rare earth recovery.
- Identify a material able to recovery efficiently rare earth elements from contaminated wastewaters

Chapter 2

Materials and methods

2.1. Reagents and solutions

Chemicals were readily available from commercial sources and were used as received without further purification: Ammonium hydroxide solution (NH_3 in H_2O, 25%, Riedel-de-Häen), Ethanol (C_2H_5OH, >99%, Panreac), Humic acid sodium salt (technical grad, Sigma-Aldrich), Iron(II) sulfate heptahydrate ($FeSO_4.7H_2O$, >99%, Merk), Graphene Oxide (0.4% wt, Graphenea, Spain), Polyethylenimine (PEI, Fluka, analytical standard 50%, w/v in water, CAS Number: 9002-98-6), Chitosan (Aldrich, CAS Number 9012-76-4), Graphite powder (EDM, 99.95% of % C, Graphit Kropfühl GmbH), Nitric acid (HNO_3, puriss. p.a., 65%, Merck), Potassium hydroxide (KOH, >98%, Pronolab), Potassium nitrate (KNO_3, >99%, Merk), Sodium hydroxide (NaOH, >98%, Pronolab), N,N-Dimethylformamide (DMF, 99.50%, Carlo Erba).

Rare earth(III) multi-element solutions were prepared by adding required volume of a certified reference solutions (1000 µg/L; Alfa Aesar Specpure®, plasma standard solutions in 5% HNO_3 for La, Eu; Gd, Tb, Dy and Y; Inorganic Ventures™, certified reference materials for ICP in 3.5% HNO_3 for Nd and Ce) to different matrixes: ultrapure Milli-Q water (produced by a Millipore system), mineral water (Serra da Estrela mineral water) and filtered real saline water (salinity 15).

2.2. Chemical synthesis of the nanomaterials

2.2.1. Synthesis of magnetic exfoliated graphite functionalized with humic acids

The synthesis of magnetic exfoliated graphite functionalized with humic acids (MEG-HA) was based on previous reports (Oliveira-Silva et al., 2014; Paul et al., 2015). Firstly, the exfoliated graphite was made and then the growth of magnetite (Fe_3O_4) nanoparticles and humic acids functionalization on the exfoliated graphite were carried out through the co-precipitation method.

The exfoliation of graphite was done by ultrasonic treatment (Sonics Vibra Cell Sonicator, VC70, 130 W, 20 kHz) in N,N-dimethylformamide (DMF). Briefly, 5.0 g of graphite powder was sonicated in 100 mL of DMF for 5 hours using a 250 mL glass beaker and kept under ice bath (0-5 ºC). Then, the mixture was centrifugated at 5000 rpm for 20 min, for purification (to separate the exfoliate graphite from the non-exfoliated graphite).

After centrifugation, exfoliated graphite (EG) was filtrated under vacuum and dried at room temperature. The desired product (EG) was obtained as a black powder.

Magnetic iron oxide NPs with an average size of 50 nm were synthesized by oxidative hydrolysis of iron(II) sulphate in alkaline conditions followed by the coating of the material (MEG) with humic acid, as follows. Ultrapure water was first deoxygenated with N_2 under vigorous stirring for 2 hours. Then, 1.90 g (34 mmol) of KOH and 1.52 g (15 mmol) of KNO_3 were added to 25 mL of deoxygenated water using a 250 mL round flask. This mixture was heated at 60ºC, under N_2, and mechanically stirred at 500 rpm. After total dissolution, 25 mL of an aqueous solution of $FeSO_4.7H_2O$ (4.75 g, 17 mmol) and EG (200 mg) previously mixed and dispersed was added drop-by-drop to the mixture and mechanical stirring was increased to 700 rpm. Immediately thereafter, 25 mL of and aqueous solution of humic acids (200 mg) was added to the mixture. The solution reacted for 30 minutes. After reaction, the round flask was transferred to a hot oil bath at 90 ºC under N_2, but without stirring, for 4 hours. Finally, the resulting black powder was washed several times with deoxygenated water and ethanol. After washing, particles were dried by evaporating the solvent in an oven at 40ºC.

2.2.2. Synthesis of graphene oxide functionalized with poly(ethyleneimine)

The synthesis of graphene oxide functionalized with poly(ethyleneimine) (GO-PEI) was based on previous reports (Cai et al., 2012; Girão et al., 2016). Briefly, a poly(ethyleneimine) (PEI) solution was prepared in distilled water and acetic acid aqueous solution (1% v/v) with a concentration of 5 mg/mL. Then, graphene oxide water dispersion was directly mixed with the PEI solution with a ratio of 24 % w/w (GO/PEI) and before shaking, the pH of the reaction was adjusted to 2. After that, the solution was then rapidly shaken for 10 seconds to form a hydrogel. After synthesis, the hydrogel was freeze-dried by lyophilization (Telstar lyoQuest HT-40, Beijer Electronics Products AB, Malmoe, Sweden) at -80 ºC obtaining three dimensional (3D) porous structures. The lyophilized sample was then washed in ultrapure water for 12 hours to remove acidic residues. Finally, the samples were freeze-dried again.

2.2.3. Synthesis of graphene oxide functionalized with chitosan

The synthesis of graphene oxide functionalized with chitosan (GO-CH) was based on previous reports (Girão et al., 2016). The experiment above was repeated but, in this synthesis, GO was directly mixed with chitosan to prepare GO-CH.

2.3. Characterization of the materials

In order to confirm the identity of the materials involved in this work and to determine some of its characteristics, a large number of characterization techniques were used.

2.3.1. General characterization methods

Fourier Transform Infrared (FT-IR) spectra (in the range 4000-350 1/cm) were recorded as KBr pellets (typically 2 mg of the sample were mixed in a mortar with *ca.* 200 mg of KBr) using a Bruker Tensor 27 spectrometer by averaging 256 scans at a maximum resolution of 4 1/cm. FT-IR spectra (in the range 4000-350 1/cm) were also recorded by directly placing of the samples on the diamond crystal unit of Reflectance Total Attenuated (ATR), using a Bruker Tensor 27 spectrophotometer after 256 scans with resolution of 4 1/cm.

Routine Power X-Ray Diffraction (PXRD) data for all materials were collected at ambient temperature on a Empyrean PANalytical diffractometer (Cu $K_{\alpha 1,2}$ X-radiation, λ_1 = 1.540598 Å; λ_2 = 1.544426 Å), equipped with an PIXcel 1D detector and a flat-plate sample holder in a Bragg-Brentano para-focusing optics configuration (45 kV, 40 mA). Intensity data were collected by the step-counting method (step 0.04º), in continuous mode, in the *ca.* $3.5 \leqslant 2\theta \leqslant 50^{\circ}$ range.

Raman spectra were obtained using a combined Raman-AFM-SNOM confocal microscope (alpha 300 RAS+, WITec, Germany). Nd:YAG laser operating at 532 nm was used as excitation source. The power of the laser was varied from 0.1 to 1 mW, in order not to damage/heat the sample.

For STEM (Scanning Transmission Electron Microscopy) analysis, samples were prepared by evaporating dilute suspensions of the nanocomposite on a copper grid coated with an amorphous carbon film. Experiments were performed on a HR-FESEM SU-70 Hitachi instrument operating at 25 kV.

Brunauer-Emmet-Teller (BET) surface area analyses were performed on an automated surface area analyser (Micromeritics Gemini 2380) by means of nitrogen adsorption-desorption.

Magnetic properties of the nanomaterial were studied by performing measurements of hysteretic cycle using the VSM magnetometer at room temperature (~ 293K). The magnetization was normalized to the total mass of the sample.

Isoelectric point of nanomaterial was determined by zeta potential measurements, using a Zetasizer Nano ZS (Malvern Instruments). A solution of nanomaterial was prepared in ultrapure water. The pH of the solution was adjusted for different pH (between 2 and 10) using NaOH or HNO_3 solutions. Furthermore, the temperature was fixed at 25ºC and three replicate measurements of zeta potential were performed for each sample.

Termogravimetric analyses (TGA) were carried out using a Shimadzu TGA 50, from ambient temperature to ca. 800 ºC, with a heating rate of 5 ºC/min, under a continuous stream of air at flow rate of 20 mL/min.

The concentration of all elements (rare earth elements(III) – Y, La, Ce, Nd, Eu, Gd, Tb, Dy and other interpretative elements such as iron, manganese, calcium, cupper, potassium, magnesium and sodium) were performed by Inductively Coupled Plasma-Optical Emission Spectometry (ICP-OES), on a Horiba Jobin Yvon Activa M spectrometer with a Burgener MiraMist nebulizer (1.0 mL/min), peristaltic sample delivery pump, argon flow plasma of 12 L/min, sheath gas of 0.8 L/min and algorithm background correction. The elements content in the materials were also determined by ICP-OES. Briefly, about 20 mg of sample were accurately weighted into an acid-washed Teflon reactor; then 3 mL of HNO_3 (70%) were added, and reactors were placed on a CEM - MDS-81D microwave digestion system (equipped with 13 pressurized vessels) at 60 °C for 30 min, and then at 100 °C for 15 min (Monterroso et al., 2003). After digestion, samples were diluted with ultrapure water and then analyzed by ICP-OES.

2.4. Sorption experiments to evaluate the removal/recovery of rare earth elements

The efficiency of the synthesized materials to remove REE(III) from aqueous solutions (ultrapure, mineral and saline waters) was evaluated by performing batch (discontinuous) experiments. In these experiments, the effect of mass of sorbent used and

the effect of increasing the ionic strength of the solution in the recovery of rare earth elements were evaluated.

2.4.1. Washing of the material used

All the glass material used in the sorption tests was properly washed before and after use to avoid possible contaminations and to minimize the impact of solute losses which can be very significant in case of low rare earths concentrations. In a first step all the material was washed with tap and distilled water. Then, it was placed in HNO_3 25% (v/v) for 24 hours. After that, the material was washed again several times with distilled water. Finally, all material was dried at room temperature and protected from the air. The SCHOOT bottles used for the sorption tests were also washed with the matrix further used in the experiments.

2.4.2. Experimental conditions

In order to study the behaviour of the different materials firstly synthesized in this work (exfoliated graphite with different oxidation levels), a set of preliminary experiments were carried out. The sorbents tested were: i) Commercial Graphite (GC); ii) Magnetic Commercial Graphite (MGC); iii) Exfoliated Graphite of 5 hours (EG-5h); iv) Magnetic Exfoliated Graphite of 5 hours (MEG-5h); v) Exfoliated Graphite of 9 hours (EG-9h); vi) Magnetic Exfoliated Graphite of 9 hours (MEG-9h); vii) Magnetic Graphene Oxide (MGO) and viii) Magnetite (Fe_3O_4). However, these experiments were not continued due to the low efficiency of the materials towards the recovery of REEs under the defined conditions and no information's regarding these materials is shown in the thesis.

Since the results obtained from the previous experiments were not as desired (high recovery rates), three new materials were tested in order to try to obtain better sorption rates. The materials chosen were magnetic exfoliated graphite functionalized with humic acid (MEG-HA), graphene oxide functionalized with 25% of polyethylenimine (GO-PEI) and graphene oxide functionalized with chitosan (GO-CH). The experimental conditions used in each test are described below:

- **Elements in study – REE(III):** Yttrium (Y), Lanthanum (La), Cerium (Ce), Neodymium (Nd), Europium (Eu), Gadolinium (Gd), Terbium (Tb), Dysprosium (Dy).

- **Initial concentrations (µg/L)*:**

Y=58.50	La=91.41	Ce=92.20
Nd=94.92	Eu=100.00	Gd=103.48
Tb=104.58	Dy=106.93	

*Theses concentrations values correspond to an initial concentration of 100 µmol/L for the elements.

- **Mass per volume ratio:** 50 and 100 mg/L**.**
- **Type of water:** ultrapure water from Milli-Q water, mineral water from Serra da Estrela water and filtered real saline water (salinity 15).
- **Contact time:**
  - To test the effect of dose of sorbent: 0, 1 and 24 hours.
  - To perform the kinetic studies: 0, 0.25, 0.5, 1, 3, 6, 12, 24 and 48 hours.
- **Initial pH:** 5.5±0.1
- **Technique used for the separation of the solid from the water:** magnetic separation (in the case of MEG-HA) and filtration (to the GO-PEI).

Results from materials comparison and mass effect were expressed in terms of recovery efficiency ($Rec\ (\%)$), eq. 1):

$$\text{Rec}\ (\%) = \frac{(C_0 - C_t)}{C_0} \times 100 \qquad (1)$$

where C_0 and C_t (both µg/L) are the initial and at time *t* concentration of each element in solution.

Kinetics of REE removal process was studied by exposing 50 and 100 mg of nanomaterials to 1 L of multi-elemental solutions of La(III), Ce(III), Nd(III), Eu(III), Gd(III), Tb(III), Dy(III) and Y(III) (solutions pH adjusted to ca. 5.5), and by collecting 10 mL of water at pre-defined times (0, 0.25, 0.5, 1, 3, 6, 12, 24 and 48 hours). The kinetic results were expressed in terms of normalized concentration (C_t/C_0) and solid loadings (eq. 2) at time t, q_t (µg/g):

$$q_t = \frac{(C_0 - C_t)}{\text{m}} \times V \qquad (2)$$

where V and m are respectively the volume of solution (L) and the mass of composite (g).

Equilibrium of rare earth recovery process was studied by exposing different amounts (50 and 100 mg/L) of composite to multi-elements solutions of the REEs in study (solutions pH adjusted to 5.5±0.1) during 24 hours. Results were expressed as solid loading at equilibrium, using Eq. 2 where $q_t = q_e$ and $C_t = C_e$.

All experiments were performed in duplicate and with controls running in parallel with the experiments and under the same experimental conditions. Solution pH was monitored at the beginning and end of the essays.

2.4.3. Kinetic models

The kinetics of the rare earth recovery from the multi-elemental solution was investigated and the experimental results were interpreted by three of the most used kinetic models (Cardoso et al., 2013; Figueira et al., 2017; Lopes et al., 2014; Tavares et al., 2012): i) Lagergren or pseudo-first order equation (Lagergren, 1898), ii) pseudo-second order equation (Ho and McKay, 1999) and iii) Elovich model (Aharoni and Tompkins, 1970).

The pseudo 1st order model after the integration is expressed by the equations 3 (3.a and 3.b):

$$\frac{dq_t}{d_t} = k_1(q_e - q_t) \quad (3.a)$$

After integration of t = 0 ($q_t = 0$) to t = t ($q_t = q_e$), the equation obtained is expressed by:

$$q_t = q_e(1 - e^{-k_1 t}) \quad (3.b)$$

q_e and q_t (mg/g) are the sorbed phase concentration at equilibrium and at time *t*, respectively, and k_1 (1/h) is the rate constant of pseudo-first order adsorption.

The pseudo-second order model can predict the system behaviour over the whole range of sorption and, is also based on the sorption capacity of the solid (Aksu, 2005; Kumar, 2006). The kinetics rate law (Ho and McKay, 1999) is described by equations 4 (4.a and 4.b):

$$\frac{dq_t}{d_t} = k_2(q_e - q_t)^2 \quad (4.a)$$

where k_2 (g/mg/h) is the rate constant of pseudo-second order sorption. After the integration with the initial condition (t = 0, qt = 0), the obtained equation (4.b) is expressed by:

$$q_t = \frac{q_e^2 k_2 t}{1+q_e k_2 t} \quad (4.b)$$

The Elovich model is also a second order model, the equation 5 does not propose a defined mechanism for the sorbent-adsorbate process and it is described by:

$$q_t = \left(\frac{1}{\beta}\right) \ln(1 + \alpha\beta t) \quad (5)$$

where α and β are, respectively, the initial sorption rate, and the desorption constant.

All models previously described were tested to study the sorption of chosen REEs and on the MEG-HA and GO-PEI composites using the GraphPad Prism 7 program.

2.4.4. Quantification of rare earth elements by inductively coupled plasma - optical emission spectrometry

The inductively coupled plasma - optical emission spectrometry (ICP-OES) is a technique used for the quantitative determination of elements at concentration levels varying from the higher concentrations values to mg/L and even μg/L in several matrices such as soils, sediments, waters, food, and others. This technique of atomic emission consists of the excitation of atoms and ions that emit energy upon returning to the fundamental state at characteristic wavelengths for each element. The intensity of this emission is indicative of the concentration of the analyte in the sample (Murray et al., 2000).

ICP-OES consists in a radio frequency generator, a plasma inductor, a torch, a sample introduction system (including a nebulizer, nebulizer chamber and injector), a collimator (lenses and mirrors), a and a detector. The emission phenomenon occurs in the plasma and the gas used is Argon, which has a high energy of ionization (15.6 eV), allowing to atomize, ionize and excite most of the elements of the periodic table. The main components of an ICP-OES are shown in figure 10 (Boss et al., 1997).

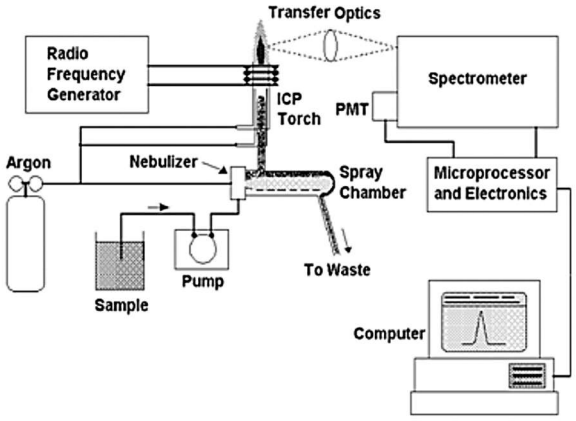

Figure 9 – Scheme of ICP-OES principal components (Boss et al., 1997).

Quality Control

Quality control is a requirement for the reliability of the results obtained in ICP-OES analysis. Thus, all the results presented in this work accomplished the following criteria.

First of all, a calibration curve – for further comparation of the analytical signal intensity of the sample – is obtained using at least 5 standards with concentrations between 4 and 100 µg/L. The standards are prepared from a multi-elemental solution; the error of each standard has to be less than 10% and the correlation coefficient has to be at least 0.9995.

The quantification limit considered in the sample analysis was 4 µg/L (the value of lower concentration standard) and the detection limit was 1.3 µg/L (one third of the quantification limit).

Additionally, to the calibration curve, it was also analysed a blank, a check standard and a replica – to verify the drift of the equipment. Finally, in each set of ten samples, a duplicate – to verify the repeatability of the quantification process – and a recovery test – to evaluate the matrix interference – are also required. The blank concentration was always inferior to 1.3 µg/L; check standard, replica and duplicate were only accepted until a maximum error of 10% and the range of accepting of recovery test varied between 85% and 115%. No certified reference material was used since there is no reference material for REEs available in the market.

Chapter 3

Results and Discussion

3.1. Structural characterization of the nanomaterials

After synthesizing the nanomaterials, it was made a set of solid state techniques to discover its structure and morphology, namely, Fourier Transform Infrared spectroscopy (FTIR), Raman spectroscopy, powder X-ray Diffraction (PXRD), Scanning Transmission Electron Microscopy (STEM), BET surface area, thermogravimetry and Zeta potential. Magnetic measurements were also performed for the magnetic nanocomposite.

3.1.1. X-ray diffraction

Single-crystal X-ray diffraction is a key technique to solve the structures of solids. However, it was not possible to obtain suitable single crystals, so it was used the powder X-ray diffraction (PXRD) technique.

Figure 11 shows the PXRD patterns of nanocomposite used (MEG-HA) and its precursors (graphite, exfoliated graphite, Fe_3O_4 NPs and humic acids). It was not possible to obtain the PXRD of GO-PEI and GO-CH composites since they are not crystalline materials.

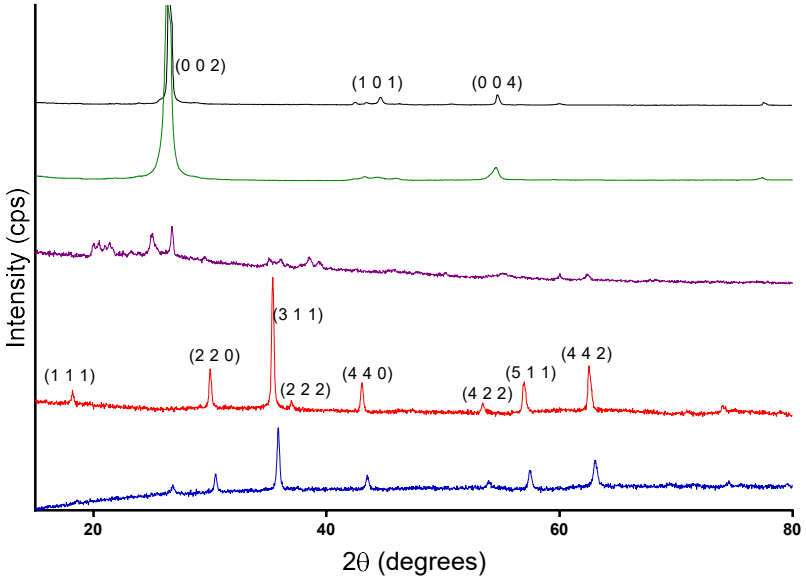

Figure 10 – Powder XRD patterns of Meg-HA (blue), Fe_3O_4 (red), humic acid (purple), EG (green) and GC (black).

Through the comparison of different PXRD patterns of the isolated compounds that compose MEG-HA (EG, Fe_3O_4 NPs and humic acids (HA)) it was possible to confirm their presence in the desired product (MEG-HA) and confirm that the synthesis was performed correctly (figure 11). The diffraction pattern of EG (figure 11 – green line) gives a narrow

peak (0 0 2) with very high intensity (2θ = 26.5º, corresponding to the interlayer distance d = 0.34 nm), characteristic of graphite (GC) (figure 11 – black line). Additionally, the broadened graphitic peak observed in EG suggests a decrease in the thickness of the samples in comparison to the precursor graphite (figure 11 – black line), confirming the exfoliation process (Song et al., 2013). In the diffractogram of Fe_3O_4 NPs (figure 11 – line red), the peaks at 2θ values of 18.19º,□30.00º, 35.39º,□36.99º,□43.06º,□53.43º,□56.98º□ and 62.54º can be assigned to (1 1 1), (2 2 0), (3 1 1), (2 2 2), (4 0 0), (4 2 2), (5 1 1) and (4 4 2) Bragg's reflections, respectively, and may be indexed on the face centred cubic structures of magnetite (Chomchoey et al., 2010; Girginova, 2009; Shen et al., 2012). The humic acid (HA) is an unknown structure, and therefore, the HA diffractogram could not be solved (figure 11 – purple line). However, the diffractogram of HA is quite important to confirm his presence in final product, MEG-HA (figure 11 – blue line). Through the diffractogram of the magnetic nanocomposite, MEG-HA (figure 11 – blue line), it is possible to confirm the presence of all the materials despite the overlap of most peaks.

3.1.2. Fourier-transform infrared spectroscopy

In order to know better the material synthesized it was made a fourier-transform in infrared spectroscopy (FT-IR) to see the links between the elements of the composites. FT-IR spectra of the composite (MEG-HA) (figure 12 – blue line) and the materials that compose it were analysed and the results are summarized in the table III. This analysis was based on a vibration frequencies table of chemical groups (Socrates, 2004) and in the information relating to the characterization of materials presented in Das et al. (2017) and in Paul et al. (2015).

Table III – Summary of some of the bands obtained in the FT-IR spectra of the MEG-HA composite (its possible correlation with the materials that compose it) and the possible correspondence with the vibrations chemical groups.

FT-IR of MEG-HA composite		
Vibrational mode	**Position (1/cm)**	**From / Present in**
ν(OH)	3664-3110	All
Functional groups* ν(C=C)	1627 and 1572	HA EG, GC and HA
δ(N-H) of NH_2	1627	HA

ν(C=O) of NHCO	1572	HA
Aromatic C-N bond	1379	HA
δ(C-C-C)	1111	HA e GC
ν(C-O)	1033	HA
ν(Fe-O)	587	Fe_3O_4

*functional groups such as aldehydes, ketones, esters, amide and carboxylic groups
δ – bending vibration, ν – stretching vibration.

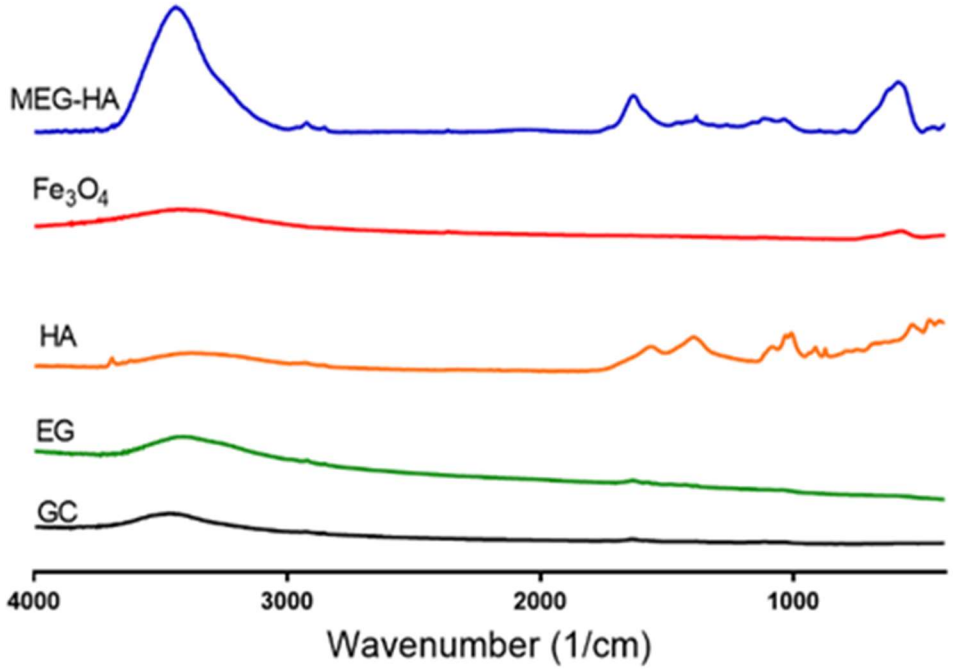

Figure 11 – FT-IR spectra of MEG-HA (in blue), Fe_3O_4 NPs (in red), HA (in orange), EG (in green) and graphite (GC, in black).

Despite the difficulty encountered in analysing the spectra and assigning the peaks to their precursors due to the overlap of the bands, it is possible to conclude, even by comparison of the spectra, that the synthesis was successful and all the precursors are present in the final product, MEG-HA.

Figure 13 illustrates the FT-IR spectra of GO-CH (in green) and GO-PEI (in black) and its analyses was summarized in table IV.

Table IV – Summary of some of the bands obtained in the FT-IR spectra of the GO-PEI and GO-CH composites and the possible correspondence with the vibrations chemical groups.

Vibrational mode	Position (1/cm)	Present in
broad ν(OH) overlapping ν(NH_2)	3525-3010	GO-CH
δ(N-H) of NH_2	1613	
δ(C-H)	1379	
ν(C-O-H)	1257	
ν(C=O) of NHCO	1052	
broad ν(OH) overlapping ν(NH2)	3710-3059	GO-PEI
$\nu_{asym}(CH_2)$	2967	
ν(-CH_2CH_2NH-)	2932	
$\nu_{sym}(CH_2)$	2861	
C-H_2 symmetry shrinkage	2359 and 2343	
Imide group ν(O=C-N-C=O)*	1716	
δ(NH_2) + ν(CH)	1386	
ν(C-O-C)	1110	
ν(C-N) and δ(C-N)	777	
ω(-NH)	617	

δ – bending vibration, ν – stretching vibration, ν_{asym} – asymmetric stretching vibration, ν_{sym} – symmetric stretching vibration, ω – wagging.

* Typical of imide carbonyl asymmetric and symmetric stretching vibration

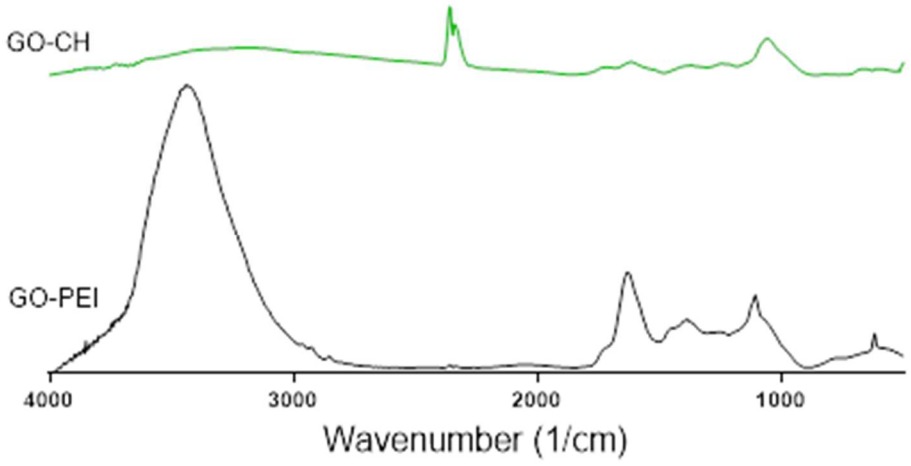

Figure 12 – FT-IR spectra of GO-CH (in green) and GO-PEI (in black).

Based on a vibration frequencies table of chemical groups (Socrates, 2004) and in the information relating to the characterization of materials presented in Itta and Tseng (2011), Kumirska et al. (2010), Yasmeen et al. (2016) and Zhang et al. (2016), it is possible to conclude that the nanocomposites were well synthesized.

3.1.3. Electron microscopy

Figure 14 illustrates the scanning electron microscopy images of GO-CH and GO-PEI composites. The samples were prepared by deposition in aluminium sample holder and with carbon coating.

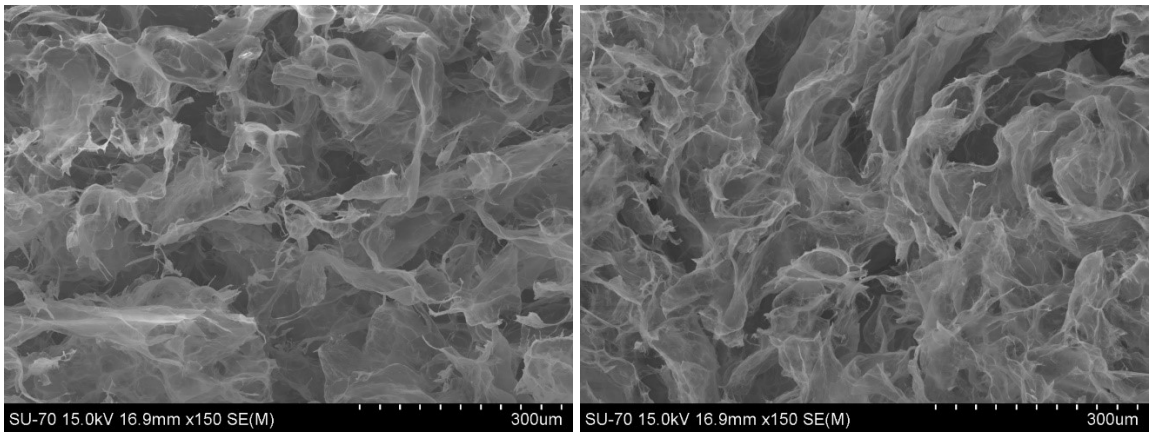

Figure 13 – SEM images of GO-CH (left) and GO-PEI (right).

The images show that the structures present similarities (due to the presence of graphene oxide nanosheets), namely a high degree of crosslinking, which results in a large surface area. It is also possible to observe that all structures are semi-transparent.
STEM images of MEG-HA were not acquired in this work, however, according BET surface area results, it seems that this material is smaller (in terms of size) than GO-PEI and GO-CH.

3.1.4. Raman spectroscopy

Figure 15 illustrates the Raman spectra of GC, EG, Fe_3O_4, MEG-HA and GO-PEI. Raman is a non-destructive technique sensitive to geometric structures and so can be used in the study of allotropes of carbon as they differ only in the nature of bonding and position of the carbon atoms.

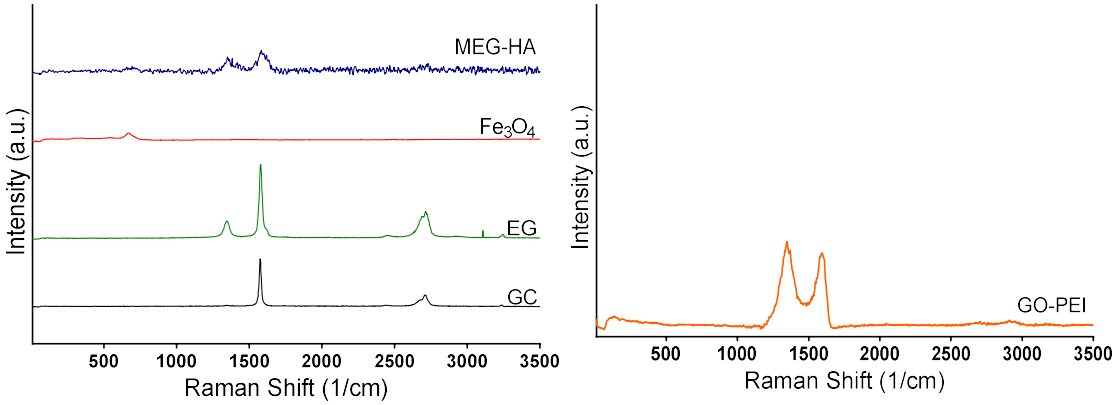

Figure 14– Raman spectra of MEG-HA (blue), Fe_3O_4 (red), EG (green) and GC (black) in the left image and GO-PEI (orange) in the right image.

The spectra of GC and EG exhibit simple structures characterized by two main bands (G- and 2D-bands, the Raman signature of graphitic sp^2 materials) in GC and a third band in the EG ascribed to the D mode that is induced by structural disorder (in this case defects and impurities in the carbon lattice, introduced during the ultrasonic treatment). The sharp and intense band that appears at around 1580 cm^{-1} in both GC and EG spectra, is the G band that corresponds to the first-order scattering of the E_{2g} mode of the sp^2 carbon atoms in a 2D hexagonal lattice (Zhang et al., 2013). Since this band arises from the stretching of the C-C bond in graphitic materials, is common to all sp^2 carbon systems. Another band that appears in the Raman spectra of all kinds of sp^2 carbon materials, usually between 2500 and 2800 cm^{-1}, is the 2D band, and results of a second-order two-phonon process. The D band (sp^3 carbon) at 1344 cm^{-1} in the EG spectrum and its inexistent in the GC spectrum, is related to the presence of structural defects that were introduced during the ultrasonic treatment. Moreover, the intensity of the G band is much higher than the one of D band for EG indicating a low number of defects in the sample. Indeed, the ratio of the D to G band (I_D/I_G) is a very useful tool to evaluate the change of defects in the carbon framework (Araújo et al., 2017).

The spectrum of MEG-HA keeps the signature of graphitic sp^2 materials (G and 2D bands), together with the D band associated with structural defects in the carbon lattice, and a peak at 670 cm^{-1} ascribed to magnetite nanoparticles (Fe_3O_4) (Chourpa et al., 2005). In comparison with the EG spectrum the I_D/I_G ratio is larger in the MEG-HA. As I_D/I_G ratio is proportional to the average size of the sp^2 carbon domain, an increase in the I_D/I_G value is attributed to the introduction of defects and to the conversion of sp^2 to sp^3 carbons.

The spectrum of GO-PEI shows clearly the D and G bands. The main feature of this spectrum is that the I_D/I_G ratio is higher than 1 (higher domain of sp^3 carbons) characteristic of graphene oxide, while in the MEG-HA the same ratio is lower than 1.

3.1.1. BET surface area

Table V shows BET surface area, pore volume and the pore diameter of the nanocomposites used in this work (GO-PEI, GO-CH and MEG-HA).

Table V – Values of BET surface area (m^2/g), pore volume (cm^3/g) and pore diameter of the different

Samples	GO-PEI	GO-CH	MEG-HA
BET surface area (m^2/g)	8.0	9.1	35.6
Pore volume (cm^3/g)	0.01	0.02	0.07
Pore diameter (nm)	9.3	6.2	9.5

Through the analysis of these results, it was verified that the MEG-HA has the largest BET surface area (35.6 m^2/g) from the three composites. These results indicate that the MEG-HA is smaller than the other two composites, since the surface area increases with the decreasing of the material size.

3.1.2. Magnetic properties

Figure 16 shows the results of magnetic measurements performed for the magnetic composite.

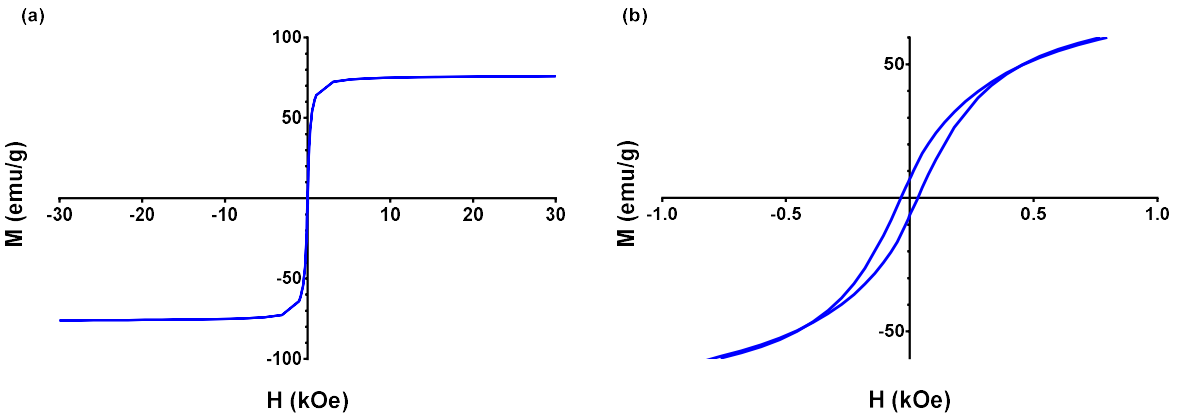

Figure 15 – Magnetization curve of the MEG-HA composite (in left (a)) and its magnification (in right (b)) as a function of the magnetic field for MEG-HA composite.

As it can be seen it the left image, the magnetization presents a fast approach to saturation in the presence of an external magnetic field (reaching saturation for about 1 kOe). The estimated saturation magnetization, at 300 K, is about 76 emu/g. The coercive field (H_c) for the MEG-HA composite is 36 Oe, at room temperature, which evidences ferrimagnetic behaviour characteristic of magnetite nanoparticles in this size range (Batlle and Labarta, 2002). The low value of H_c indicates that the material is easily demagnetized.

3.1.1. Zeta potential

Zeta potential is a physical parameter, which can be used to quantify the electrical potential of the solid particle surface at different pH level. This technique is usually used to determine the isoelectric point (or the point of zero charge) of the nanomaterials.

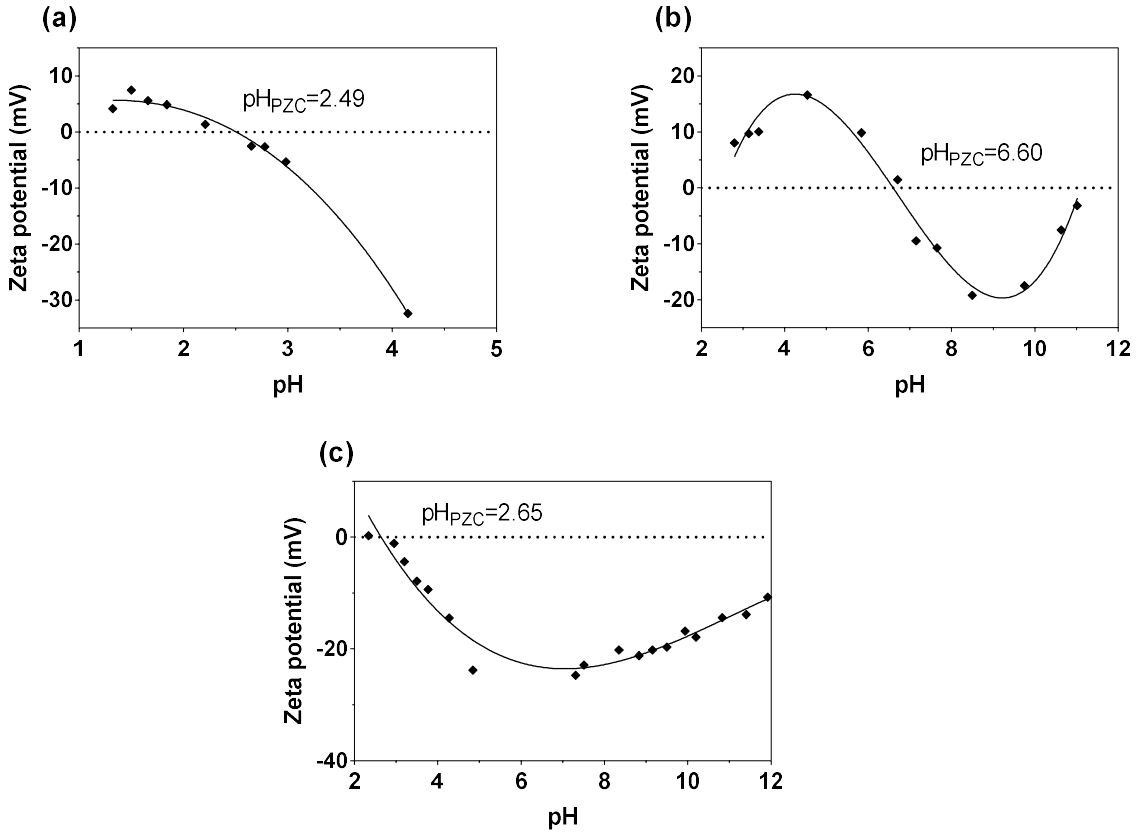

Figure 16 – Zeta potential of MEG-HA (a), GO-CH (b) and Go-PEI (c) composites.

Through the potential zeta analysis of MEG-HA (figure 17, a)), it was verified that the surface charge of MEG-HA is only positive at very low pH values since the isoelectric point is a pH = 2.49. From the $pH_{PZC,}$ the zeta potential remained negative under the pH studied.

In contrast, the zeta potential of GO-CH (figure 17, b)) remained positive over a broad pH range (2.8-6.5) and negative between 6.7 and 11.0 The isoelectric point determined was at pH = 6.60.

Lastly, the zeta potential of GO-PEI was also negative over the almost investigated pH range (figure 17, c)). The isoelectric point was achieved at pH=2.65).

3.1.2. Thermogravimetry

The thermal behaviour of MEG-HA composite (figure 18) and GO-PEI composite (figure 19) was investigated between ambient temperature and ca. 800 ºC from thermogravimetric analysis.

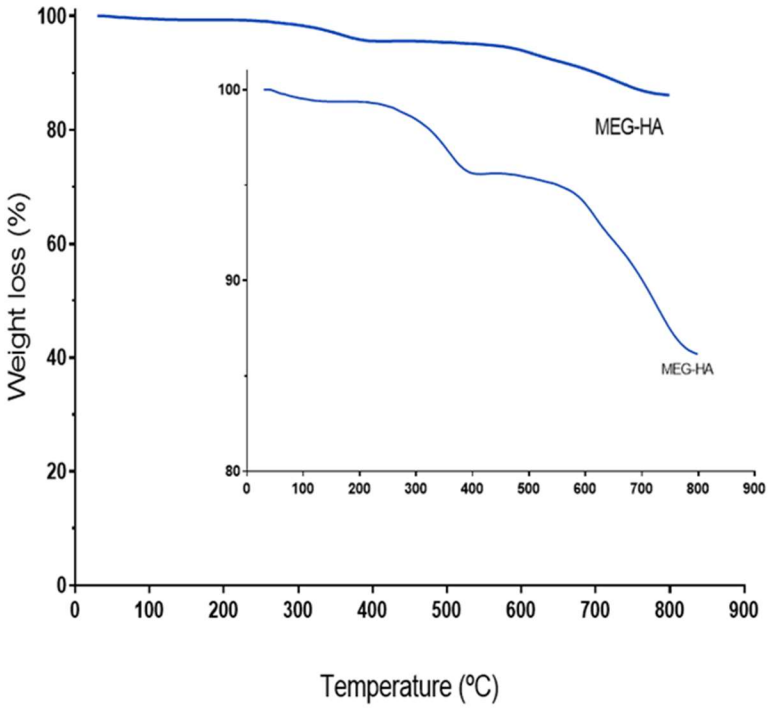

Figure 17 – Thermogram of the MEG-HA composite

From the thermogravimetric curve of MEG-HA it is possible to observe three weight losses: the first (of ca. 0.5%) occurs up to 100 ºC which indicates the presence of water, the

second (of ca. 4%) occurs (between ca. 265 ºC and 400 ºC) and the third weight loss (of ca. 9.5%) occurs between ca. 500 ºC and 790 ºC. These losses are related with the decomposition of the organic components. Note that this material shows an outstanding high thermal stability which can be a great advantage over other materials in applications that requires more severe conditions.

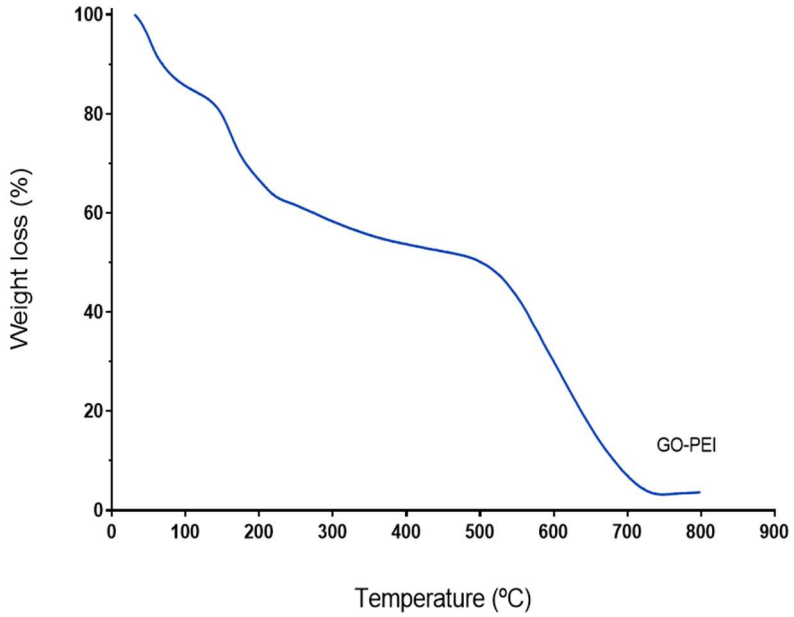

Figure 18 – Thermogram of the GO-PEI composite

From the thermogravimetric curve of GO-PEI it is possible to observe four weight losses: the first (of ca. 16%) occurs up to 100 ºC which indicates the presence of water. Then, between ca. 125 ºC and 380 ºC occurs the decomposition of the ethyleneimine polymer with a weight loss of ca. 28% which is in agreement with the data found in the literature (Zhang et al., 2016) and the last weight loss (of ca. 45%) occurs between ca. 500 ºC and 760 ºC which are related to the decomposition of the GO leading to the collapse and total degradation of the material. This thermogram indicates that the synthesis of GO-PEI was successful. Note that TGA of GO-CH were not acquire since this material was not studied with detail in this work.

3.2. Sorption experiments to evaluate the recovery of rare earth elements

After the synthesis and characterization of the nanomaterials (MEG-HA, GO-PEI and GO-CH), its efficiency was studied in the removal and recovery of rare earth elements

present in aqueous solutions. In this work, recovery studies using multi-element solutions of REEs (La, Ce, Nd, Eu, Gd, Tb, Dy and Y) were carried out. For this purpose, the following tests were performed: (i) evaluate the influence of the amount of sorbent mass, (ii) evaluate the effect of salinity and (iii) study the kinetic behaviour of the recovery process. The results presented were calculated through equation 1. All experiments were performed at an inicial pH *ca.* 5.5. This work pH was choose because the pH of common wastewater from REE mines and refineries is usually about 6 or less (Chen et al., 2014b). However, other REEs recovery applications from e-waste can work at lower pH values. In order to facilitate the discussion among the rare earths elements, such as, the different behaviours evidenced in the analysis of the results, the REEs were grouped in three categories: light REE (LREE: La, Ce and Nd), medium REE (MREE: Eu and Gd) and heavy REE (HREE: Tb, Dy and Y).

3.2.1. Effect of amount of sorbent

The effect of the amount of sorbent in the recovery of REE(III) was studied, since it is an important parameter to evaluate the sorption capacity of the materials. For this purpose, the masses of sorbent used were 50 and 100 mg/L while the other experimental conditions were kept the same. In Figure 20, it is possible to observe the recovery (%) of REEs [100 µmol/L] from ultrapure water at pH *ca.* 5.5 and room temperature, using the three nanocomposites after 1 and 24 hours of contact time.

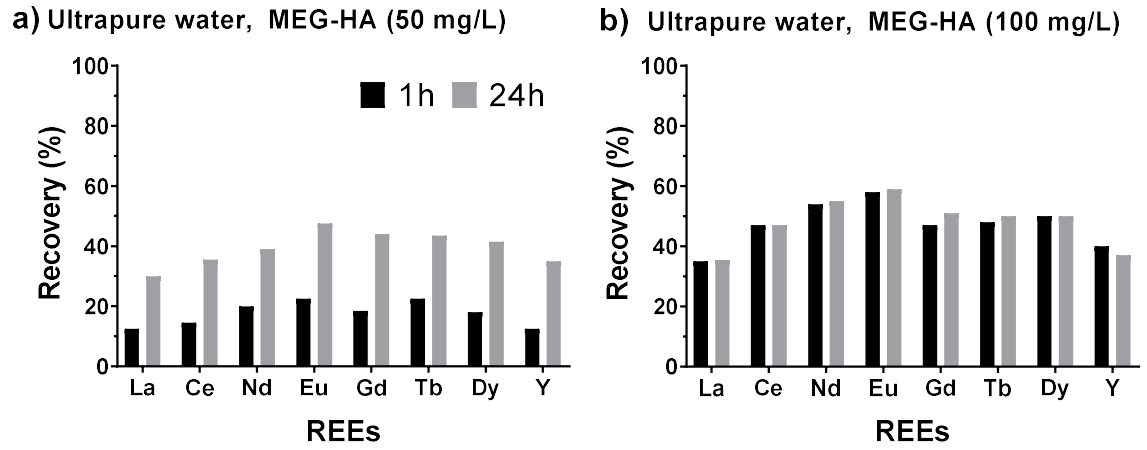

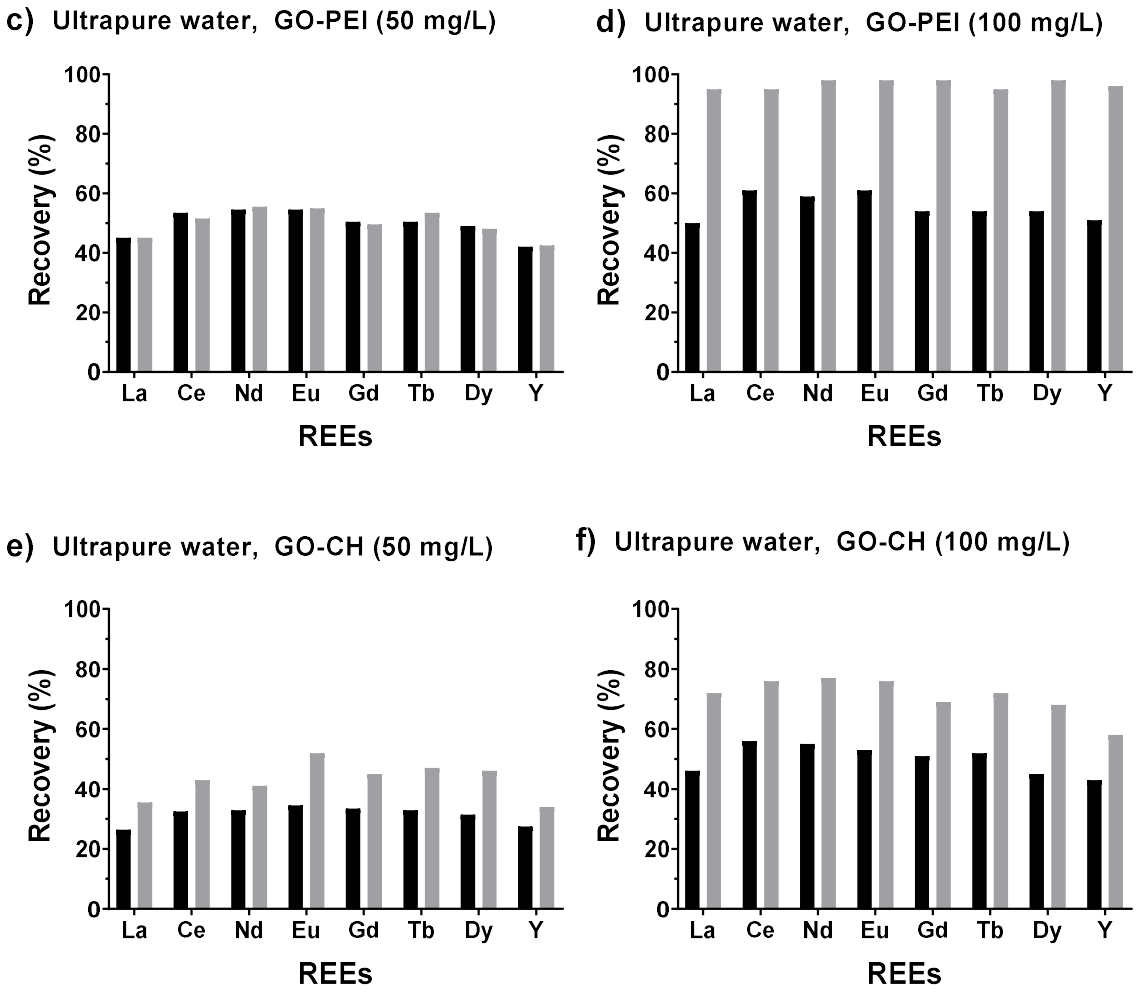

Figure 19 – Recovery percentages of rare earths elements (%) in aqueous solution (ultrapure water) after 1 (black) and 24 hours (grey) of contact time, pH ca. 5.5, $C_{REE(III)}$=100 µmol/L, T=25 ºC, m/V=50 and 100 mg/L (in left and right sides, respectively). Each graphic represents one material by the following order: a) MEG-HA (50 mg/L), b) MEG-HA (100 mg/L), c) GO-PEI (50 mg/L), d) GO-PEI (100 mg/L), e) GO-CH (50 mg/L), f) GO-CH (100 mg/L).

The results obtained show recoveries of REEs in all the experiments and the effect of the amount of sorbent was verified. The experiments where it was used a mass sorbent of 50 mg/L, it was achieved an average recovery of 44% and when using 100 mg/L of sorbent mass, it was achieved an average recovery of 72%. It is also possible do observe that GO-PEI and GO-CH need more time to achieve the maximum capacity of sorption than MEG-HA. The nanomaterial that achieved the best sorption percentage was GO-PEI (100 mg/L) around 100%, the other materials (GO-CH and MEG-HA) achieved sorption around 70 and 50%, respectively.

In the case of MEG-HA composite, the recovery of REEs using 50 and 100 mg/L was not statistically different, with only a 7% of improvement (from 40 to 47%). However, it is possible to verify that the equilibrium was reached faster using the larger mass since it took only 1 hour to achieve the maximum recovery (47%). As for the differences between the elements, it was verified that MREE were the most recovered in general, with Eu being the most recovered element (48 and 59% using 50 and 100 mg/L of sorbent, respectively). On the other hand, light REE (LREE) were the least recovered, with La being the least recovered element (30 and 31% for a mass of sorbent of 50 and 100 mg/L, respectively).

As for GO-PEI composite, the increase in the amount of sorbent was very evident, with a ranged of recovery of 50% (using a m/V ratio of 50 mg/L) and 97% (using a m/V ratio of 100 mg/L). As for the differences between the elements, it was verified that in general in the lower mass (50 mg/L) the MREE were the most recovered elements and the heavy REE (HREE) were the least ones.

For GO-CH composite, the increase of the amount of elements removed with the increase on mass of sorbent was also verified, with a range between 43% (using a m/V ratio of 50 mg/L) and 71% (using a m/V ratio of 100 mg/L). Yttrium was the least recovered element (34 and 58% for a mass of sorbent of 50 and 100 mg/L, respectively), and HREE showed the worst removal percentages. The values presented here were obtained after 24 hours of contact time.

After the analysis of the results it was decided to perform further studies with only 2 nanomaterials: GO-PEI and MEG-HA. GO-PEI was chosen since it showed the most promising results and the choice of MEG-HA was due to its magnetic properties since it offers more practicable in the separation of the nanomaterial from the solution; moreover, it has a different chemistry and it is cheaper than GO-PEI or GO-CH (which are similar).

3.2.2. Effect of ionic strength

To evaluate the ionic strength effect, 100 mg/L of MEG-HA and GO-PEI were used for the REEs recovery (100 µmol/L) from ultrapure, mineral and saline water at pH *ca*. 5.5 and room temperature.

Figure 21 and 22 show the variation of the normalized concentration (ratio between the concentration at time t, C_t, and the initial concentration, C_0) over time for rare earth elements, in the presence of 100 mg/L of MEG-HA and GO-PEI, respectively.

a) Ultrapure water, MEG-HA (100 mg/L)

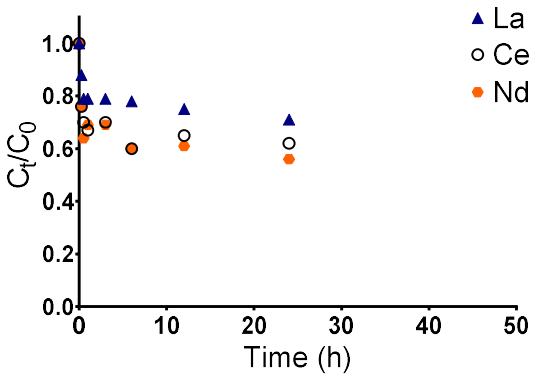

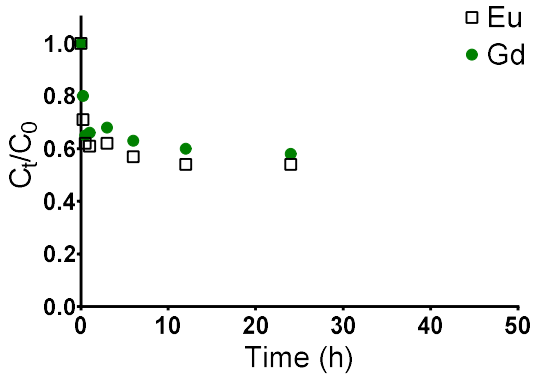

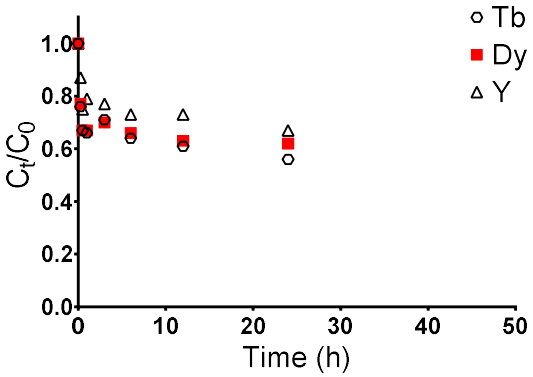

b) Mineral water, MEG-HA (100 mg/L)

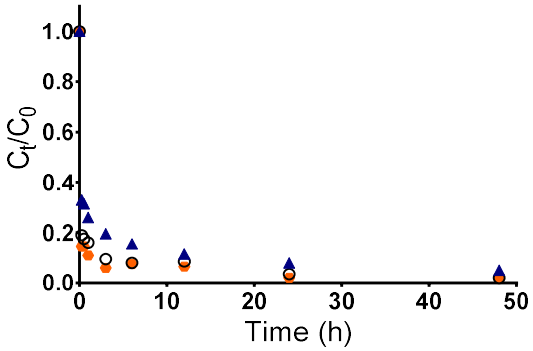

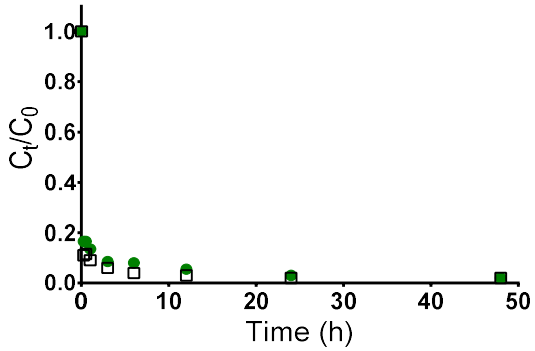

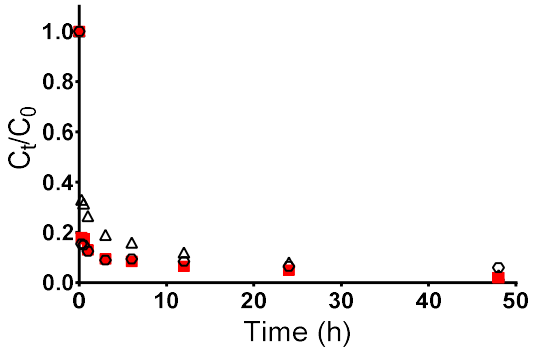

c) Saline water, MEG-HA (100 mg/L)

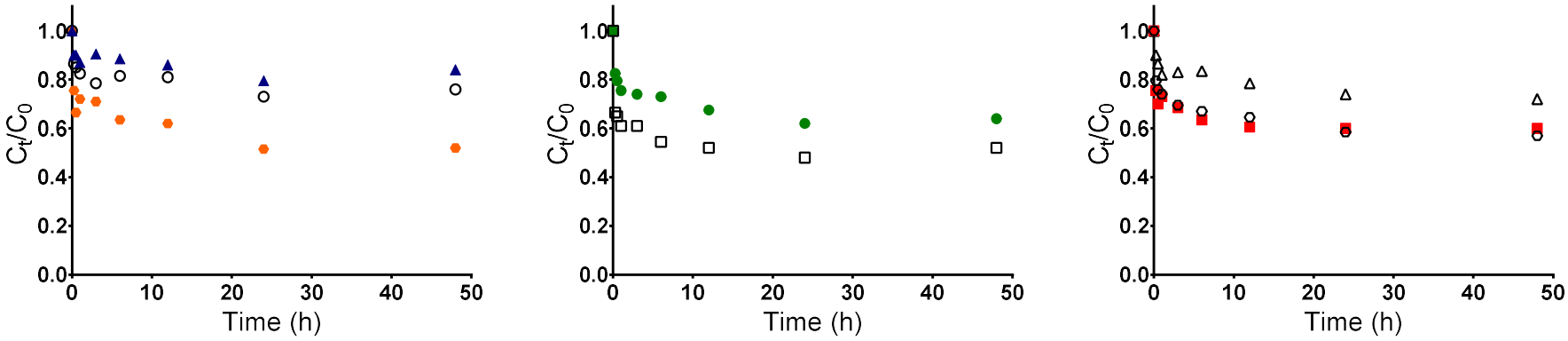

Figure 20 – Variation profile of normalized concentrations of rare earth elements multi-elemental solution (100 µmol/L) in waters (ultrapure (a), mineral (b) and saline (c) waters), in function of contact time with the MEG-HA (100 mg/L). Note that the values represented in the graphics are average values. The data were separated in three graphics for a better visualization of the results: left - LREEs (La, Ce and Nd), centre - MREEs (Eu and Gd), and right - HREEs (Tb, Dy and Y).

For the tests in mineral water using MEG-HA (figure 21-b), it can be observed that the normalized concentration in solution of each REE showed a fast decrease in the first minutes, pointing to a high recovery rate of REEs (> 95%) from solutions. Then, for a short period of time, evolves into a slower kinetics reaching equilibrium in less than 3 hours. This behaviour is explained by the large mass transport driving forces observed at the beginning of the experiment, since the composite is free of REE ions. The decrease on REEs concentration can be related to the nanocomposites since in its absence, the REE concentration in solution remained nearly constant. Regarding the test in ultrapure and saline water, the recovery rates were not so good; even so, REEs concentration decreases to almost half of the initial concentration. Overall, it is possible to conclude that regardless the water type, the equilibrium is reached fast (few hours). Comparing the results between the REEs, it is possible to observe that regardless the water type: i) for MREEs, Eu(III) have better recovery rates than Gd(III); ii) for HREEs, Y(III) is the least recovered element and iii) in the LREE, Nd(III) is the most recovered element, mainly when comparing the results obtained with La(III).

The recovery of only *ca.* 50% for all the REEs in ultrapure water can be explained by the low ionic conductivity of this kind of water, that can difficult the movement of the ions in solution and its transport to the material surface. Regarding the results obtained in mineral water, there is a significant increase in the recovery percentage which means that, or there is no formation of competitive complexes for the binding sites of MEG-HA (despite the increase of ions in solution) or the increase in conductivity originated from the introduction of more ions is greater than possible negative effects arising from the increase in matrix complexity. The percentage recovery in saline water (that is the more complex water type tested in this work) is the lower one, suggesting the occurrence of complexation of REE with water constituents which could change the affinity of the REEs for the material.

a) **Ultrapure water, GO-PEI (100 mg/L)**

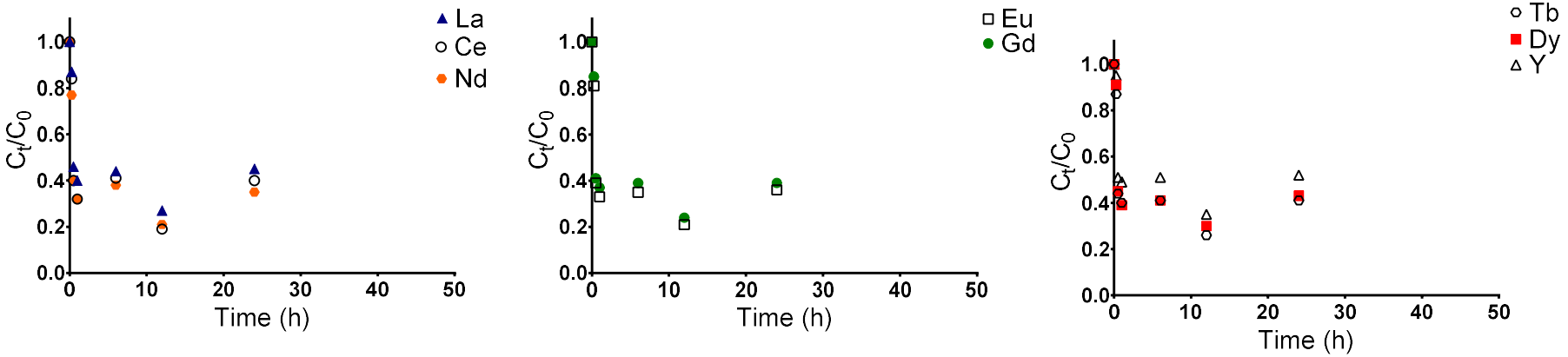

b) **Mineral water, GO-PEI (100 mg/L)**

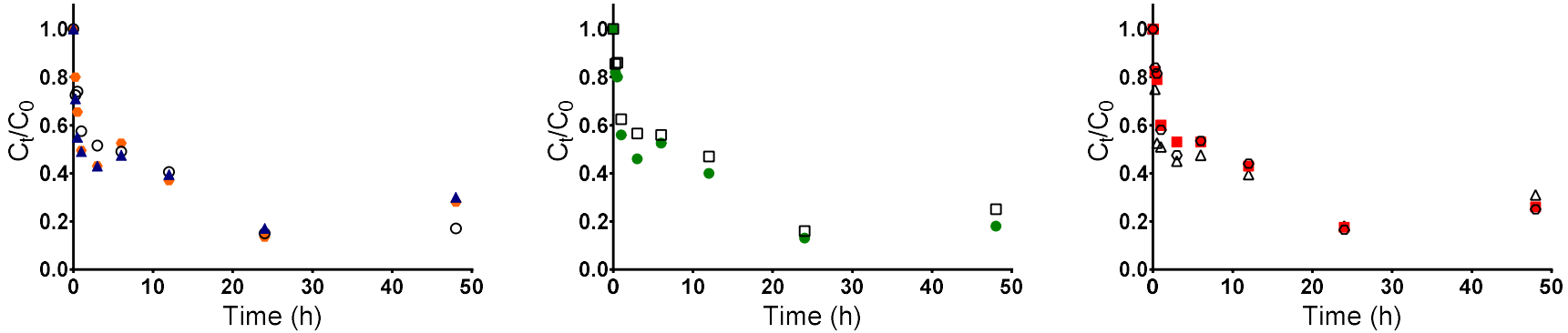

c) Saline water, GO-PEI (100 mg/L)

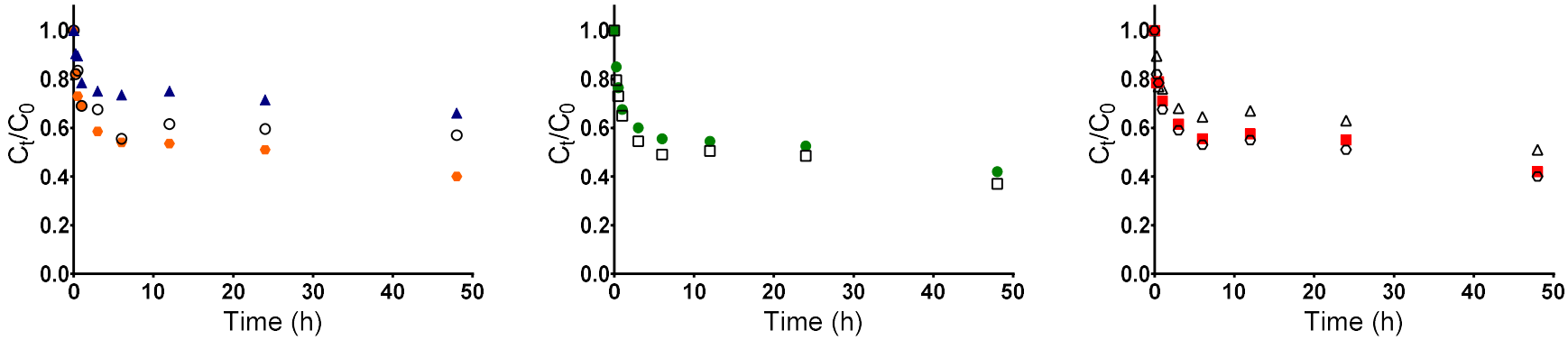

Figure 21 – Variation profile of normalized concentrations of rare earth elements multi-elemental solution (100 µmol/L) in waters (ultrapure (a), mineral (b) and saline (c) waters), in function of contact time with the GO-PEI (100 mg/L). Note that the values represented in the graphics are average values. The data were separated in three graphics for a better visualization of the results: left - LREEs (La, Ce and Nd), centre - MREEs (Eu and Gd), and right - HREEs (Tb, Dy and Y).

The removal of REEs from different water types using GO-PEI is shown in Figure 21-b, and it can be observed that best results were achieved for mineral water. Overall, in these experiments it was obtained recoveries around 90% in mineral water and 60% in ultrapure and saline water. The explanations for these observations are analogous to those referred for MEG-HA.

Note that either using MEG-HA or GO-PEI, in some cases, the recovery rate of REEs decreases between 24 and 48 hours. This decrease was previously reported in the literature (Carvalho et al., 2016) and can be explained by the possible presence hydroxo(oxo) or carbonated species; these species are insoluble, so they can originate competitive equilibria, affecting the recovery efficiency of REEs for prolongated contact time with sorbent. Nevertheless, this decrease is not significant when compared to the initial concentration of REEs.

Figure 23 resumes the recovery of REEs from the figures 21 and 22, after 24 hours of contact time with 100 mg/L of two different sorbents: MEG-HA (a) e GO-PEI (b).

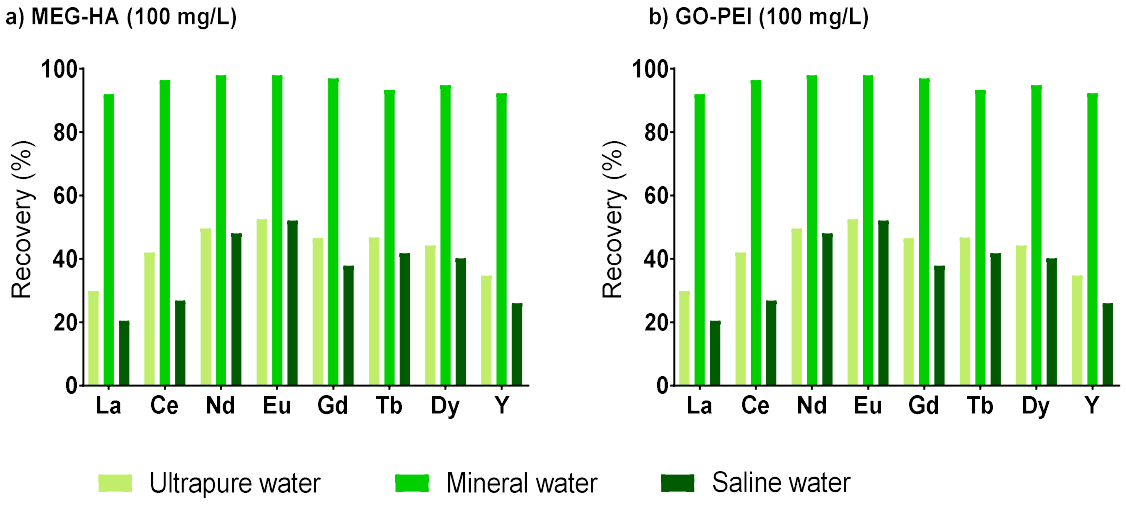

Figure 22 - Recovery of rare earths elements (%) in aqueous solution (ultrapure, mineral and saline waters) after 24 hours of contact time, pH ca. 5.5, CREE(III)=100 µmol/L, T=25 ºC, using 100 mg/L of MEG-HA (a) and GO-PEI (b).

Comparing the results obtained for the recovery of each REE after 24 hours of contact with the two nanocomposites, it is possible to conclude that the removal percentage of each REE is similar whatever the material used and for all the water types. This can be explained by the similar PZC of both materials (2.49 for MEG-HA and 2.65 for GO-PEI). Although, the similar PZC values, the sorption mechanism for both materials is different.

For the GO-PEI, PEI molecules played bilateral roles: on one hand they serve as the binding bridge for conjugation and on the other hand they improve the sorption affinity of the material to REEs (Wang et al., 2013). Thus, REEs species can sorbed in any of the adsorption sites (−N=, −NH−, $-NH_2$, $-NH_3$) (Choi et al., 2018) of PEI: through covalent bonds directly with N atoms or through hydrogen bonding with the functional group NH_3^+. We could confirm theses hypothesis by performing XPS analyses, however it was not possible to acquire for this work. Regarding the MEG-HA, the sorption process of REEs using humic acids functionalized materials is general associated to surface complexation (Yang et al., 2012).

Thus, MEG-HA would be a better choice for the recovery of REEs due to its magnetic properties, facilitating the recovery process and it is possible to observe a higher removal of MREEs using both of materials.

3.2.3. Kinetic studies

The application of kinetic models allows to understand the interaction dynamics between solid (adsorbent) and liquid (adsorbate), namely, the speed at which this interaction occurs. The sorption rate depends on the structural properties of the solid (porosity, specific area and particle size), liquid properties (such as concentration) and the type of interactions between the adsorbate and the active sites of the adsorbent (Oliveira et al., 2005).

Only results were the correlation between experimental data and model estimates were considered higher than the statistically accepted value for a probability of 99% and for a data of n=17 were considered.

The experimental kinetic data of the REEs recovery from a multi-elemental solution (100 µmol/L) in mineral and saline waters by MEG-HA (100 mg/L) and in saline water by GO-PEI (100 mg/L) composites at room temperature were fitted by pseudo-first order, pseudo-second order and Elovich models, represented by equations (3), (4) and (5).

The solid loadings of REEs on the MEG-HA and GO-PEI composites (q_t, µg/g) *versus* contact time (t), for mineral (a) and saline waters (b), is shown in Figures 24 and 25, respectively. For all sorbent-sorbate(s) systems the kinetic profiles are characterized by an abrupt increase of the solid loading of the rare earths in the nanocomposites, followed by a less pronounced increase, reaching a horizontal branch (*plateau*). The fit parameters for each data set are summarized in Table VI, VII and VIII.

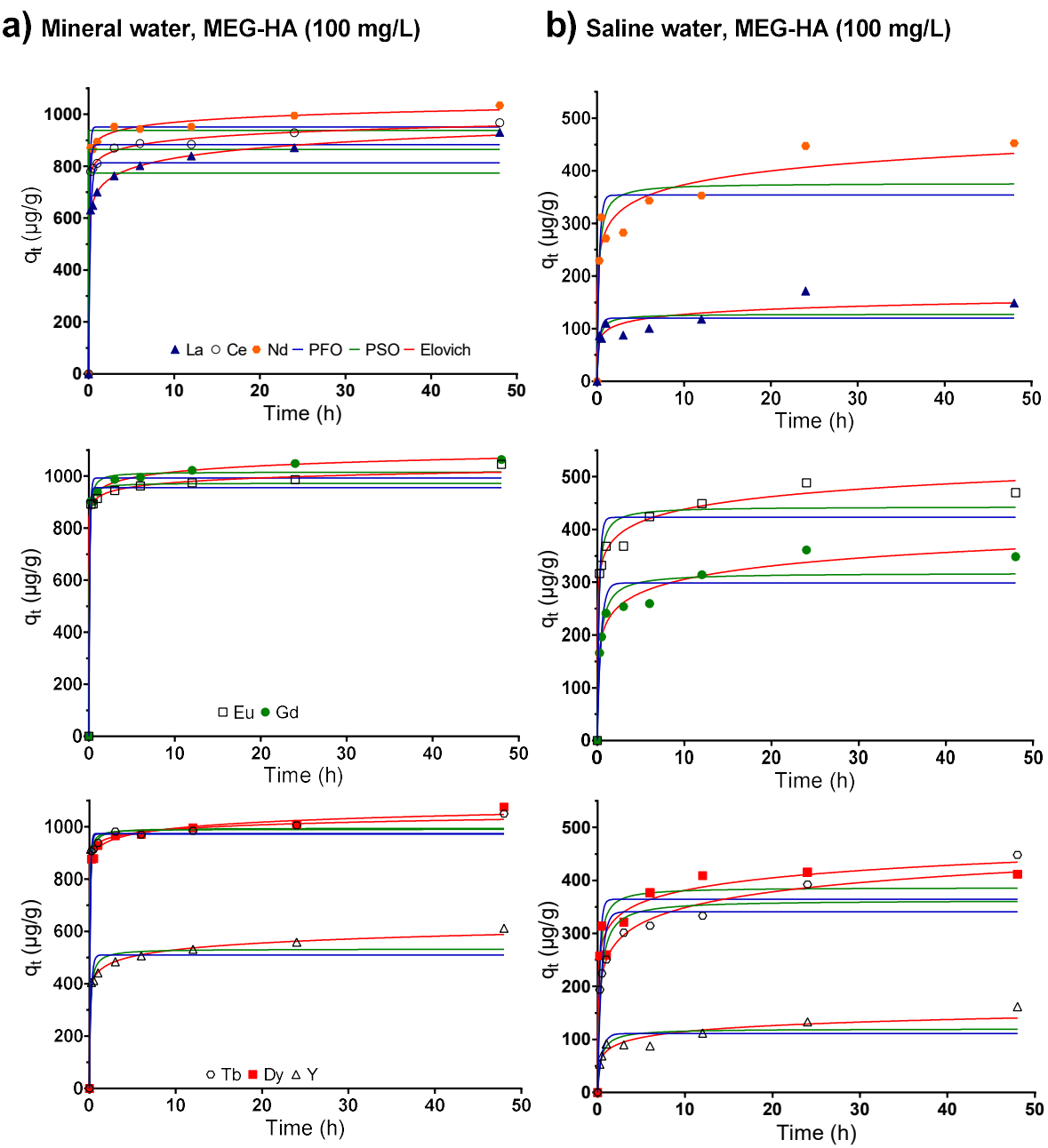

Figure 23 – Adjustment of the kinetic models (pseudo-first order, pseudo-second order and Elovich) to the best result obtained in REEs recovery (100 mg/L of MEG-HA composite in mineral (a) and saline (b) waters).

Table VI - - Values obtained in the adjustment of experimental results to the pseudo 1st order, pseudo 2nd order and Elovich's models, using the software GraphPad Prism 7. These results were obtained in the recovery of REEs using 100 mg/L of MEG-HA, in mineral waters.

Material	Matrix	Element	q_e exp (µg/g)	Degrees of Freedom	Pseudo first order model				Pseudo second order model				Elovich's model			
					Parameters		Adjustment		Parameters		Adjustment		Parameters		Adjustment	
					k_1	q_e (µg/mg)	R^2	$s_{y/x}$	k_2	q_e (µg/mg)	R^2	$s_{y/x}$	α	β	R^2	$s_{y/x}$
MEG-HA (100 mg/L)	Mineral water	La	929.6	15	5.0	801.7	0.9293	74.32	0.011	835.9	0.9653	52.03	1.41E+07	0.01777	0.9906	27.13
		Ce	967.3	15	8.2	875.3	0.965	56.83	0.022	898.4	0.9779	44.88	1.00E+12	0.02939	0.9873	33.96
		Nd	1034.0	15	9.5	944.4	0.9691	57.23	0.028	965.0	0.9784	47.90	5.49E+14	0.03400	0.9855	39.23
		Eu	1045.3	15	10.3	955.3	0.9732	53.90	0.034	972.6	0.9796	47.10	1.30E+17	0.03947	0.9852	40.03
		Gd	1063.4	15	8.9	992.4	0.9752	53.67	0.024	1016.0	0.9860	40.29	6.97E+13	0.03019	0.9930	28.51
		Tb	1050.3	15	10.2	974.3	0.9862	39.23	0.035	990.7	0.9916	30.53	4.85E+18	0.04254	0.9951	23.30
		Dy	1075.7	15	8.5	972.0	0.9775	50.02	0.023	994.8	0.9883	36.04	2.58E+13	0.02983	0.9951	23.32
		Y	611.8	15	5.00	510.3	0.9175	51.41	0.017	532.9	0.9562	37.46	5.61E+06	0.02685	0.9893	18.49

Table VII - Values obtained in the adjustment of experimental results to the pseudo 1st order, pseudo 2nd order and Elovich's models, using the software GraphPad Prism 7. These results were obtained in the recovery of REEs using 100 mg/L of MEG-HA, in saline waters.

Material	Matrix	Element	q_e exp (µg/g)	Degrees of Freedom	Pseudo first order model				Pseudo second order model				Elovich's model			
					Parameters		Adjustment		Parameters		Adjustment		Parameters		Adjustment	
					k_1	q_e (µg/mg)	R^2	$s_{y/x}$	k_2	q_e (µg/mg)	R^2	$s_{y/x}$	α	β	R^2	$s_{y/x}$
MEG-HA (100 mg/L)	Saline water	La	148.5	15	3.5	120.1	0.6098	32.28	0.03969	127.5	0.6547	30.36	1.26E+04	0.07169	0.7439	26.15
		Ce	214.3	15	3.0	178.6	0.3240	86.83	0.02569	187.5	0.3429	85.61	3.18E+04	0.05286	0.3664	84.07
		Nd	452.3	15	3.9	353.8	0.6387	90.56	0.01442	376.3	0.6771	85.62	7.05E+04	0.02633	0.7383	77.08
		Eu	469.7	15	4.3	422.9	0.7639	79.06	0.01644	443.0	0.7995	72.87	1.12E+06	0.02896	0.8295	67.19
		Gd	348.4	15	2.4	298.6	0.8653	40.76	0.01057	317.6	0.9150	32.38	1.51E+04	0.02724	0.9632	21.29
		Tb	448.3	15	2.2	341.0	0.8397	51.14	0.008865	362.6	0.8974	40.91	1.42E+04	0.02325	0.9588	25.93
		Dy	411.8	15	4.2	364.3	0.7903	63.34	0.01559	386.7	0.8430	54.80	2.59E+05	0.02948	0.8861	46.67
		Y	161.7	15	2.1	111.1	0.6982	25.89	0.02146	120.0	0.7432	23.88	1.81E+03	0.06108	0.8186	20.07

Overall, the fitting curves based on three kinetic models, namely, pseudo-first order, pseudo-second order and Elovich provided good adjustments to the experimental data corresponding to the recovery using MEG-HA in mineral water, with most of the coefficient of determination (R^2) above 0.95. Regarding the recovery with the same material but from saline water, despite the coefficients of determination were not so good, the values of R^2 are within the expected for adjustment obtained for the recovery of cerium (n=17 experimental values and an alpha of 0.01).

For the experiments using MEG-HA, the fitting of the Elovich model presents the highest coefficient of determination. This means that the sorption mechanism between REEs and MEG-HA may correspond to chemisorption (Jacinto et al., 2018).

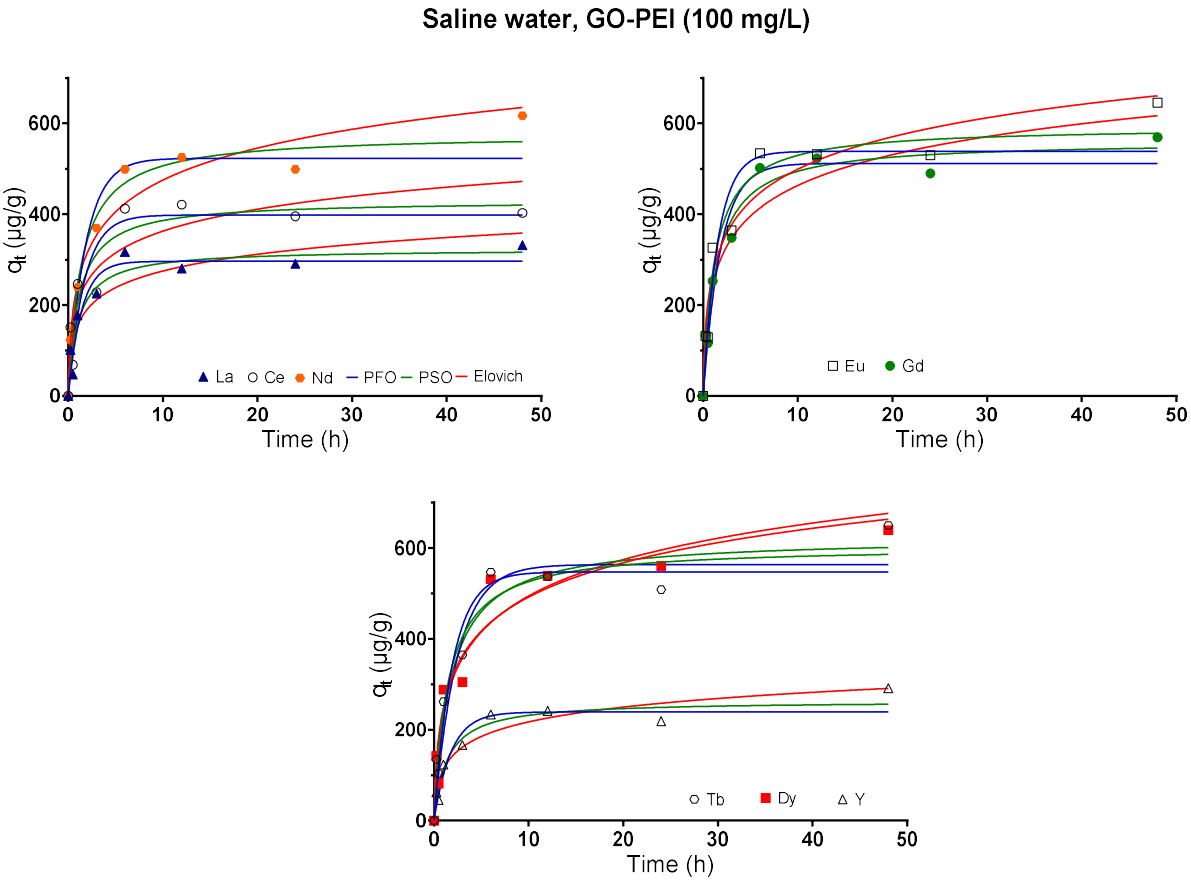

Figure 24 – Adjustment of the kinetic models(pseudo-first order, pseudo-second order and Elovich) to the best result obtained in REEs recovery (100 mg/L of MEG-HA composite and saline water).

Table VIII - Values obtained in the adjustment of experimental results to the pseudo 1st order, pseudo 2nd order and Elovich's models, using the software GraphPad Prism 7. These results were obtained in the recovery of REEs using 100 mg/L of GO-PEI, in saline waters.

Material	Matrix	Element	q_e exp (µg/g)	Degrees of Freedom	Pseudo first order model				Pseudo second order model				Elovich's model			
					Parameters		Adjustment		Parameters		Adjustment		Parameters		Adjustment	
					k_1	q_e (µg/mg)	R^2	$s_{y/x}$	k_2	q_e (µg/mg)	R^2	$s_{y/x}$	α	β	R^2	$s_{y/x}$
GO-PEI	Saline water	La	331.7	15	0.71	296.4	0.8852	42.00	0.0029	323.1	0.8870	41.67	915.3	0.01873	0.8487	48.22
		Ce	402.9	15	0.59	398.2	0.7971	75.37	0.0021	429.7	0.8193	71.13	1239	0.01429	0.7995	74.94
		Nd	616.9	15	0.55	522.9	0.8760	77.62	0.0013	575.8	0.8897	73.23	1047	0.009762	0.8718	78.95
		Eu	645.4	15	0.65	538.1	0.8391	93.01	0.0014	592.3	0.8599	86.79	1283	0.009675	0.8449	91.32
		Gd	569.3	15	0.54	511.7	0.9076	64.31	0.0013	560.7	0.9174	60.81	1083	0.01017	0.8891	70.45
		Tb	649.8	15	0.51	547.3	0.8344	97.41	0.0011	603.8	0.8401	95.72	958.1	0.009106	0.8174	102.3
		Dy	639.2	15	0.41	563.4	0.7998	110.0	0.00090	623.3	0.8167	105.3	795.4	0.008570	0.8097	107.3
		Y	291.4	15	0.55	239.0	0.8618	38.09	0.0028	263.4	0.8714	36.75	467.7	0.02120	0.8500	39.68

Overall, the fitting curves based on three kinetic models, namely, pseudo-first order, pseudo-second order and Elovich provided reasonable adjustments to the experimental data corresponding to the recovery using GO-PEI in saline water, with most of the coefficient of determination (R^2) above 0.80, which is within the expected value for n=17 and an alpha of 0.01.

In the experiments using GO-PEI, the fitting of the pseudo second order model presents the highest coefficient of determination. This means that the sorption mechanism between REEs and the nanocomposite is of chemical nature involving covalent or ionic forces and as the material surface is heterogeneous more than one type of interactions could occur simultaneously (Ho and McKay, 1999).

The following analysis concerns only the best results, namely, recovery of REEs from mineral waters using MEG-HA. Thus, comparing the values obtained for the parameters of Elovich model in its application to the recovery of REEs, it is noted that the α value corresponding to recovery of Tb(III) and Eu(III) is higher than that obtained for the recovery of the other REEs and the lowest α value corresponds to the recovery of La(III) and Y(III). This means that the initial rate of sorption of Tb(III) and Eu(III) is, in that case, much higher than the other REEs, which translates to higher affinity of Tb(III) and Eu(III) to MEG-HA. So, in the affinity of REEs to MEG-HA is as follows: Tb(III) ~ Eu(III) > Nd(III) ~ Gd(III) ~ Dy(III) ~ Ce(III) > La(III) ~ Y(III).

Chapter 4

Conclusions and suggestions for future work

4.1. Conclusions and Future work

The world has never been so much dependent on electronic devices as it is today and that means, consequently, REEs dependency. The problem of the electronic devices is the fact they become obsolete too quickly which generate great amounts of e-waste. E-waste is already a worldwide problem due to the enormous amount produced annually, making it very difficult to manage. It is known that an incorrect approach in the treatment and storage of e-waste can cause serious damage to the environment. For this reason, it is necessary to create and promote recycling approaches to the e-waste.

Recently, increasing attention has been given to carbon nanostructure materials. A review of the literature published in the last decade about carbon-based materials as sorbents to remove rare earth elements or technology-critical elements from spiked waters was presented here. Most of the studies tested high REE concentrations, tens to hundreds mg/L of single elements, in deionised waters. So, this work intended to recovery the rare earth elements under realistic conditions, with more complex water types, using lower element concentrations, and in multi-elemental systems using different carbon composites, like magnetic exfoliated graphite functionalized with humic acids (MEG-HA), graphene oxide functionalized with *ca.* 25% of polyethylenimine (GO-PEI) and graphene oxide functionalized with chitosan (GO-CH), that were synthetized and characterized, and then, their ability for the recovery of REEs was evaluated.

Regarding the results obtained for the effect of the amount of sorbent, it was possible to conclude that this factor has impact on the recovery percentage, ranging between 44 to 72% by doubling the mass of sorbent 50 to 100 mg/L). It is also possible do observe that GO-PEI and GO-CH need more time to achieve the maximum removal capacity than MEG-HA. In the case of the recovery of REEs from different matrices using MEG-HA or GO-PEI, it is possible to conclude that the composite has its most efficiency in mineral water with recovery rates around 100%, followed by saline water and ultrapure waters.

In the kinetic studies it was concluded that the Elovich model presents the highest coefficient of determination which means that the sorption mechanism between REEs and MEG-HA may correspond to chemisorption, being that Tb(III) and Eu(III) are the REEs with higher affinity to the materials. As for the kinetic studies of GO-PEI the pseudo second order model presents the highest coefficient of determination which indicates that the sorption mechanism between REEs and the nanocomposite is of chemical nature involving

covalent or ionic forces and as the material surface is heterogeneous more than one type of interactions could occur simultaneously.

As a suggestion for future work, it will be of interest to conduct regeneration studies by desorption processes. Also, it could be interesting to test other functionalizations methods and other ligands as functionalizations. Regarding the removal/recovery studies, it will be interest to apply these nanocomposites in the recovery of rare earths from real wastewaters and also from e-waste.

In addition to kinetic evaluation, it would be also necessary to perform equilibrium studies in order to determine the maximum sorption capacity of the materials as well as to confirm the sorption mechanisms involved in the REEs removal.

Chapter 5

References

Abrahami ST, Xiao Y, Yang Y. Rare-earth elements recovery from post-consumer hard-disc drives. Miner Process Extr Metall 2015;124:106–15.

Agrawal YK. Poly(β-Styryl)-(1,2-Methanofullerene-C60)-61-Formo Hydroxamic Acid for the Solid Phase Extraction, Separation and Preconcentration of Rare Earth Elements. Fullerenes, Nanotub Carbon Nanostructures 2007;15:353–65.

Aharoni C, Tompkins FC. Kinetics of Adsorption and Desorption and the Elovich Equation, 1970, p. 1–49. doi:10.1016/S0360-0564(08)60563-5.

Aksu Z. Application of biosorption for the removal of organic pollutants: A review. Process Biochem 2005;40:997–1026. doi:10.1016/j.procbio.2004.04.008.

Araújo MP, Soares OSGP, Fernandes AJS, Pereira MFR, Freire C. Tuning the surface chemistry of graphene flakes: new strategies for selective oxidation. RSC Adv 2017;7:14290–301. doi:10.1039/C6RA28868E.

Ashour RM, Abdelhamid HN, Abdel-Magied AF, Abdel-Khalek AA, Ali MM, Uheida A, et al. Rare Earth Ions Adsorption onto Graphene Oxide Nanosheets. Solvent Extr Ion Exch 2017;35:91–103.

Atibu EK, Devarajan N, Laffite A, Giuliani G, Salumu JA, Muteb RC, et al. Assessment of trace metal and rare earth elements contamination in rivers around abandoned and active mine areas. The case of Lubumbashi River and Tshamilemba Canal, Katanga, Democratic Republic of the Congo. Chemie Der Erde 2016;76:353–62.

Baldé CP, Forti V, Gray V, Kuehr R, Stegmann P. The Global E-Waste Monitor - 2017. Bonn/Geneva/Vienna: 2017.

Baldé CP, Wang F, Kuehr R, Huisman J. The Global E-Waste Monitor - 2014. Bonn, Germany: 2015.

Batlle X, Labarta A. Finite-size effects in fine particles: Magnetic and transport properties. J Phys D Appl Phys 2002;35:15–42.

Behdani FN, Rafsanjani AT, Torab-Mostaedi M, Mohammadpour SMAK. Adsorption ability of oxidized multiwalled carbon nanotubes towards aqueous Ce(III) and Sm(III). Korean J Chem Eng 2013;30:448–55.

Binnemans K, Jones PT. Perspectives for the recovery of rare earths from end-of-life fluorescent lamps. J Rare Earths 2014;32:195–200.

Boss CB, Boss CB, Fredeen KJ, Fredeen KJ. Concepts, Instrumentation and Techniques in Inductively Coupled Plasma Optical Emission Spectrometry. third. 1997. doi:10.1017/CBO9781107415324.004.

Branger C, Meouche W, Margaillan A. Recent advances on ion-imprinted polymers. React Funct Polym 2013;73:859–75.

Cai X, Lin M, Tan S, Mai W, Zhang Y, Liang Z, et al. The use of polyethyleneimine-modified reduced graphene oxide as a substrate for silver nanoparticles to produce a material with lower cytotoxicity and long-term antibacterial activity. Carbon N Y 2012;50:3407–15.

Cao W, Hu S-S, Ye L-H, Cao J, Xu J-J, Pang X-Q. Trace-chitosan-wrapped multi-walled carbon nanotubes as a new sorbent in dispersive micro solid-phase extraction to determine phenolic compounds. J Chromatogr A 2015;1390:13–21.

Cardoso SP, Lopes CB, Pereira E, Duarte AC, Silva CM. Competitive removal of Cd2+and Hg2+ions from water using titanosilicate ETS-4: Kinetic behaviour and selectivity. Water Air Soil Pollut 2013;224. doi:10.1007/s11270-013-1535-z.

Carvalho RS, Daniel-Da-Silva AL, Trindade T. Uptake of Europium(III) from Water using Magnetite Nanoparticles. Part Part Syst Charact 2016;33:150–7.

Chen C, Hu J, Xu D, Tan X, Meng Y, Wang X. Surface complexation modeling of Sr(II) and Eu(III) adsorption onto oxidized multiwall carbon nanotubes. J Colloid Interface Sci 2008;323:33–41.

Chen CL, Wang XK, Nagatsu M. Europium Adsorption on Multiwall Carbon Nanotube/Iron

Oxide Magnetic Composite in the Presence of Polyacrylic Acid. Environ Sci Technol 2009;43:2362–7.

Chen S, Xiao M, Lu D, Zhan X. Carbon nanofibers as solid-phase extraction adsorbent for the preconcentration of trace rare earth elements and their determination by inductively coupled plasma mass spectrometry. Anal Lett 2007a;40:2105–15.

Chen S, Xiao M, Lu D, Zhan X. Use of a microcolumn packed with modified carbon nanofibers coupled with inductively coupled plasma mass spectrometry for simultaneous on-line preconcentration and determination of trace rare earth elements in biological samples. Rapid Commun Mass Spectrom 2007b;21:2524–8.

Chen W, Wang L, Zhuo M, Liu Y, Wang Y, Li Y. Facile and highly efficient removal of trace Gd(III) by adsorption of colloidal graphene oxide suspensions sealed in dialysis bag. J Hazard Mater 2014a;279:546–53.

Chen W, Wang L, Zhuo M, Wang Y, Fu S, Li Y, et al. Reusable colloidal graphene oxide suspensions combined with dialysis bags for recovery of trace Y(III) from aqueous solutions. RSC Adv 2014b;4:58778–87.

Chomchoey N, Bhongsuwan D, Bhongsuwan T. Magnetic Properties of Magnetite Nanoparticles Synthesized by Oxidative Alkaline Hydrolysis of Iron Powder 2010;971:963–71.

Chourpa I, Douziech-Eyrolles L, Ngaboni-Okassa L, Fouquenet J-F, Cohen-Jonathan S, Soucé M, et al. Molecular composition of iron oxide nanoparticles, precursors for magnetic drug targeting, as characterized by confocal Raman microspectroscopy. Analyst 2005;130:1395. doi:10.1039/b419004a.

Cobelo-García A, Filella M, Croot P, Frazzoli C, Du Laing G, Ospina-Alvarez N, et al. COST action TD1407: network on technology-critical elements (NOTICE)—from environmental processes to human health threats. Environ Sci Pollut Res 2015;22:15188–94.

Das T, Kalita G, Bora PJ, Prajapati D, Baishya G, Saikia BK. Humi-Fe3O4 nanocomposites from low-quality coal with amazing catalytic performance in reduction of nitrophenols. J Environ Chem Eng 2017;5:1855–65. doi:10.1016/j.jece.2017.03.021.

Directorate General Enterprise and Industry. EU critical raw materials profiles 2014:77–85. doi:Ref. Ares(2015)1819595 - 29/04/2015.

Dupont D, Brullot W, Bloemen M, Verbiest T, Binnemans K. Selective Uptake of Rare Earths from Aqueous Solutions by EDTA- Functionalized Magnetic and Nonmagnetic Nanoparticles. ACS Appl Mater Interfaces 2014;6:4980−4988.

Dutta T, Kim KH, Uchimiya M, Kwon EE, Jeon BH, Deep A, et al. Global demand for rare earth resources and strategies for green mining. Environ Res 2016;150:182–90.

Environmental Law Alliance Worldwide. Overview of Mining and its Impacts. Guideb. Eval. Min. Proj. EIAs, 2014, p. 3–18.

European Comission. EU Critical Raw Materials Profiles. 2014.

European Rare Earths Competency Network (ERECON). Strengthening the European Rare Earths Supply-Chain. Challenges and policy options. 2014.

Fakhri H, Mahjoub AR, Aghayan H. Effective removal of methylene blue and cerium by a novel pair set of heteropoly acids based functionalized graphene oxide: Adsorption and photocatalytic study. Chem Eng Res Des 2017;120:303–15.

Fan QH, Shao DD, Hu J, Chen CL, Wu WS, Wang XK. Adsorption of humic acid and Eu(III) to multi-walled carbon nanotubes: Effect of pH, ionic strength and counterion effect. Radiochim Acta 2009;97:141–8.

Farzin L, Shamsipur M, Shanehsaz M, Sheibani S. A new approach to extraction and preconcentration of Ce(III) from aqueous solutions using magnetic reduced graphene oxide decorated with thioglycolic-acid-capped CdTe QDs. Int J Environ Anal Chem 2017;97:854–67.

Figueira P, Lourenço MAO, Pereira E, Gomes JRB, Ferreira P, Lopes CB. Periodic mesoporous organosilica with low thiol density - A safer material to trap Hg(II) from water. J Environ Chem Eng 2017;5. doi:10.1016/j.jece.2017.09.032.

Firdaus M, Rhamdhani MA, Durandet Y, Rankin WJ, McGregor K. Review of High-Temperature Recovery of Rare Earth (Nd/Dy) from Magnet Waste. J Sustain Metall 2016;2:276–95.

Fisher A, Kara D. Determination of rare earth elements in natural water samples – A review of sample separation, preconcentration and direct methodologies. Anal Chim Acta 2016;935:1–29.

Francisquini E, Schoenmaker J, Souza JA. Nanopartículas Magnéticas e suas Aplicações. Química Supramol e Nanotecnologia 2014:269–88.

Gad HMH, Awwad NS. Factors affecting on the sorption/desorption of Eu (III) using activated carbon. Sep Sci Technol 2007;42:3657–80.

Ghazaghi M, Mousavi HZ, Rashidi AM, Shirkhanloo H, Rahighi R. Graphene-silica hybrid in efficient preconcentration of heavy metal ions via novel single-step method of moderate centrifugation-assisted dispersive micro solid phase extraction. Talanta 2016;150:476–84.

Giakisikli G, Anthemidis AN. Magnetic materials as sorbents for metal/metalloid preconcentration and/or separation. A review. Anal Chim Acta 2013;789:1–16.

Girão AF, Gonçalves G, Bhangra KS, Phillips JB, Knowles J, Irurueta G, et al. Electrostatic self-assembled graphene oxide-collagen scaffolds towards a three-dimensional microenvironment for biomimetic applications. RSC Adv 2016;6:49039–51.

Girginova P llieva. Novel magnetic materials: from coordination compounds to nanomaterials. University of Aveiro, 2009.

Gonzalez V, Vignati DAL, Leyval C, Giamberini L. Environmental fate and ecotoxicity of lanthanides: Are they a uniform group beyond chemistry? Environ Int 2014;71:148–57.

Hao Z, Li Y, Li H, Wei B, Liao X, Liang T, et al. Levels of rare earth elements, heavy metals and uranium in a population living in Baiyun Obo, Inner Mongolia, China: A pilot study. Chemosphere 2015;128:161–70.

Hatje V, Bruland KW, Flegal AR. Determination of rare earth elements after pre-concentration using NOBIAS-chelate PA-1®resin: Method development and application in the San Francisco Bay plume. Mar Chem 2014;160:34–41.

Hidayah NN, Abidin SZ. The evolution of mineral processing in extraction of rare earth elements using solid-liquid extraction over liquid-liquid extraction: A review. Miner Eng 2017;112:103–13.

Ho YS, McKay G. Pseudo-second order model for sorption processes. Process Biochem 1999;34:451–65. doi:10.1016/S0032-9592(98)00112-5.

Hobohm J, Kuchta K. Innovative recovery strategies of rare earth and other critical metals from electric and electronic waste. 2015.

Hu Y, Pan J, Zhang K, Lian H, Li G. Novel applications of molecularly-imprinted polymers in sample preparation. Trends Anal Chem 2013;43:37–52.

Huang C. Rare Earth Coordination Chemistry: Fundamentals and Applications. 2010. doi:10.1002/9780470824870.

Huang C, Hu B. Silica-coated magnetic nanoparticles modified with γ-mercaptopropyltrimethoxysilane for fast and selective solid phase extraction of trace amounts of Cd, Cu, Hg, and Pb in environmental and biological samples prior to their determination by inductively co. Spectrochim Acta - Part B At Spectrosc 2008;63:437–44.

Innocenzi V, Ippolito NM, De Michelis I, Prisciandaro M, Medici F, Vegliò F. A review of the processes and lab-scale techniques for the treatment of spent rechargeable NiMH batteries. J Power Sources 2017;362:202–18.

Jacinto J, Henriques B, Duarte AC, Vale C, Pereira E. Removal and recovery of Critical

Rare Elements from contaminated waters by living Gracilaria gracilis. J Hazard Mater 2018;344:531–8. doi:10.1016/j.jhazmat.2017.10.054.

Juère E, Florek J, Larivière D, Kim K, Kleitz F. Support effects in rare earth element separation using diglycolamide-functionalized mesoporous silica. New J Chem 2016;40:4325–34.

Kaya M. Recovery of metals and nonmetals from electronic waste by physical and chemical recycling processes. Waste Manag 2016;57:64–90.

Kiew SF, Kiew LV, Lee HB, Imae T, Chung LY. Assessing biocompatibility of graphene oxide-based nanocarriers: A review. J Control Release 2016;226:217–28.

Kilian K, Pyrzyńska K, Pęgier M. Comparative Study of Sc(III) Sorption onto Carbon-based Materials. Solvent Extr Ion Exch 2017;35:450–9.

Kim D, Powell LE, Delmau LH, Peterson ES, Herchenroeder J, Bhave RR. Selective Extraction of Rare Earth Elements from Permanent Magnet Scraps with Membrane Solvent Extraction. Environ Sci Technol 2015;49:9452–9.

Koochaki-Mohammadpour SMA, Torab-Mostaedi M, Talebizadeh-Rafsanjani A, Naderi-Behdani F. Adsorption Isotherm, Kinetic, Thermodynamic, and Desorption Studies of Lanthanum and Dysprosium on Oxidized Multiwalled Carbon Nanotubes. J Dispers Sci Technol 2014;35:244–54.

Kulaksiz S, Bau M. Anthropogenic dissolved and colloid/nanoparticle-bound samarium, lanthanum and gadolinium in the Rhine River and the impending destruction of the natural rare earth element distribution in rivers. Earth Planet Sci Lett 2013;362:43–50.

Kumar KV. Linear and non-linear regression analysis for the sorption kinetics of methylene blue onto activated carbon. J Hazard Mater 2006;137:1538–44. doi:10.1016/j.jhazmat.2006.04.036.

Kumirska J, Czerwicka M, Kaczyński Z, Bychowska A, Brzozowski K, Thöming J, et al.

Application of spectroscopic methods for structural analysis of chitin and chitosan. Mar Drugs 2010;8:1567–636. doi:10.3390/md8051567.

Lagergren S. About the theory of so-called adsorption of soluble substances. K Sven Vetenskapsakademiens Handl 1898;24:1–39.

Li C, Huang Y, Lin Z. Fabrication of titanium phosphate@graphene oxide nanocomposite and its super performance on Eu3+ recycling. J Mater Chem A 2014;2:14979–85.

Li D, Zhang B, Xuan F. The sorption of Eu(III) from aqueous solutions by magnetic graphene oxides: A combined experimental and modeling studies. J Mol Liq 2015;211:203–9.

Li K, Gao Q, Yadavalli G, Shen X, Lei H, Han B, et al. Selective Adsorption of Gd3+ on a Magnetically Retrievable Imprinted Chitosan/Carbon Nanotube Composite with High Capacity. ACS Appl Mater Interfaces 2015;7:21047–55.

Liang T, Li K, Wang L. State of rare earth elements in different environmental components in mining areas of China. Environ Monit Assess 2014;186:1499–513.

Lister TE, Wang P, Anderko A. Recovery of critical and value metals from mobile electronics enabled by electrochemical processing. Hydrometallurgy 2014;149:228–37.

Lopes CB, Oliveira JR, Rocha LS, Tavares DS, Silva CM, Silva SP, et al. Cork stoppers as an effective sorbent for water treatment: The removal of mercury at environmentally relevant concentrations and conditions. Environ Sci Pollut Res 2014;21:2108–21. doi:10.1007/s11356-013-2104-0.

Martins MA, Trindade T. Os nanomateriais e a descoberta de novos mundos na bancada do químico. Quim Nova 2012;35:1434–46. doi:10.1590/S0100-40422012000700026.

Marwani HM, Albishri HM, Jalal TA, Soliman EM. Study of isotherm and kinetic models of lanthanum adsorption on activated carbon loaded with recently synthesized Schiff's base. Arab J Chem 2017;10:1032–40.

Medas D, Cidu R, De Giudici G, Podda F. Geochemistry of rare earth elements in water and solid materials at abandoned mines in SW Sardinia (Italy). J Geochemical Explor 2013;133:149–59.

Meryem B, JI H, GAO Y, DING H, LI C. Distribution of rare earth elements in agricultural soil and human body (scalp hair and urine) near smelting and mining areas of Hezhang, China. J Rare Earths 2016;34:1156–67.

Monterroso P, Abreu SN, Pereira E, Vale C, Duarte AC. Estimation of Cu, Cd and Hg transported by plankton from. Acta Oecologica 2003;24:351–7.

München DD, Veit HM. Neodymium as the main feature of permanent magnets from hard disk drives (HDDs). Waste Manag 2017;61:372–6.

Murray RW, Miller DJ, Kryc KA. Analysis of Major and Trace Elements in Rocks, Sediments, and Interstitial Waters by Inductively Coupled Plasma-Atomic Emission Spectrometry. ODP Techical Note, 2000, p. 1–27.

Noack CW, Perkins KM, Callura JC, Washburn NR, Dzombak DA, Karamalidis AK. Effects of ligand chemistry and geometry on rare earth element partitioning from saline solutions to functionalized adsorbents. ACS Sustain Chem Eng 2016;4:6115–24.

Ogata T, Narita H, Tanaka M. Adsorption mechanism of rare earth elements by adsorbents with diglycolarnic acid ligands. Hydrometallurgy 2016;163:156–60.

Oliveira-Silva R, Pinto da Costa J, Vitorino R, Daniel-da-Silva AL. Magnetic chelating nanoprobes for enrichment and selective recovery of metalloproteases from human saliva. J Mater Chem B 2014;3:238–49.

Oliveira EA, Montanher SF, Andrade AD, Nóbrega JA, Rollemberg MC. Equilibrium studies for the sorption of chromium and nickel from aqueous solutions using raw rice bran. Process Biochem 2005;40:3485–90. doi:10.1016/j.procbio.2005.02.026.

Pagano G, Aliberti F, Guida M, Oral R, Siciliano A, Trifuoggi M, et al. Rare earth elements

in human and animal health: State of art and research priorities. Environ Res 2015;142:215–20.

Paul B, Parashar V, Mishra A. Graphene in the Fe3O4 nano-composite switching the negative influence of humic acid coating into an enhancing effect in the removal of arsenic from water. Environ Sci Water Res Technol 2015;1:77–83. doi:10.1039/C4EW00034J.

Perreault LL, Giret S, Gagnon M, Florek J, Larivière D, Kleitz F. Functionalization of Mesoporous Carbon Materials for Selective Separation of Lanthanides under Acidic Conditions. ACS Appl Mater Interfaces 2017;9:12003–12.

Płotka-Wasylka J, Szczepańska N, de la Guardia M, Namieśnik J. Miniaturized solid-phase extraction techniques. Trends Anal Chem 2015;73:19–38.

Pyrzynska K, Kubiak A, Wysocka I. Application of solid phase extraction procedures for rare earth elements determination in environmental samples. Talanta 2016;154:15–22.

Quina FH. Nanotecnologia e o meio ambiente: perspectivas e riscos. Quim Nova 2004;27:1028–9. doi:10.1590/S0100-40422004000600031.

Ramos SJ, Dinali GS, Oliveira C, Martins GC, Moreira CG, Siqueira JO, et al. Rare Earth Elements in the Soil Environment. Curr Pollut Reports 2016;2:28–50.

Rim K-T. Effects of rare earth elements on the environment and human health: A literature review. Toxicol Environ Health Sci 2016;8:189–200.

Rim KT, Koo KH, Park JS. Toxicological Evaluations of Rare Earths and Their Health Impacts to Workers: A Literature Review. Saf Health Work 2013;4:12–26.

Royen H, Fortkamp U. Rare Earth Elements - Purification, Separation and Recycling. Stockholm, Sweden: 2016.

Ruiz-Mercado GJ, Gonzalez MA, Smith RL, Meyer DE. A conceptual chemical process for the recycling of Ce, Eu, and Y from LED flat panel displays. Resour Conserv Recycl

2017;126:42–9.

Saha D, Akkoyunlu SD, Thorpe R, Hensley DK, Chen J. Adsorptive recovery of neodymium and dysprosium in phosphorous functionalized nanoporous carbon. J Environ Chem Eng 2017;5:4684–92.

Schischke K, Clemm C. Environmental Responsibility Report. Berlin: 2016.

Sengupta A, Deb AKS, Dasgupta K, Adyaa VC, Ali SM. Diglycolamic acid-functionalized multiwalled carbon nanotubes as a highly efficient sorbent for f-block elements: Experimental and theoretical investigations. New J Chem 2017;41:4531–45.

Shen M, Cai H, Wang X, Cao X, Li K, Wang SH, et al. Facile one-pot preparation, surface functionalization, and toxicity assay of APTS-coated iron oxide nanoparticles. Nanotechnology 2012;23:105601. doi:10.1088/0957-4484/23/10/105601.

Shriver D, Weller M, Overton T, Rourke J, Armstrong F. Inorganic Chemistry. 2014.

Smith YR, Bhattacharyya D, Willhard T, Misra M. Adsorption of aqueous rare earth elements using carbon black derived from recycled tires 2016;296:102–11.

Socrates G. Infrared and Raman characteristic group frequencies. Third. 2004.

Song WL, Cao MS, Lu MM, Liu J, Yuan J, Fan LZ. Improved dielectric properties and highly efficient and broadened bandwidth electromagnetic attenuation of thickness-decreased carbon nanosheet/wax composites. J Mater Chem C 2013;1:1846–54. doi:10.1039/c2tc00494a.

Su S, Chen B, He M, Hun B, Xiao Z, Hu B, et al. Determination of trace/ultratrace rare earth elements in environmental samples by ICP-MS after magnetic solid phase extraction with Fe3O4@SiO2@polyaniline-graphene oxide composite. Talanta 2014;119:458–66.

Sun Y, Shao D, Chen C, Yang S, Wang X. Highly efficient enrichment of radionuclides on graphene oxide-supported polyaniline. Environ Sci Technol 2013;47:9904–10.

Sun Y, Wang Q, Chen C, Tan X, Wang X. Interaction between Eu(III) and Graphene Oxide Nanosheets Investigated by Batch and Extended X-ray Absorption Fine Structure Spectroscopy and by Modeling Techniques. Environ Sci Technol 2012;46:6020–7.

Sun Z, Xiao Y, Agterhuis H, Sietsma J, Yang Y. Recycling of metals from urban mines - A strategic evaluation. J Clean Prod 2016;112:2977–87.

Tan Q, Li J, Zeng X. Rare Earth Elements Recovery from Waste Fluorescent Lamps: A Review. Crit Rev Environ Sci Technol 2015;45:749–76.

Tansel B. From electronic consumer products to e-wastes: Global outlook, waste quantities, recycling challenges. Environ Int 2017;98:35–45.

Tavares DS, Lopes CB, Coelho JP, Sánchez ME, Garcia AI, Duarte AC, et al. Removal of arsenic from aqueous solutions by sorption onto sewage sludge-based sorbent. Water Air Soil Pollut 2012;223. doi:10.1007/s11270-011-1025-0.

Tong S, Zhao S, Zhou W, Li R, Jia Q. Modification of multi-walled carbon nanotubes with tannic acid for the adsorption of La, Tb and Lu ions. Microchim Acta 2011;174:257–64.

Tripathi AC, Saraf SA, Saraf SK. Carbon nanotropes: A contemporary paradigm in drug delivery. Materials (Basel) 2015;8:3068–100.

Tsamis A, Coyne M. Recovery of Rare Earths from Electronic Wastes: An Opportunity for High-Tech SMEs. Brussels, Belgium: 2015.

Vogel N. Rare Earth Elements. 2011. doi:10.1007/978-3-642-35133-4.

Wang Y, Liang S, Chen B, Guo F, Yu S, Tang Y. Synergistic Removal of Pb(II), Cd(II) and Humic Acid by Fe3O4@Mesoporous Silica-Graphene Oxide Composites. PLoS One 2013;8:2–9. doi:10.1371/journal.pone.0065634.

Wei B, Li Y, Li H, Yu J, Ye B, Liang T. Rare earth elements in human hair from a mining area of China. Ecotoxicol Environ Saf 2013;96:118–23.

Wu Y, Yin X, Zhang Q, Wang W, Mu X. The recycling of rare earths from waste tricolor phosphors in fluorescent lamps: A review of processes and technologies. Resour Conserv Recycl 2014;88:21–31.

Xiaoqi S, Yang J, Ji C, Jiutong M. Solvent impregnated resin prepared using task-specific ionic liquids for rare earth separation. J Rare Earths 2009;27:932–6.

Xie Y, Helvenston EM, Shuller-Nickles LC, Powell BA. Surface Complexation Modeling of Eu(III) and U(VI) Interactions with Graphene Oxide. Environ Sci Technol 2016;50:1821–7.

Yadav KK, Dasgupta K, Singh DK, Anitha M, Varshney L, Singh H. Solvent impregnated carbon nanotube embedded polymeric composite beads: An environment benign approach for the separation of rare earths. Sep Purif Technol 2015;143:115–24.

Yang L, Wang X, Nie H, Shao L, Wang G, Liu Y. Residual levels of rare earth elements in freshwater and marine fi sh and their health risk assessment from Shandong , China. Mar Pollut Bull 2016;107:393–7.

Yang S, Zong P, Ren X, Wang Q, Wang X. Rapid and Highly E ffi cient Preconcentration of Eu(III) by Core − Shell Structured Fe3O4@Humic Acid Magnetic Nanoparticles. ACS Appl Mater Interfaces 2012;4:6891–900.

Yang Y, Walton A, Sheridan R, Güth K, Gauß R, Gutfleisch O, et al. REE Recovery from End-of-Life NdFeB Permanent Magnet Scrap: A Critical Review. J Sustain Metall 2017;3:122–49.

Yao T, Xiao Y, Wu X, Guo C, Zhao Y, Chen X. Adsorption of Eu(III) on sulfonated graphene oxide: Combined macroscopic and modeling techniques. J Mol Liq 2016;215:443–8.

Yasmeen S, Kabiraz M, Saha B, Qadir M, Gafur M, Masum S. Chromium (VI) Ions Removal from Tannery Effluent using Chitosan-Microcrystalline Cellulose Composite as Adsorbent. Int Res J Pure Appl Chem 2016;10:1–14. doi:10.9734/IRJPAC/2016/23315.

Yoon H-SS, Kim C-JJ, Chung K-WW, Kim S-DD, Lee J-YY, Kumar JR. Solvent extraction, separation and recovery of dysprosium (Dy) and neodymium (Nd) from aqueous solutions: Waste recycling strategies for permanent magnet processing. Hydrometallurgy 2016;165:27–43.

Zaimes GG, Hubler BJ, Wang S, Khanna V. Environmental Life Cycle Perspective on Rare Earth Oxide Production. ACS Sustain Chem Eng 2015;3:237–44.

Zepf V. Rare Earth Elements, 2013. doi:10.1007/978-3-642-35458-8.

Zhang W, Shi X, Zhang Y, Gu W, Li B, Xian Y. Synthesis of water-soluble magnetic graphene nanocomposites for recyclable removal of heavy metal ions. J Mater Chem A 2013;1:1745–53. doi:10.1039/C2TA00294A.

Zhao F, Repo E, Meng Y, Wang X, Yin D, Sillanpää M. An EDTA-b-cyclodextrin material for the adsorption of rare earth elements and its application in preconcentration of rare earth elements in seawater. J Colloid Interface Sci 2016;465:215–24.

Zhu LL, Guo L, Zhang ZJ, Chen J, Zhang SM. The Preparation of Supported Ionic Liquids (SILs) and Their Application in Rare Metals Separation. ChemInform 2012;55:1479–87.

Zhuang M, Zhao J, Li S, Liu D, Wang K, Xiao P, et al. Concentrations and health risk assessment of rare earth elements in vegetables from mining area in Shandong, China. Chemosphere 2016;168:578–82.

Chapter 6

Attachments

Table A1 - Recovery of REEs using Graphene oxide (GO) composites and the respectively experimental conditions used as reported in the literature.

Ref.	Sorbent	Type of water	Type of system	REEs (III)	$[REEs]_0$ (µg/L)	pH	T (ºC)	Time of contact (h)	m (sorbent)/ V(solution) (mg/L)	q_m (mg/g) or REEs adsorption (%)
(Ashour et al., 2017)	GO colloid	Ultrapure	Multi elements	La, Nd, Gd, Y	5×10^3	6	r.t.	0.5	10×10^2	La = 85.67 mg/g Nd = 188.6 mg/g Gd = 225.5 mg/g Y = 135.7 mg/g
(Ashour et al., 2017)	GO colloid	Ultrapure	Multi elements	La, Nd, Gd, Y	$(5 – 50) \times 10^3$	3-8	5-45	0.02-2	10×10^2	
(Li D. et al., 2015)	GO	Ultrapure	Mono element	Eu	10×10^3 $NaClO_4$= 0.01 mol/L	4.5, 7	20	0-24	10×10^2	90 %, 89.654 mg/g
(Li D. et al., 2015)	MGO	Ultrapure	Mono element	Eu	10×10^3 $NaClO_4$= 0.01 mol/L	4.5, 7	20	0-24	10×10^2	80 %, 70.15 mg/g
(Li D. et al., 2015)	GO e MGO	Ultrapure	Mono element	Eu	$(1– 50) \times 10^3$	2-11	20, 40, 60	0-24	10×10^2	
(Sun et al., 2012)	GONS	Ultrapure	Mono element	Eu [(1)]	51×10^3 $NaClO_4$= 0.01 mol/L	2 4.5 6 7	25	48	2×10^2	65 %, 167.16 mg/g 161.29 mg/g 175.44 mg/g 100 %
(Sun et al., 2012)	GONS	Ultrapure	Mono element	Eu	51×10^3 $NaClO_4$= 0.01 mol/L	2-11	25,45, 65	48	2×10^2	

Ref.	Sorbent	Type of water	Type of system	REEs (III)	$[REEs]_0$ (µg/L)	pH	T (ºC)	Time of contact (h)	m (sorbent)/ Vsolution (mg/L)	q_m (mg/g) or REEs adsorption (%)
(Yao et al., 2016)	GO	Ultrapure	Mono element	Eu	10×10^3 NaCl= 0.1, 0.01, 0.001 mol/L	5.5	20	0-24	5×10^2	100%, 142.8 mg/g
(Yao et al., 2016)	GO-OSO_3H	Ultrapure	Mono element	Eu	10×10^3 NaCl= 0.1, 0.01, 0.001 mol/L	5.5	20	0-24	5×10^2	90%, 125.0 mg/g
(Yao et al., 2016)	GO e GO-OSO_3H	Ultrapure	Mono element	Eu	10×10^3 NaCl= 0.1, 0.01, 0.001 mol/L	1-11	20	0-24	5×10^2	
(Chen et al., 2014a)	GO colloid	Ultrapure	Mono element	Gd	12×10^3	5.9 (2-11)	30	0.5	0.4×10^2	286.86 mg/g
(Chen et al., 2014b)	GO colloid	Ultrapure	Mono element	Y	12×10^3	5.9	30, 40	0.42	0.4×10^2	190.48 mg/g
(Xie et al., 2016)	GO	Ultrapure	Mono element	Eu	0.01×10^3 NaCl= 0.01M	5.0, 2.7-7.3	r.t.	48	1×10^2	78 mg/g, 97%
(Xie et al., 2016)	GO	Ultrapure	Mono element	Eu	(0.01–100) $x10^3$	1-8 2,4,6	r.t.	48	1×10^2	
(Kilian et al., 2017)	GO	Ultrapure	Mono element	Sc	300×10^3	2 4	r.t.	4	50×10^2	~ 95%, 36.5 mg/g 39.7 mg/g

Ref.	Sorbent	Type of water	Type of system	REEs (III)	$[REEs]_0$ (µg/L)	pH	T (ºC)	Time of contact (h)	m (sorbent)/ Vsolution (mg/L)	q_m (mg/g) or REEs adsorption (%)
(Kilian et al., 2017)	GO	Milli-Q	Mono element	Sc	(1-300) $x10^3$	1-5.5	r.t.	0.02-0.5	50 x 10^2	
(Fakhri et al., 2017)	30%Mo_4W_8@EDMG, 30%Mo_2W_{10}@EDMG	Milli-Q	Mono element	Ce	10 x 10^3	6 (2-6)	20	0.08-3	17 x 10^2	90.90 mg/g, 96.15 mg/g
(Su et al., 2014)	MPANI-GO	Milli-Q	Multi elements	Y, La, Ce, Pr, Nd, Sm, Eu, Gd, Tb, Dy, Ho, Er, Tm, Yb, Lu	0.01 x 10^3	4	r.t.	0.33	4 x 10^2	~ 95% Y=8.1, La=15.5, Ce=8.6, Pr=11.1, Nd=8.5, Sm=7.7, Eu=11, Gd=16.3, Tb=11.8, Dy=16, Ho=8.1, Er=15.2, Tm=10.4, Yb=10.3, Lu=14.9 mg/g
(Su et al., 2014)	MPANI-GO	Milli-Q	Multi elements	Y, La, Ce, Pr, Nd, Sm, Eu, Gd, Tb, Dy, Ho, Er, Tm, Yb, Lu	(0.00025, 0.0005, 0.001, 0.002, 0.01) $x10^3$	2-9	r.t.	0.02-0.25, 0.33	(0.25-20) $x10^2$	
(Sun et al., 2013)	PANI@GO	$HClO_4$ (aq) 0.01 mol/L	Mono element	Eu	15 x 10^3	3	25	48	2.5 x 10^2	250.74 mg/g

Ref.	Sorbent	Type of water	Type of system	REEs (III)	$[REEs]_0$ (µg/L)	pH	T (ºC)	Time of contact (h)	m (sorbent)/ Vsolution (mg/L)	q_m (mg/g) or REEs adsorption (%)
(Farzin et al., 2017)	TGA/CdTeQDs/Fe3O4/rGONS	Distilled	Mono element	Ce	0.05×10^3 (1-100) $\times 10^3$	5.0	35	0.17	7×10^2	95 % 56.82 mg/g
(Farzin et al., 2017)	TGA/CdTeQDs/Fe3O4/rGONS	Distilled	Mono element	Ce	(1-100) $\times 10^3$	2-8	35	0.02-0.25	(2 – 9) $\times 10^2$	
(Li C. et al., 2014)	GTiP-1	Milli-Q	Mono element	Eu	100×10^3	1 3.7 5.5 7.3	25	2	10×10^2	~ 3 % ~ 32 % 35 % ~ 72 %
((Li C. et al., 2014)	GTiP-2	Milli-Q	Mono element	Eu	100×10^3	1 3.7 5.5 7.3	25	2	10×10^2	~ 10 % ~ 45 % 50 % ~ 80 %
(Li C. et al., 2014)	GO	Milli-Q	Mono element	Eu	100×10^3	1 3.7 5.5 7.3	25	2	10×10^2	~ 7 % ~ 20 % 20 % ~ 28 %
(Li C. et al., 2014)	GO, GTiP-1, GTiP-2	Milli-Q	Mono element	Eu	(5-200)$\times 10^3$ Na^+= 1, 10, 100, 1000 mM	1.7, 3.7, 5.5, 7.3	25	2, 4	$10\,000 \times 10^2$	

(1) Adsorptions experiments were conducted under N_2 conditions.

Note that the optimal experimental conditions are represented by shading and the other conditions tested and described in the papers are represented on a white background (without shading).

Table A2 - Recovery of REEs using Carbon nanotubes (CNTs) and the respectively experimental conditions used as reported in the literature.

Ref.	Sorbent	Type of water	Type of system	REEs (III)	$[REEs]_0$ (µg/L)	pH	T (ºC)	Time of contact (h)	m (sorbent)/ Vsolution (mg/L)	qm (mg/g) or REEs adsorption (%)
(Kilian et al., 2017)	CNTs-COOH	Milli-Q	Mono element	Sc	300 x 10^3	2 4	r.t.	4	50 x 10^2	37.9 mg/g 42.5 mg/g
(Kilian et al., 2017)	CNTs-COOH	Milli-Q	Mono element	Sc	(1-300) x10^3	1-5.5	r.t.	0.02-0.5	50 x 10^2	-
(Behdani et al., 2013)	MWCNTs-oxidized	Distilled	Multi elements	Ce	20 x 10^3 20 x 10^3 10 x 10^3	5	30	2	12 x 10^2 10 x 10^2 10 x 10^2	~ 87 % ~ 82 % ~ 97 %
(Behdani et al., 2013)	MWCNTs-oxidized	Distilled	Multi elements	Sm	20 x 10^3 20 x 10^3 10 x 10^3	5	30	2	12 x 10^2 10 x 10^2 10 x 10^2	~ 98 % ~ 95 % ~ 100 %
(Behdani et al., 2013)	MWCNTs-oxidized	Distilled	Multi elements	Ce, Sm –	(10, 20,50, 75, 100, 150, 200) x 10^3	2-8	30, 40, 50, 60	0.08,0.17, 0.25,0.33, 0.5, 0.67,0.83, 1, 1.25, 1.5, 2	(2, 4, 6, 8, 10, 12) x10^2	-
(Koochaki-Mohammadpour et al., 2014)	MWCNTs-oxidized	Distilled	Multi elements	La	20 x 10^3 20 x 10^3 10 x 10^3	5	30	2	12 x 10^2 10 x 10^2 10 x 10^2	80 % 80 % 93 %
(Koochaki-Mohammadpour et al., 2014)	MWCNTs-oxidized	Distilled	Multi elements	Dy	20 x 10^3 20 x 10^3 10 x 10^3	5	30	2	12 x 10^2 10 x 10^2 10 x 10^2	98 % 97 % 98 %

Ref.	Sorbent	Type of water	Type of system	REEs (III)	$[REEs]_0$ (µg/L)	pH	T (ºC)	Time of contact (h)	m (sorbent)/ Vsolution (mg/L)	qm (mg/g) or REEs adsorption (%)
(Koochaki-Mohammadpour et al., 2014)	MWCNTs-oxidized	Distilled	Multi elements	La, Dy –	(10 – 200) $x10^3$	2-6	30, 40, 50, 60	0.08,0.17, 0.25,0.33, 0.5,0.67, 0.83, 1, 1.25,1.5, 2	(2-12) $x10^2$	-
(Tong et al., 2011)	TA-MWCNTs	Distilled	Multi elements	La Tb Lu	40 x 10^3	5	20	1	50 x 10^2	5.35 mg/g, 8.55 mg/g, 3.97 mg/g
(Tong et al., 2011)	TA-MWCNTs	Distilled	Mono element	La	40 x 10^3	5	20	1	50 x 10^2 (with 0.12x10^2 being TA)	75 %
(Tong et al., 2011)	TA-MWCNTs	Distilled	Multi elements	(La, Tb, Lu)	40 x 10^3	1.5-4	20	1	50 x 10^2	0.4-6.0 mg/g
(Tong et al., 2011)	TA-MWCNTs	Distilled	Multi elements	(La, Tb, Lu)	(5 – 50) $x10^3$	1.5-7	20	0.08-2	(20-200) $x10^2$	-
(Fan et al., 2009)	MWCNTs-oxidized	Milli-Q	Mono element	Eu	0.99 x 10^3	5 (2-8)	25	96	6 x 10^2	90 %
(Chen et al., 2009)	MWCNTs/Fe_3O_4 composite	Milli-Q	Mono element	Eu [a]	0.061 x 10^3 $NaClO_4$= 0.1 mol/L	5.5	25	48	6 x 10^2	~ 100 %
(Chen et al., 2009)	MWCNTs/Fe_3O_4 composite	Milli-Q	Mono element	Eu [a]	0.61 x 10^3, 6.1 x 10^3	2.5-7	25	48	6 x 10^2	-

Ref.	Sorbent	Type of water	Type of system	REEs (III)	$[REEs]_0$ (µg/L)	pH	T (°C)	Time of contact (h)	m (sorbent)/ Vsolution (mg/L)	qm (mg/g) or REEs adsorption (%)
(Yadav et al., 2015)	PES/PVA/MWCNT/ D2EHPA beads	HCl (aq, 0.5 mol/L)	Mono element	Y	1000×10^3	–	30	8	1000×10^2	95 %
(Yadav et al., 2015)	PES/PVA/MWCNT/ D2EHPA beads	HCl (aq, 0.5 mol/L)	Mono element	Y	$(80\text{-}3300) \times 10^3$	–	30-65	0-8	1000×10^2	44.09 mg/g
(Yadav et al., 2015)	PES/PVA/MWCNT/ D2EHPA beads	HCl (aq, 0.5 mol/L)	Multi element	Y Sm La	100×10^3	–	30	4	1000×10^2	94 % 82% 30%
(Yadav et al., 2015)	PES/PVA/MWCNT/ D2EHPA beads	HCl (aq, 0.5 mol/L)	Multi element	Y Sm La	$(150–1000) \times 10^3$	–	30	0-8	1000×10^2	-
(Chen et al., 2008)	MWCNTs-oxidized	Distilled	Mono element	Eu	0.03×10^3 $NaClO_4$= 0.001, 0.01, 0.1 mol/L	6 (2-7)	25	48	6×10^2	98 % for all the ionic strengths
(Li K. et al., 2015)	mIIP-CS/CNT composite	Distilled	Multi elements	Gd [b]	10×10^3	7	20 33 43	4	20×10^2 [c]	79.48 mg/g 109.3 mg/g 121.51 mg/g
(Li K. et al., 2015)	mNIP-CS/CNT composite	Distilled	Multi elements	Gd [b]	10×10^3	7	33	4	20×10^2 [c]	96.15 mg/g
(Li K. et al., 2015)	mIIP-CS/CNT and mNIP-CS/CNT composites	Distilled	Multi elements	Gd [b]	$(2, 10, 50, 100, 200) \times 10^3$	2-7	20, 33, 43	0.05-8	20×10^2 [c]	-

[a] Adsorptions experiments under N_2 conditions. [b] Gd^{3+} adsorption experiments with two competitive ions (La^{3+} and/or Ce^{3+}). [c]10 mg of IIP-CS/CNT (or NIP-CS/CNT) and 30 mg of $SiO_2@Fe_3O_4$ were added into a vial, which contained 20 mL of REEs.

- the optimal experimental conditions are represented by shading and the others conditions tested and described in the papers are represented on a white background (without shading).

Table A3 - Recovery of REEs using other carbon materials ((Activated Carbon, Fullerene, C-Dots, Carbon Black, Mesoporous Carbon, Carbon nanofibers)) and the respectively experimental conditions used as reported in the literature.

Ref.	Sorbent	Type of water	Type of system	REEs (III)	$[REEs]_0$ (µg/L)	pH	T (ºC)	Time of contact (h)	m (sorbent)/ Vsolution (mg/L)	qm (mg/g) or REEs adsorption (%)
(Sun et al., 2012)	AC (Activated Carbon)	Milli-Q	Mono element	Eu	10×10^3 $NaClO_4$= 0.01 mol/L	4.5	25	48	2×10^2	20 mg/g
(Kilian et al., 2017)	AC-COOH	Milli-Q	Mono element	Sc	300×10^3	2	r.t.	4	50×10^2	2.1 mg/g
	AC-COOH	Milli-Q	Mono element	Sc	300×10^3	4	r.t.	4	50×10^2	2.2 mg/g
	AC-COOH	Milli-Q	Mono element	Sc	(1-300) $\times 10^3$	1-5.5	r.t.	0.02-4	50×10^2	
(Smith et al., 2016)	F-CCB (Functionalized commercial carbon black)	Milli-Q	Multi elementar	La, Ce, Nd, Sm, Y	100×10^3	Natural pH	25	24	0.25×10^2	La = 15 % Ce = 41 % Nd = 22.5 % Sm = 14 % Y = 17 %
	F-CCB (Functionalized commercial carbon black)	Milli-Q	Multi elementar	La, Ce, Nd, Sm, Y	100×10^3	Natural pH	25	24	**(0.03, 0.05, 0.15) $\times 10^2$**	La = 12%, 13%, 14% Ce = 35.5%, 36%, 35% Nd = 10%, 12%, 16% Sm = 10%, 10%, 12.5% Y = 12%, 13%, 13%
	RTCB (Recycled tire carbon black)	Milli-Q	Multi elementar	La, Ce, Nd, Sm, Y	100×10^3	Natural pH	25	24	0.25×10^2	La = 27.5 % Ce = 68 % Nd = 34 % Sm = 41 % Y = 28 %

Ref.	Sorbent	Type of water	Type of system	REEs (III)	$[REEs]_0$ (µg/L)	pH	T (ºC)	Time of contact (h)	m (sorbent)/ Vsolution (mg/L)	qm (mg/g) or REEs adsorption (%)
(Smith et al., 2016)	RTCB (Recycled tire carbon black)	Milli-Q	Multi elementar	La Ce Nd Sm Y	100 x 10^3	Natural pH	25	24	**(0.03, 0.05, 0.15) x10^2**	La = 3.5%, 6%, 17.5% Ce = 11%, 15%, 42% Nd = 5%, 7.5%, 22% Sm = 5.5%, 9%, 25.5% Y = 3.5%, 6%, 17.5%
	F-AC (Functionalized activated carbon)	Milli-Q	Multi elementar	La Ce Nd Sm Y	100 x 10^3	Natural pH	25	24	0.25 x 10^2	La = 7.5 % Ce = 12 % Nd = 31 % Sm = 7.5 % Y = 12.5 %
	F-AC (Functionalized activated carbon)	Milli-Q	Multi elementar	La Ce Nd Sm Y	100 x 10^3	Natural pH	25	24	**(0.03, 0.05, 0.15) x10^2**	La = 1.5%, 2.5%, 6.5% Ce = 2.5%, 8%, 11% Nd = 9%, 17%, 24% Sm = 0%, 7.5%, 5% Y = 6%, 9%, 11%
	CCB (commercial carbon black)	Milli-Q	Multi elementar	La Ce Nd Sm Y	100 x 10^3	Natural pH	25	24	**(0.15, 0.25)** x10^2	La = 2.5%, 2.5% Ce = 1%, 1% Nd = 5%, 8% Sm = 1%, 2.5% Y = 2.5%, 3%
	CCB (commercial carbon black)	Milli-Q	Multi elementar	La Ce Nd Sm Y	100 x 10^3	Natural pH	25	24	**(0.03, 0.05)** x10^2	La = 2.5%, 2.5% Ce = 1%, 1% Nd = 5%, 5% Sm = 1%, 1% Y = 2.5%, 2.5%

X

Ref.	Sorbent	Type of water	Type of system	REEs (III)	$[REEs]_0$ (µg/L)	pH	T (ºC)	Time of contact (h)	m (sorbent)/ Vsolution (mg/L)	qm (mg/g) or REEs adsorption (%)
(Smith et al., 2016)	AC	Milli-Q	Multi elementar	La Ce Nd Sm Y	100 x 10^3	Natural pH	25	24	**(0.15, 0.25) x10^2**	La = 1%, 1% Ce = 1%, 1% Nd = 12.5%, - Sm = 0%, 0% Y = 0%, 0%
	AC	Milli-Q	Multi elementar	La Ce Nd Sm Y	100 x 10^3	Natural pH	25	24	**(0.03, 0.05) x10^2**	La = 1%, 1.5% Ce = 1%, 1% Nd = 7.5%, 8% Sm = 0%, 1% Y = 1.5%, 1%
	RTCB (Recycled tire carbon black)	Milli-Q	Multi elementar	La Ce Nd Sm Y	20 x 10^3	Natural pH	80	1	0.5 x 10^2	La = 40%, Ce = 95% Nd = 75%, Sm = 80% Y = 63%
	RTCB (Recycled tire carbon black)	Milli-Q	Multi elementar	La Ce Nd Sm Y	20 x 10^3	Natural pH	80	2	0.5 x 10^2	La = 45%, Ce = 95% Nd = 80%, Sm = 82% Y = 72%
	RTCB (Recycled tire carbon black)	Milli-Q	Multi elementar	La Ce Nd Sm Y	20 x 10^3	Natural pH	80	12	0.5 x 10^2	La = 75%, Ce = 95% Nd = 91%, Sm = 95% Y = 90%

Ref.	Sorbent	Type of water	Type of system	REEs (III)	$[REEs]_0$ (µg/L)	pH	T (ºC)	Time of contact (h)	m (sorbent)/ Vsolution (mg/L)	qm (mg/g) or REEs adsorption (%)
(Smith et al., 2016)	RTCB (Recycled tire carbon black)	Milli-Q	Multi elementar	La Ce Nd Sm Y	20×10^3	Natural pH	25	1	0.5×10^2	La = 25% Ce = 85% Nd = 68% Sm = 60% Y = 48%
	RTCB (Recycled tire carbon black)	Milli-Q	Multi elementar	La Ce Nd Sm Y	20×10^3	Natural pH	25	2	0.5×10^2	La = 45% Ce = 90% Nd = 70% Sm = 73% Y = 60%
	RTCB (Recycled tire carbon black)	Milli-Q	Multi elementar	La Ce Nd Sm Y	20×10^3	Natural pH	25	12	0.5×10^2	La = 60% Ce = %, 95% Nd = 83% Sm = 88% Y = 77%
	RTCB (Recycled tire carbon black)	Milli-Q	Multi elementar	La,Ce Nd, Sm Y	100×10^3	Natural pH	40	24	0.05×10^2	La= 5.5%, Ce= 23% Nd= 9%, Sm= 9% Y= 9%
	RTCB (Recycled tire carbon black)	Milli-Q	Multi elementar	La, Ce Nd, Sm Y	100×10^3	Natural pH	60	24	0.05×10^2	La= 7.5%, Ce= 25% Nd= 16%, Sm= 16% Y= 16%
	RTCB (Recycled tire carbon black)	Milli-Q	Multi elementar	La, Ce Nd, Sm Y	100×10^3	Natural pH	80	24	0.05×10^2	La= 12.5%, Ce= 30% Nd= 20%, Sm= 20% Y= 21%

Ref.	Sorbent	Type of water	Type of system	REEs (III)	$[REEs]_0$ (µg/L)	pH	T (ºC)	Time of contact (h)	m (sorbent)/ Vsolution (mg/L)	qm (mg/g) or REEs adsorption (%)
(Smith et al., 2016)	RTCB (Recycled tire carbon black)	Milli-Q	Multi elementar	La, Ce, Nd, Sm, Y	100×10^3	Natural pH	40	24	0.25×10^2	La= 29% Ce = 75% Nd = 40% Sm = 40% Y = 40%
	RTCB (Recycled tire carbon black)	Milli-Q	Multi elementar	La, Ce, Nd, Sm, Y	100×10^3	Natural pH	60	24	0.25×10^2	La= 32.5% Ce = 81% Nd = 50%, Sm = 55%, Y = 50%,
	RTCB (Recycled tire carbon black)	Milli-Q	Multi elementar	La, Ce, Nd, Sm, Y	100×10^3	Natural pH	80	24	0.25×10^2	La= 48% Ce = 84% Nd = 58% Sm = 60% Y = 60%
	RTCB (Recycled tire carbon black)	Milli-Q	Multi elementar	La, Ce, Nd, Sm, Y	100×10^3	Natural pH	40	24	0.5×10^2	La= 45% Ce = 85% Nd = 65% Sm = 68% Y = 60%
	RTCB (Recycled tire carbon black)	Milli-Q	Multi elementar	La, Ce, Nd,Sm, Y	100×10^3	Natural pH	60	24	0.5×10^2	La= 51.5%, Ce = 90% Nd = 70%, Sm = 72% Y = 70%

Ref.	Sorbent	Type of water	Type of system	REEs (III)	$[REEs]_0$ (µg/L)	pH	T (ºC)	Time of contact (h)	m (sorbent)/ Vsolution (mg/L)	qm (mg/g) or REEs adsorption (%)
	RTCB (Recycled tire carbon black)	Milli-Q	Multi elementar	La, Ce, Nd, Sm, Y	100×10^3	Natural pH	80	24	0.5×10^2	La= 69%, Ce = 90% Nd = 75%, Sm = 75% Y = 75%
	F-CCB, RTCB, F-AC, AC	Milli-Q (Shaker: 200 rpm)	Multi elementar	La, Ce, Nd, Sm, Y	(100-200) $x10^3$	Natural pH	r.t. (25), 40, 60, 80	1-24	(0.25-0.5) $x10^2$	
(Gad and Awwad, 2007)	H-APC AC (HPO_4-APC activated carbon)	Milli-Q	Mono elementar	Eu	50×10^3	5	20	2	2.5×10^2 5×10^2 7.5×10^2 10×10^2 12.5×10^2 15×10^2 17.5×10^2	45 % 60 % 60 % 72 % 80 % 90 % 93 %
	H-APC AC	Milli-Q	Mono elementar	Eu	50×10^3	2 5 6 7	20	2	10×10^2	20 mg/g 32 mg/g 47 mg/g 50 mg/g
(X. Sun et al., 2016)	Carbonized polydopamine nano carbon shells (C-Dots)	Milli-Q	Multi elementar	La, Pr, Nd, Eu, Gd,Dy, Ho, Er, Tm, Yb, Lu	-	5.3	r.t.	1	20×10^2	-

Ref.	Sorbent	Type of water	Type of system	REEs (III)	$[REEs]_0$ (µg/L)	pH	T (ºC)	Time of contact (h)	m (sorbent)/ Vsolution (mg/L)	qm (mg/g) or REEs adsorption (%)
(Gad and Awwad, 2007)	H-APC AC	Milli-Q	Mono elementar	Eu	50 x 10^3	5	20	1 2	10 x 10^2	29 mg/g 29 mg/g
	H-APC AC	Milli-Q	Mono elementar	Eu	50 x 10^3	5	20 40 60	2	10 x 10^2	28.9 mg/g 29 mg/g 29.9 mg/g
	H-APC AC	Laboratory wastewaters	Mono elementar	Eu	-	5	20	0.7	5 x 10^2 10 x 10^2 15 x 10^2 20 x 10^2 25 x 10^2	97.55 98.47 98.63 99.07 99.10
(Marwani et al., 2017)	AC-DETADHBA	Distilled	Multi elementar	La	5 x 10^3	6 5 4	25	1	25 mg*	99. 60%, 144.80 mg/g 85% 40%
	AC-DETADHBA	Distilled	Multi elementar	La	5 x 10^3	6	25	0.17 0.5 1	25 mg*	121 mg/g 135 mg/g 144.80 mg/g
	AC-COOH	Distilled	Multi elementar	La	5 x 10^3	6	25	1	25 mg*	89.50 mg/g
	AC-DETADHBA	Distilled	Multi elementar	La	(10-400) x10^3	1-7	25	0.002, 0.0083, 0.17, 0.33, 0.5, 0.67, 0.83, 1	25 mg*	

Ref.	Sorbent	Type of water	Type of system	REEs (III)	$[REEs]_0$ (µg/L)	pH	T (ºC)	Time of contact (h)	m (sorbent)/ Vsolution (mg/L)	qm (mg/g) or REEs adsorption (%)
(Marwani et al., 2017)	AC-DETADHBA	Tap water	Mono elementar	La	5×10^3 10×10^3 50×10^3	6	25	1	25 mg*	98.54 % 100 % 95.76 %
	AC-DETADHBA	Lake water	Mono elementar	La	5×10^3 10×10^3 50×10^3	6	25	1	25 mg*	100 % 100 % 93.48 %
	AC-DETADHBA	Seawater	Mono elementar	La	5×10^3 10×10^3 50×10^3	6	25	1	25 mg*	98.86 % 99.65 % 93.24 %
(Saha et al., 2017)	Phosphorous functionalized nanoporous carbon	Milli-Q	Multi elementar	Nd Dy	0.5×10^3	6.1 6.6	25	4	10×10^2	Nd= 335.5 mg/g Dy= 344.6 mg/g
		Milli-Q	Multi elementar	Nd Dy	0.5×10^3	**6.1** **6.6**	25	**3** **0.033**	10×10^2	Nd= 68% Dy= 67%
	Phosphorous functionalized nanoporous carbon	Milli-Q	Multi elementar	Nd Dy	$(0.05\text{-}0.5) \times 10^3$	2, 4, 6.1 or 6.6	25	0.033, 0.25, 0.67, 1, 2, 3, 4	10×10^2	
(Perreault et al., 2017)	CMK-8	Milli-Q	Multi elementar	Sm	0.02×10^3	2.6	r.t.	0.5 2.5	10×10^2	1 mg/g 1.5 mg/g
	CMK-8-O (CMK-8-Oxidezed)	Milli-Q	Multi elementar	Sm	0.07×10^3	2.6	r.t.	0.5 1 2.5	10×10^2	14 mg/g 13.8 mg/g 13 mg/g

Ref.	Sorbent	Type of water	Type of system	REEs (III)	$[REEs]_0$ (µg/L)	pH	T (ºC)	Time of contact (h)	m (sorbent)/ Vsolution (mg/L)	qm (mg/g) or REEs adsorption (%)
(Perreault et al., 2017)	CMK-8-DGO (DGO: diglycolyl-type organic)	Milli-Q	Multi elementar	La	0.04 $x10^3$	2.6	r.t.	0.5 1 2.5	10 x 10^2	10 mg/g 9 mg/g 9 mg/g
	CMK-8-DGO (DGO: diglycolyl-type organic)	Milli-Q	Multi elementar	La	0.0003 $x10^3$	2.6 3.8 5.7	r.t.	4	10 x 10^2	23 mg/g 27 mg/g 22 mg/g
	CMK-8	Milli-Q	Multi elementar	Sm	(0.0025-0.025) $x10^3$	2.6	r.t.	4	10 x 10^2	8 mg/g
	CMK-8-O (CMK-8-Oxidezed)	Milli-Q	Multi elementar	Sm	(0.05-0.2) $x10^3$	2.6	r.t.	4	10 x 10^2	23 mg/g
	CMK-8-DGO (DGO: diglycolyl-type organic)	Milli-Q	Multi elementar	La	(0.01-0.1) $x10^3$	2.6	r.t.	4	10 x 10^2	10 mg/g
(Turanov and Karandashevb , 2009)	FB-D2EHPA sorbent (Fullerene Black functionalized)	HNO_3 (0.0031 M)	Multi elementar	La, Ce, Pr, Nd, Sm,Eu, Gd, Tb, Dy,Ho, Er, Tm, Yb, Lu	(0.02-1) $x10^{-3}$	-	20	2	100 x 10^2	-

*There are not any mention of the volume of REEs solution used.

- The optimal experimental conditions are represented by shading and the others conditions tested and described in the papers are represented on a white background (without shading

Table A4 - Values obtained in the adjustment of experimental results to the pseudo 1st order, pseudo 2nd order and Elovich's models, using the software GraphPad Prism 7. These results were obtained in the recovery of REEs using 100 mg/L of GO-PEI, in mineral waters.

Material	Matrix	Element	q_e exp (µg/g)	Degrees of Freedom	Pseudo first order model				Pseudo second order model				Elovich's model			
					Parameters		Adjustment		Parameters		Adjustment		Parameters		Adjustment	
					k_1	q_e (µg/mg)	R^2	$s_{y/x}$	k_2	q_e (µg/mg)	R^2	$s_{y/x}$	α	β	R^2	$s_{y/x}$
GO-PEI (100 mg/L)	Mineral water	La	304.5	15	5.098	391.7	0.2577	189.7	0.01337	418.4	0.2797	186.9	1.66E+05	0.02583	0.3113	182.7
		Ce	416.3	15	1.213	440.6	0.3478	178.5	0.003031	485.0	0.4184	168.6	4.34E+03	0.01469	0.4734	160.4
		Nd	374.6	15	1.823	449.5	0.2992	202.8	0.003956	495.4	0.3578	194.1	7.56E+03	0.01531	0.4045	186.9
		Eu	473.6	15	0.2138	552.3	0.5037	167.9	0.0006634	586.3	0.5461	160.6	7.35E+02	0.009773	0.5825	154.0
		Gd	464.7	15	0.9508	510.2	0.3492	210.1	0.002090	564.3	0.4158	199.1	3.43E+03	0.01205	0.4674	190.1
		Tb	486.3	15	0.3212	560.6	0.4517	187.6	0.001018	594.1	0.5099	177.3	1.32E+03	0.01021	0.5521	169.5
		Dy	459.6	15	0.5723	509.1	0.4238	183.9	0.001486	558.9	0.4911	172.8	1.94E+03	0.01139	0.5363	165.0
		Y	214.2	15	2.928	257.6	0.3191	109.8	0.01128	279.8	0.3647	106.1	1.56E+04	0.03168	0.4016	102.9